NATIONAL TECHNICAL UNIVERSITY OF ATHENS

SCHOOL OF CHEMICAL ENGINEERING

INTER-DEPARTMENTAL POSTGRADUATE COURSE

'COMPUTATIONAL MECHANICS'

NUMERICAL SIMULATION OF THE HYDROELASTIC INTERACTION BETWEEN TSUNAMI WAVES AND VERY LARGE FLOATING STRUCTURES OR ICE SHEETS

POST-GRADUATE THESIS

towards the fulfilment of the requirements for a specialisation diploma in

Computational Mechanics

by

ANGELIKI KARPERAKI

Thesis Supervisors: Prof Efstathios E.Theotokoglou

Dr Theodosios K. Papathanasiou

ATHENS, JULY 2014

Page intentionally left blank

Acknowledgments

The author feels the need to thank both supervisors Professor E. E Theotokoglou and Dr T. Papathanasiou for the guidance, support and patience they showed during the preparation of the present work. In particular, if it was not for the insightful comments and sheer dedication of Dr Papathanasiou, who also provided the motivation for this research, the author would not have gone far. His input in the error estimation for the finite elements and the a priori stability estimates for the weak solution ,were more than valuable.

I would also like to thank Professor K. Belibassakis for his feedback regarding result presentation and the physical interpretation of the phenomenon.

Finally, I would like to thank my parents and everyone who made this project enjoyable.

Page intentionally left blank

Abstract

Ice caps act as climate controllers, regulating temperature, ocean circulation and affecting global weather patterns. The disintegration of ice shelves and sea ice in recent years has gathered scientific attention as the stability of ice formations is being re-evaluated. The detrimental interaction between ice sheets and long waves has been recently advocated, showing the need for a thorough investigation of the phenomenon. Simultaneous technological advancements in marine engineering provide a different motivation for the study of the transient response of Very Large Floating Structures (VLFS) under long wave excitation.

In the present thesis, the elastic Euler Bernoulli beam model and the shallow water equations are coupled in order to derive a 1-D hydroelastic system. Two specific problems are defined, the one of a floating cantilever, a fixed-edge plate, able to simulate an ice shelf or moored VLFS, and one of a freely floating plate approximating the configuration of an ice floe or a pontoon VLFS.

Stability estimates of the variational form of the governing equations and the energy conservation principle are studied for both problems. The finite element method is employed for the solution of the problems in question. Special hydroelastic elements incorporating various polynomial degrees are developed in order to cater for the coupling in the hydroelasticity dominated regions of the problem. In addition, error estimates for the semi-discrete form are derived. The finite element solution is compared against the eigenfunction expansion method of Sturova (2009).

Finally, two examples are explored for each of the problems along with a geophysical case study based on the Sulzberger Ice Shelf calving event in 2011. Additionally, results presented as collaboration, by the author, at the European Geosciences General Assembly 2014 are given. The presence of the fixed boundary and its effect on the bending moment and shear force distributions are explored. Thickness variations are shown to have an effect on shear force distribution while the distance from the free edge of a cantilever plate where the maximum bending moment appears is relatively insensitive of the incoming tsunami wavelength.

Page intentionally left blank

Abstract in Greek

Εκτεταμένη Περίληψη

Οι συνέπειες της κλιματικής αλλαγής τόσο στο περιβάλλον, όσο και στην ανθρώπινη δραστηριότητα αποτελεί αντικείμενο εντατικής έρευνας. Με την αύξηση της θερμοκρασίας, το ενδιαφέρον στρέφεται στις Πολικές ζώνες και στην ευπαθή ισσορροπία τους. Ως ρυθμιστές του παγκόσμιου κλίματος, οι Αρκτικές ζώνες επηρεάζουν την θερμοκρασία και την ωκεάνια κυκλοφορία. Την ίδια στιγμή, ο καταγεγραμμένος 'κατακερματισμός'των στρωμάτων πάγου (ice shelves) ή παγετώνων στην Ανταρκτική και η σημαντική μείωση του θαλάσσιου πάγου στην Αρκτική, φαίνονται να επηρεάζουν άμεσα τις εμπορικές δραστηριότητες και να επιβεβαιώνουν την αρχή μιας σειράς κλιματικών διαταραχών.

Η κυματική διέγερση των στρωμάτων πάγου έχει συνδεθεί με τα φαινομενα απόσχισης σωμάτων πάγων και το σχηματισμό ροών (ice floes). Η παλιρροιακή δράση και η συνεχής καταπόνηση των κυμάτων, σε συνδιασμό με τις εγγενείς ατέλειες του πάγου οδηγεί σε καμπτική αστοχία και την τελική απόσχιση τμημάτων πάγου. Οι μεγάλες οριζόντιες διαστάσεις, σε σχέση με το πάχος των στρωμάτων πάγου, καθιστά τις ελαστικές παραμορφώσεις κυρίαρχες των κινήσεων στερεού σώματος. Επομένως, η μελέτη της απόκρισης στρωματών πάγων υπο κυματική καταπόνιση εμπίπτει στη περιοχή της υδροελαστικότητας.

Ανθρώπινες κατασκευές που μοιράζονται τα ίδια χαρακτηριστικά με τα στρώματα πάγου, όπως οι Μεγάλες Πλώτες Κατασκευές (Very Large Floating Structures, VLFS) αποτελούν εφαρμογές της υδροελαστικότητας. Συνεπώς, η υδροελαστική ανάλυση πλωτών στρωμάτων υπο κυματική καταπόνιση είναι κοινό έδαφος για εφαρμογές τοσο στη γεωφυσική όσο και στη μηχανική κλίμακα.

Ιδιαίτερο ενδιαφέρον παρουσιάζει η μελέτη των επιπτωσεων μακρών κυμάτων (long waves), σε στρώματα πάγου. Το κίνητρο της παρούσας εργασίας εντοπίζεται σε συμβάν αποσχισης σώματος πάγου απο το στρωμα Sulzberger στη θάλασσα Ross, έπειτα απο χτύπημα κύματος tsunami που δημιουργήθηκε απο σεισμο του 2011, με επικεντρο το Honshu της Ιαπωνίας. Απο το συμβαν δημιουργήθηκαν δύο νέα παγόβουνα με καταστροφικές συνέπειες για το μέχρι πρότινος ευσταθές στρώμα.

Η μελέτη της δράσης μακρών κυμάτων αφορα εξίσου και τις εφαρμογές των VLFS, καθώς οι πιο συνήθεις κατασκευές με ποντόνια εξυπηρετούν παράκτιες περιοχές όπου και το πλάτος των μακρών κυμάτων αυξάνεται δραματικά.

Στην παρούσα εργασία εξετάζεται η απόκριση πλωτών στρωμάτων ύπο την καταπόνηση μακρών κυμάτων. Για την ανάλυση, επιδιώκεται η μονοδιάστατη σύζευξη του μοντέλου λεπτής, ελαστικής δοκού Euler Bernoulli και των γραμμικοποιημένων εξισώσεων ρηχών υδάτων. Ορίζονται δύο ξεχωριστά προβλήματα. Το πρώτο πρόβλημα αφορά μια πλωτή πλάκα με ένα πακτωμέμο άκρο ενώ το δεύτερο εξετάζει μια ελεύθερη πλωτή πλάκα.

Στη συνέχεια παρουσιάζεται η ανάλυση ευστάθειας της ισχυρής διατύπωσης των δύο προβλήματων και μελετάται η αρχή της διατήρησης της ενέργειας για κάθε σύστημα. Στη συνέχεια, για την επίλυση γίνεται χρήση της μεθόδου των πεπερασμένων στοιχείων. Ειδικά πεπερασμένα στοιχεία κατασκευάζονται με διαφορους πολυωνυμικούς βαθμούς, για την προσεγγιση της λύσης στις περιοχές της υδροελαστικής σύζευξης. Επιπλέον παρατίθεται και η εκτίμηση σφάλματος για την ημι-διακριτή μορφή στο χώρο. Στη συνέχεια η λύση των πεπερασμένων στοιχείων συγκρίνεται με διαφορετική μέθοδο (Sturova 2009) που βασίζεται στην ανάπτυξη της ανύψωσης ελεύθερης επιφάνειας σε ιδιοσυναρτήσεις της δοκού in vacuo.

Τέλος, παρουσιάζονται δύο παραδείγματα για το κάθε ένα απο τα προβλήματα καθώς και το παράδειγμα του στρώματος Sulzberger. Επίσης, δίνονται αποτελέσματα που παρουσιάστηκαν στο European Geosciences Union Assembly 2014, με συμμετοχή της συγγραφέα. Η ανάλυση επιβεβαιώνει την επίδραση του πάχους της πλάκας στη διασπορά του υδροελαστικού κύματος καθώς και στην κατανομή των ροπών και τεμνουσών. Η απόσταση της μέγιστης ροπής φαίνεται να εξαρταται απο το πάχος αλλά όχι απο το μήκος κύματος της καταπόνησης.

Table of Contents

Page intentionally left blank

List of Figures

Summary

It is the scope of this study to examine the hydroelastic interaction between long waves and Very Large Floating Structures (VLFS) or Ice sheets. The conjunction link in the title is based on the similarity found in the response analysis techniques for all thin floating structures, either man-made or of geophysical origin. Six chapters constitute the present thesis.

In **Chapter 1** the motivation and the goals of the present work are given. A brief introduction on ice formations and VLFS is also provided in different sections. Finally a state of the art review in hydroelasticity is provided.

Chapter 2 outlines basic theoretical concepts, essential for the analysis that follows. Serving a complementary role, chapter 2 can be entirely omitted.

In **Chapter 3** the governing equations of the hydroelastic problem for any number of floating bodies over shallow water are presented. In addition, two sub cases of significance for environmental and technological applications are analysed in detail. These cases are the floating cantilever and the single freely floating plate. The corresponding initial boundary value problems, are termed problem Π_1 and problem Π_2 respectively.

In **Chapter 4** the variational formulation of problems Π_1, Π_2 is presented. The principle of energy conservation is examined for all three configurations and finally *a priori* stability estimates for the weak solutions are derived.

In **Chapter 5** the semi-discrete formulation of the aforementioned problems is given along with error estimates. The development of special hydroelastic elements and the finite element method implementation are discussed in subsequent sections of the chapter.

Chapter 6 presents a series of results for selected examples. Discussion of the results, conclusion and future research goals are also included in the chapter.

Page intentionally left blank

CHAPTER 1

Introduction

Adverse climatic trends and modern technological advances in marine engineering have brought the study of large floating bodies under the spotlight. Polar researchers employ hydroelasticity in the study of ice shelf or ice floe dynamic response under ocean wave excitation, while marine engineers engage its principles in Very Large Floating Structures (VLFS) design. In this first chapter, an introduction to both bodies of work is given along with a survey of literature in hydroelasticity. The aims and objectives of the current thesis are given at the end of the chapter.

1.1 Introduction and research motivation

The effects of climate change are bound to influence human activity globally, an issue currently discernible at the Polar Regions.

Polar Regions form a transient terrain, which is not only the ground for commercial human activities, but also the natural habitat of distinct fauna. The climatic effects of the arctic zones are profound. For example, the annual formation and thawing of sea ice, along with its breaking and dispersion due to wave excitation, is a significant mechanism of natural climate control trough melt water circulation and temperature regulation. The scientific attention received by ice self 'disintegration', referring to sudden ice shelf retreat events during extended warm seasons, is indicative of the grave importance of the matter. In such occasions, ice shelves weakened by unusually long summer periods, finally broke off into

the sea. The calving, usually initiated by ocean wave excitation, results in a floating mass of ice with an area often reaching hundreds of square meters, drifting away due to currents and wind loads. Apart from the obvious environmental hazard, caused by ice cap depletion, the floating ice formations are also endangering commercial ship-routes and the presence of off-shore structures.

Hence, it is evident that accurate modelling of ice formations response to external forcing is valuable for future projections. Moreover, as Arctic shipping routes are becoming accessible for longer periods during the year [1], there is a certain monetary end to accurate weather and sea forecasts, for the given region.

Interestingly enough, motivation for the present thesis was found in the 2011 Sulzberger Ice shelf calving event, when the Tsunami succeeding the Honshu earthquake on March 11th, reached the ice shelf and triggered the separation of two large icebergs. At the given incident a total of 125 km^2 of ice was separated from Sulzberger Ice Self, with satellite pictures exposing the effect of events taking place as far as 13000 km away [2].

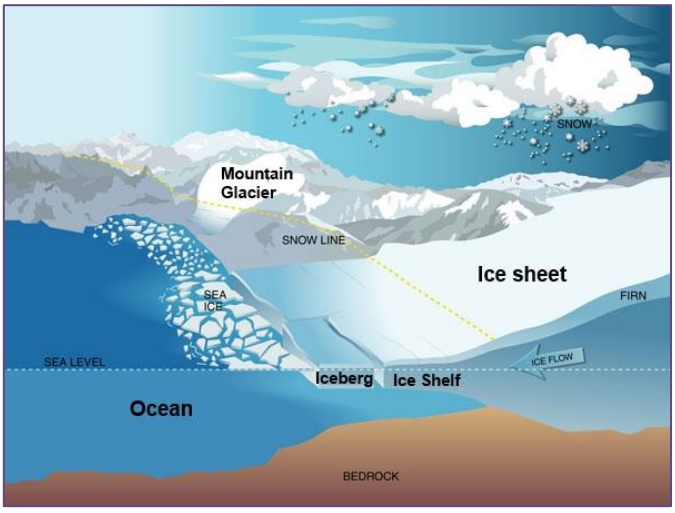

Figure 1 Ice shelf schematic (source: http://earthobservatory.nasa.gov/NaturalHazards)

On a related note, recent advances in marine technology have led to the emergence of Very Large Floating Structures (VLFS). Popular, current applications of VLFS span between floating bridges and oil storage facilities. Between the two areas of polar geophysics and marine engineering, there exists a certain link, the study of hydroelasticity.

Ice floes and floating pontoon type VLFS, as will be discussed later, share certain properties, namely their large length compared to thickness and small flexural rigidity. Due to the above, hydroelastic effects are dominant under water wave excitation and their study preoccupies both bodies of work.

1.2 Sea Ice

Ice physics and sea ice distribution has gathered scientific attention due to its direct association with global climate; large ice caps serve as climate controllers by affecting temperature and ocean current movement. Adding to the above geophysical reasoning behind the study of sea-ice interaction, other human activity related applications should be considered as drives for research. Such examples are the emergency landing and take-off of airplanes [3], ice floe impact with offshore structures and structural integrity of an ice floe when it comes to erecting a temporary base camp for polar expeditions. In the past decade acknowledgement of the adverse effects of climate change has enhanced scientific fervour in the field of ocean wave-ice interaction, as wave trains are bound to become rougher [4], while elevated temperatures weaken ice formations.

(a) **(b)**

Figure 2 (a) Ice floes in the MIZ, **(b)** Ice shelf extending into the ocean

Ice-ocean interaction is manifested through the break-up of pack ice. Calving of glaciers and ice shelves is a phenomenon endorsed by simultaneous processes, the primary factor being ice structure itself, along with local temperature. Tidal effects and wave excitations add to the inherent structural imperfections in the ice body, while oscillatory flexural bending caused by the excitation ultimately leads to the break off of ice shelves or the splitting of ice sheets. The detrimental effects of gravity wave forcing on Antarctic ice shelves, are explored in a recent work by Bromirski and Stephen [5], speculating a direct correlation between sea-level rise and ice shelf dynamics.

Train waves reaching the tip of ice shelves traverse the Marginal ice zone (MIZ), a region covered with ice floes at the boundary of pack ice shoreline and the open ocean induced by

wave action. The ice floe sizes, found in the MIZ, decrease with increasing distance from the ice cap. Thus, the smallest fragments are to be found at the ocean front [6]. The size of the zone itself depends on both seasonal temperature and wave forcing. The waves coming in the MIZ travel finite distances as energy is dissipated through additional floe cracking and scattering. Short waves are scattered at every imperfection found in their path, prone to the irregular geometry of the ice floes. As a result the zone acts as a dampener, shielding the ice shelf from further breaking. This 'buffer' zone suffers due to severe sea ice reduction observed the last decades [7]. As a general rule, less sea ice means that greater sums of wave energy, or simply waves of greater amplitude, reach the ice shelf leading to its disintegration. In addition, the disappearance of sea ice is linked to the rise in frequency of ocean surges. This coupling leads to the mutual catalysis of both phenomena

Finally, it would be useful for the reader to consider that sea ice exhibits a highly complex material behaviour, often a place of disagreement in modelling attempts [51]. Due to the difficulty of access to samples, experimental testing is limited. As a quasi-brittle material, sea ice properties are dominated by the presence of a characteristic length which mandates the derivation of a scaling law in order to connect laboratory testing with the geophysical scales of interest [52]. The engineering properties of sea ice are summarised in a review paper by Timco & Weeks [8], while the reader could benefit from a recent review on the modern multiscale modelling techniques applied to ice deformation behaviour [9].

1.3 Very Large floating Structures (VLFS)

Very large floating structures or VLFS begun as a futuristic vision a couple of decades back, inspired by population densification and the bitter realisation of its harmful impact on both social and environmental grounds.

The population movement towards coastal regions and the subsequent increase in size of coastal cities is well documented, as is the need for proper shoreline protection measures and allowances in order to contain the damage of excessive urbanization [10]. Creating satellite floating structures to accommodate the need for space was considered an appealing alternative to its counterparts, expanding inland and costly land reclamation. The socio-economic drives behind the development of VLFS are thoroughly examined in the work of Wang, Watanabe and Utsunomiya [10].

Away from population relief, the VLFS idea was soon extended to fit military applications, civil infrastructure and industry. Typical examples of VLFS projects include bridges, breakwaters, solar and wind power plants, oil and gas drilling and storage facilities, military bases, emergency bases and industrial space. Notable examples of existing VLFS projects include the 1km long floating test runaway known as the Mega-Float in Tokyo Bay, the floating oil storage bases in Shirashima and Kamigoto islands, the floating Washington bridge in Seattle and the floating piers in Ujina port [11].

(a) **(b)**

Figure 3 Pontoon type VLFS applications (a) *Mega-Float-Tokyo Bay* (b) *floating oil storage base -Kamigoto island* (source: [11])

VLFS are classified under two main categories; semi-submersible and pontoon (or mat-like) type. The above figures (see *figures 3(a) and 3(b))* illustrate pontoon applications exclusively. While the first type facilitates ballast structural elements in order to minimize wave impact and maintain a constant buoyancy force, the latter resembles a plate (or any box-like structure) laying on water surface. The semi-submersible type is suitable for open ocean applications, such as oil and gas platforms, as it can sustain large amplitude wave forcing. The pontoon type, on the other hand is suitable for applications on calm waters, relatively close to the shoreline. When horizontal dimension exceeds 60 meters, the pontoon VLFS is often referred to as Mega-float. In order to shield against harsh seas, a combination of a breakwater system and mooring facility accompanies pontoon type VLFS

Both types have distinct hydrodynamic qualities, namely their large length and small bending rigidity which renders hydroelastic effects dominant. Thus, an elastic plate resting on water surface is an appropriate model for calculating the dynamic response of a mega-float.

1.4 Hydroelasticity : a brief review

Research on sea-ice interaction focuses on both the study of waves passing through the MIZ, sea ice formations and their resultant effect on the ice. Mathematical models are distinguished between those incorporating continuous ice shelves in the form of a constrained infinite or semi-infinite plate, extending into the ocean, and those dealing with solitary floes of finite dimensions, free to move in all directions. The response of solitary ice floes has been studied primarily in the frequency domain under harmonic excitation, while a number of works consider the time-domain response analysis of a compliant raft, thus accounting for irregular wave forcing [4]. Distinct hydrodynamic qualities, namely their large length and small bending rigidity, renders hydroelastic effects dominant when it comes to the study of the dynamic response of ice floes. Hence, ice floes are commonly modelled as floating thin plates with zero or non-zero draft. Some notable contributions in solitary ice floe models include those of Meylan and Squire [13] andAdrianov and Hermans [14] who consider a two-dimensional plate floating over arbitrary depth. Meylan [18] considers an ice floe of arbitrary geometry. While the majority of works are preoccupied with the freely floating ice sheet problem, a recent work of Bhattacharjee and Soares [15] considers the frequency domain problem of a floating semi-infinite plate near a vertical wall. A series of plate edge conditions are examined, including free, fixed and pinned at the vertical wall interface. An analytical solution to the problem of a clamped semi-infinite, homogeneous, elastic plate over flat seabed is presented by Brocklehurst *et al*. [16]. In Tkacheva, a modal expansion technique is performed in order to determine the response of either a free or a fixed, semi-infinite elastic plate over infinite depth [17].

Given recent technological advances in offshore engineering, it is very difficult to ignore the fact that a significant amount of work lends itself well when it comes to hydroelastic analysis of floating bodies. The study of VLFS emerged and evolved in parallel with marine geophysics and as thoroughly depicted by V.A. Squire [19], despite the common ground there has been little effort to unify the fields. Pontoon type VLFS share the same hydrodynamic qualities with ice floes and as a result the methodologies developed for their study bear a great resemblance. The foundation of both fields is set on hydroelasticity, the branch of science concerned with the response of deformable immersed bodies under sea excitation [20]. Applications of hydroelasticity span from ships [21] to VLFS [20], [22], [23], to floating ice bodies [12], [24]. Research on the hydroelastic response of floating bodies is primarily preoccupied with the frequency domain analysis of deformations, a

technique suitable for harmonic wave excitations. In the frequency domain, the methods incorporate either the mode expansion method or mesh methods [12], [14]. Modal expansion is based on the separation between the solid and the fluid part. The elastic deformation is deduced by the superposition of distinct modes of motion, while hydrodynamic forces are treated primarily through the employment of the Green function method or the eigenfunction expansion matching method [20]. Exemplary works in frequency domain analysis employing the modal expansion method are those of Kashiwagi [25], Taylor and Ohkusu [26], Kim and Ertekin [27] and Meylan and Squire [13].

A number of researchers have focused on the time dependant analysis of elastic floating bodies, allowing for irregularities in wave forcing and moving loads. Some of these studies incorporate direct time integration schemes [28], [29] and others employ Fourier transform [30], [31], [32], [33]. Sturova [34] employs a modal expansion technique, with respect to the beam 'dry' modes in order to solve for the transient response of a freely floating body over shallow waters.

Variable bathymetry considerations are also apparent in the literature. Owing to the great length to thickness ratio, both VLFS and ice floes are expected to span over variable bathymetries. While a uniform and flat bottom is a common assumption among researchers, a few attempts have been made to incorporate the real-life topography of the seabed in calculation models. Sun et al [35] consider a sloping seabed while others account for a arbitrary bathymetry [36], [37], [38].

In the literature, attempts have been made to account for irregular waves and non-linear wave effects. These models may refer to tsunami wave impact, storm surges and wave breaking. Masuda *et a.l* [39], [40] considered the effect of a tsunami wave on the response of a plate floating in shallow water. Wen and Shinozuka [41] and Wen [42] also consider tsunami and other as well as wind induced waves in their analysis. Finally, the work of Ohmatsu and Ohta account for irregular waves [32].

For the modelling of the floating body, the Kirchoff thin plate assumption is considered by the majority of studies [25], [27], [44] for both VLFS and ice floes. Thin plate models however are bound to become restrictive and unrealistic in the following decades [19], [11]. Chen [20] explores the shortcomings of linear plate models when incident waves are not normal to the plate and in subsequent works non-linear models like the von-Karman plate are employed [45]. Endo and Yoshida [36] apply the Timoshenko equation theory for a floating body, while a recent article by Hegarty and Squire [47] warns against the

application of the eigenfunction matching method in higher order models due to inherent singularities. The need for the successful incorporation of models accounting for large deflections is phrased in recent reviews [22].

Another focus of interest is in the fact that both ice floes and VLFS are heterogeneous bodies, the former on the grounds of intrinsic imperfections and naturally occurring thickness variations and the latter due to its complex interconnecting parts. Special models have been developed by polar modellers accounting for both inherent cracks [48], [49] and geometrical variations [50].

1.5 Research aim and objectives

The literature review in hydroelacity, revealed that few works have focused on the transient response of floating bodies. Meanwhile, the need to successfully incorporate irregular wave forcing in the analysis is proven essential by documented cases of tsunami induced ice shelf disintegration and harsh seas projections.

The aim of the present thesis is to employ the finite element method in the calculation of the transient response of floating bodies under long wave excitation. The objectives of this work include,

- The mathematical formulation of the general, 1-D hydroelastic problem of a floating body over shallow water regions.
- Derivation and study of the weak form of the aforementioned problem.
- Development of a special hydroelastic element, able to approximate the coupling between the elastic body and the fluid layer.
- Comparison and validation of the finite element solution.
- Examination of several combinations of floating body and bathymetry configurations representing real-life applications.

References

[1] Stephenson, S. R., Smith, R. C. & Agnew J. A. (2011) Divergent long-term trajectories of human access to the Arctic, *Nature Climate Change 1*, p.156-160.

[2] Brunt K. M. *et al.* (2011) Antarctic ice shelf calving triggered by the Honsu (Japan) Earthquake and tsunami, March 2011, *Journal of Glaciology 57(205)*, p. 785-788

[3] Squire, V. A., Hosking, R. J., Kerr, A. D. & Langhorne, P. J. (1996). *Moving Loads on Ice Plates*, Boston and London: Kluwer Academic Press, *ISBN 0-7923-3953-3.*

[4] Bromirski, P. D. , Cayan, D. R. & Flick, R. E. (2005)Wave spectral energy variability in the northeast Pacific, *Journal of Geophysical Research 110,* C03005, (DOI: 10.1029/2004JC002398).

[5] Bromirski, P. D. & Stephen, R. A. (2012) Response of the Ross Ice Shelf, Antarctica, to ocean gravity-wave forcing, *Annals of Glaciology 53(60),* p. 163-172.

[6] Williams, D. T., Bennets, L. G., Squire, V. A., Dumont, D. & Bertino, L. (2013) Wave-ice interactions in the Marginal Ice Zone. Part 1: Theoretical foundations, *Ocean Modelling 71*, p. 81-91.

[7] De la Mare, W. K. (1997) Abrupt mid-twentieth century decline in Antarctic sea ice extent from whaling records, *Nature 389*, p.57-60.

[8] Timco, G. W. & Weeks, W. F. (2010) A review of the engineering properties of sea ice, *Cold Regions Science and Technology 60*, p. 107-129.

[9] Montagmat, M. *et al.*(2014) Multiscale modelling of ice deformation behaviour, *Journal of Structural Geology 61*, p. 78-108.

[10] Wang, C. M., Watanabe, E. & Utsunomiya, T. (eds.) (2008) *Very Large Floating Structures*, New York: Taylor & Francis.

[11] Watanabe, E., Wang, C. M, Utsonomiya T. & Moan. T. (2004) *Very large Floating Structures: Applications, Analysis and Design*, CORE Report No. 2004-02, University of Singapore *(http://www.eng.nus.edu.sg/core).*

[12] Squire, V. A. (2007) Of ocean waves and sea-ice revisited, *Cold Regions Science and Technology 49*, p. 110-133

[13] Meylan, M. H. & Squire, V. A. (1994) The response of ice floes to ocean waves, *Journal of Geophysical Research 99* (C1), 899–900.

[14] Andrianov, A. I., & Hermans, A. J., (2004). Hydroelasticity of elastic circular plate. In: Landrini, M., Campana, E.F., Iafrati, A. (Eds.), *Proceedings 19th International Workshop on Water Waves and Floating Bodies*, Istituto Nazionale Studi ed Esperienze di Architettura Navale, Cortona, Italy.

[15] Bhattacharjee, J. & Guedes Soares C., (2012) Flexural gravity wave over a floating ice sheet near a vertical wall, *Journal of Engineering Mathematics 75*, p. 29-48.

[16] Blocklehurst, P., Korobkin, A. A. & Părău, E. I. (2010) Interaction of hydro- elastic waves with a vertical wall, *Journal of Engineering Mathematics 68*, p. 215-231.

[17] Tkacheva L. A., (2013) Interaction of Surface and flexural gravity waves in ice cover with vertical wall, *Journal of Applied Mechanics and Technical Physics 54*, p. 651-661

[18] Meylan, M. H. (2002) Wave response of an ice floe of arbitrary geometry, *Journal of Geophysical Research 107*, p. 5.1-5.11 (DOI:10.1029/2000JC000713).

[19] Squire, V. A. (2008) Synergies Between VLFS Hydroelasticity and Sea Ice Reasearch, *International Journal of Offshore and Polar Engineering 18 (3)*, p. 1-13.

[20] Chen, X. J., Wu, Y. S., Cui, W. C. & Jensen, J. (2006) Review of Hydroelasticity Theories for Global Response of Marine Structures, *Ocean Engineering (33)*, p. 439–457.

[21] Bishop, R. E. D., Price, W. G, & Wu, Y. (1986) A General Linear Hydroelasticity Theory of Floating Structures Moving in a Seaway, *Philosophical Transactions of the Royal Society A (316)*, No. 1538, p. 375–426.

[22] Watanabe, E., Utsunomiya, T., & Wang, C. M. (2004) Hydroelastic Analysis of Pontoon-type VLFS: A Literature Survey, *Engineering Structures (26)*, p. 245–256.

[23] Ohmatsu, S. (2005) Overview: Research on Wave Loading and Responses of VLFS, *Marine Structures (18)*, p. 149–168.

[24] Squire, V. A., Dugan, J. P., Wadhams, P., Rottier, P. J. & Liu, A. K., (1995) Of ocean waves and sea-ice, *Annual Review of Fluid Mechanics (27)*, p. 115–168.

[25] Kashiwagi M. (1998) A B-spline Galerkin scheme for calculating the hydroelastic response of a very large floating structure waves, *Journal of Marine Science and Technology (3)*, p. 37–49.

[26] EatockT. R., Ohkusu M. (2000) Green functions for hydroelastic analysis of vibrating free-free beams and plates, *Applied Ocean Research (22)*, p. 295–314.

[27] Kim J. W. & Ertekin R. C. (1998) An eigenfunction-expansion method for predicting hydroelastic behaviour of a shallow-draft VLFS :*Proceedings of the 2nd International Conference on Hydroelasticity in Marine Technology,* ed. Kashiwagi M.,Koterayama, W & Ohkusu, M., RIAM, Japan, p. 47-59.

[28] Watanabe, E., & Utsunomiya, T. (1996) Transient response analysis of a VLFS at airplane landing : *Proceedings of the International Workshop on Very Large Floating Structures*, ed. Watanabe, E., Japan, p. 243–247.

[29] Watanabe, E., Utsunomiya, T. & Tanigaki, S. (1998) A transient response analysis of a very large floating structure by finite element method, *JSCE Structural Engineering/Earthquake Engineering (15)*, p. 155s–163s.

[30] Endo, H. (2000) The behaviour of a VLFS and an airplane during takeoff/landing run in wave condition, *Marine Structures (13)*, p. 477–491.

[31] Kashiwagi, M. (2000) A time-domain mode-expansion method for calculating transient elastic responses of a pontoon-type VLFS, *Journal of Marine Science and Technology (5)*, p. 89–100.

[32] Ohmatsu, S. (1998) Numerical calculation of hydroelastic behaviour of VLFS in time domain: *Proceedings of 2nd International Conference on Hydroelastic Marine Technology*, Hawaii, p. 89–97.

[33] Endo, H. & Yago, K. (1999) Time history response of a large floating structure subjected to dynamic load, *Journal of the Society of Naval Architects of Japan 186*, p. 369–376.

[34] Sturova, I. V. (2009) Time-dependent response of a heterogeneous elastic plate floating on shallow water of variable bathymetry, *Journal of Fluid Mechanics (637)*, p. 305-325.

[35] Sun, H., Cui, W. C., Liu, Y. Z. & Liao, S.J., (2003) Hydroelastic response analysis of mat-like VLFS over a plane slope in head seas, *China Ocean Engineering (17)*, p. 315–326.

[36] Utsunomiya, T. & Watanabe, E. (2001) Fast multipole method for hydrodynamic analysis of very large floating structures: Proceedings of the 16th International Workshop on Water Waves and Floating Bodies, Hiroshima, Japan, p. 161–164.

[37] Belibassakis, K. A. & Athanassoulis, G. A. (2005) A Coupledmode Model for the Hydroelastic Analysis of Large Floating Bodies over Variable Bathymetry Regions, *Journal of Fluid Mechanics (531)*, p. 221–249.

[38] Takagi, K. & Kohara, K. (2000) Application of the ray theory to hydroelastic behaviour of VLFS: *Proceedings of The 10th International Offshore Polar Engineerging Conferance*, ISOPE, USA, p. 72–77.

[39] Masuda, K., Ikoma, T., Kobayashi, A. & Uchida, M. (2003) Effect of Tsunami Wave Profile on the Response of a Floating Structure in Swallow Sea: *Proceedings of The 13th (2003) International Offshore and Polar Engineering Conference*, Honolulu, Hawaii, USA

[40] Masuda, K., Miyazaki, T. & Takamura, H., (1998) Study on estimation method for motions and mooring tensions of moored floating structure in offshore area under tsunami: Proceedings of 14th (1998) Ocean Engineering Symposium, p. 161–166.

[41] Wen, Y. K & Shinozuka M. (1972) Analysis of floating plate under oceanwaves. J Waterways, *Harbors Coastal Engineering Division (98)*, ASCE, p. 177–90

[42] Wen, Y. K. (1974) Interaction of ocean waves with floating plate, *Journal of Engineering Mechanics Division (100)*, p. 375-395.

[43] Ohmatsu, S. (1998) Time Domain Analysis of Hydroelastic Behavior of VLFS in Waves, *Journal of the Society of Naval Architects of Japan (184)*, pp. 223-230.

[44] Ohkusu, M. & Namba, Y., (1996) Analysis of hydroelastic behaviour of a large floating platform of thin plate configuration in waves: *Proceedings of the International Workshop on Very Large Floating Structures*, ed. Watanabe, E., Japan, p. 143-148.

[45] Chen, X. J., Jensen, J. J., Cui, W. C. & Fu, S. X. (2003) Hydroelasticity of a floating plate in multidirectional waves, *Ocean Engineering (30)*, p. 1997–2017.

[46] Endo, H. & Yoshida, K. (1998) Timoshenko Equation of Vibration for Plate-Like Floating Structures: *Proceedings of the 2nd International Conference on Hydroelasticity in Marine Technology*, ed. Kashiwagi M., Koterayama, W & Ohkusu, M., RIAM, Japan, p. 255–264.

[47] Hegarty, G. M. & Squire, V. A. (2008) A Boundary Integral Method for the Interaction of Large Amplitude Waves with a Compliant Floating Raft such as a Sea-ice Floe, *Journal of Engineering Mathematics (62)*, p. 355-372

[48] Williams, T. D. & Squire, V. A. (2002) Wave Propagation Across an Oblique Crack in an Ice Sheet, *International Journal of Offshore and Polar Engineering (12)*, p. 157–162.

[49] Porter, R, & Evans, D. V. (2006) Scattering of Flexural Waves by Multiple Narrow Cracks in Ice Sheets Floating on Water, *Wave Motion (43)*, p. 425–443.

[50] Williams, T. D. & Squire, V. A. (2006) Scattering of Flexural gravity Waves at the Boundaries between Three Floating Sheets with Applications, *Journal of Fluid Mechanics (569)*, p. 113–140.

[51] Dempsey, J. P, Adamson, R. M. & Mulmule, S. V. (1999) Scale effects on the in-situ tensile strength and fracture of ice. Part II: First–year Sea ice at resolute, N. W. T., *International Journal of Fracture (95)*, p. 347-366.

[52] Bažant, Z. P. (2005) *Scaling of Structural Strength*, Oxford: Elsevier Butterworth-Heinemann.

CHAPTER 2

Theoretical Background

Shallow water theory, the study of long waves and the propagation of waves in elastic media constitute an essential foundation for the analysis in the following chapters of the present work. The sections below do not provide a full account of the topics but rather a brief introduction, drawing attention to significant notions that will be touched upon in the analysis and modelling of hydroelastic problems.

2.1 Shallow water theory

The swallow-water model is a simplistic geophysical model accounting for gravity wave propagation in swallow depth, extremely useful in coastal engineering. The theory is derived under the assumption that the horizontal length scale is significantly greater than the vertical one, which is the case for tidal waves and tsunamis. Swallow water theory is considered valid over regions, where $kh < 10^{-1}\pi$ with k being the wave number and h the water depth, holds for wave propagation.

A basic derivation of the swallow water equations is presented below (*see also* figure 4). Initially, the following 2-D boundary value problem is defined.

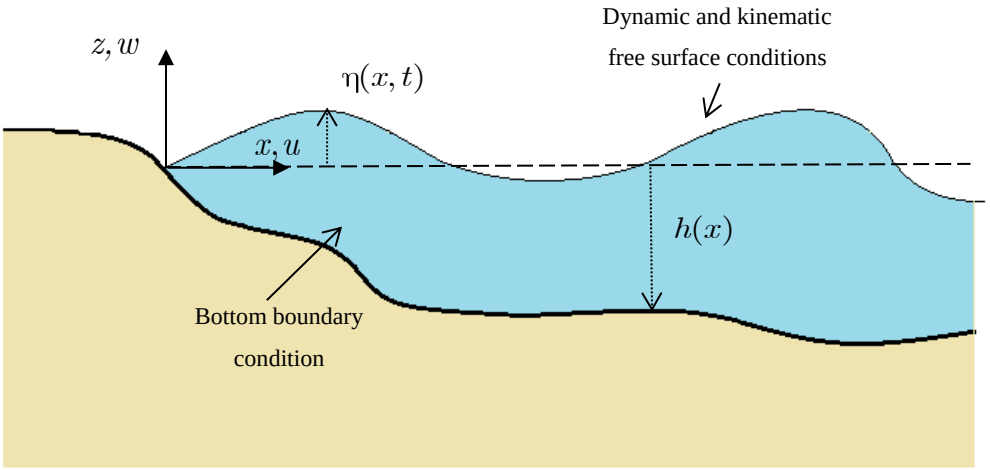

Figure 4 General vertical 2-D configuration

For the fluid region depicted above the mass continuity equation holds, hence

$$\frac{1}{\rho}\frac{D\rho}{Dt}+\frac{\partial u}{\partial x}+\frac{\partial w}{\partial z}=0, \tag{2.1}$$

where $\frac{D}{Dt}\bullet$ is the total derivative with respect to time, ρ is the fluid density and u,w are the fluid velocity components as shown in the figure above.

Now, by use of the common incompressibility assumption for water, equation (2.1) is reduced to,

$$\nabla\cdot\mathbf{u}=0.$$

By incorporating the additional assumption of fluid irrotationality and introducing the scalar velocity potential function, the Laplace equation is satisfied within the fluid region,

$$\nabla^2\varphi=0. \tag{2.2}$$

In order to complete the formulation of the problem, the governing equation defined above needs to be complimented by certain physical conditions at the boundaries or interfaces. The velocity components need to satisfy certain kinematic conditions at any fluid boundary. Based on the straightforward assumption that no particle cross over (flow) should exist between the fluid region and any given interface (in order for the interface to exist), kinematic conditions are expressed as $Df(x,z,t)/Dt=0$, where $f\left(x,z,t\right)=0$ is the surface equation.

The free water surface is described by $f(x,z,t) = z - \eta(x,t)$, with $\eta(x,t)$ being the water surface displacement. Hence applying the kinematic condition at $z = \eta(x,t)$ results in,

$$\partial_t \eta + u\Big|_{z=\eta} \partial_x \eta - w\Big|_{z=\eta} = 0\,. \tag{2.3}$$

Similarly, at the fixed bottom ($z = -h(x)$, see fig. 4), where the surface is given by $f(x,z) = z + h(x)$, the kinematic condition at, becomes

$$u\Big|_{z=-h} \partial_x h + w\Big|_{z=-h} = 0. \tag{2.4}$$

In addition to the boundary conditions (2.3) and (2.4) another physical restriction is posed in the free water surface stemming from its inability to sustain pressure variations. Hence at $z = \eta(x,t)$ the linearised Bernoulli equation provides the necessary dynamic condition,

$$-\partial_t \varphi + (P - P_{atm}) / \rho_w + g\eta = 0 \tag{2.5}$$

where P_{atm} is the atmospheric pressure, g is the acceleration of gravity and ρ_w is the water density. At the free water surface $P_{atm} = P$ and the pressure term is omitted from the dynamic condition (2.5.) .

Based on the 2-D problem posed, a few reasonable assumptions lead to shallow water theory or long wave theory.

Derivation of the non-linear water theory begins by integrating equation (2.1) over depth,

$$\int_{-h}^{\eta} \partial_x u dz + w\Big|_{z=\eta} - w\Big|_{z=-h} = 0\,. \tag{2.6}$$

Substituting (2.3) and (2.4) into (2.6) the following is derived

$$\left(\int_{-h}^{\eta} u dz\right)_x = -\partial_t \eta. \tag{2.7}$$

It must be noted that up to equation (2.7), the mathematical manipulations carry no assumptions. In Swallow water theory the primary assumption is that the vertical acceleration of the fluid particles is negligible and has no effect on pressure, or equivalently that the pressure is given solely by its hydrostatic component $p = g\rho(\eta - z)$. By differentiating with respect to x, it can be immediately observed that $\partial_x p = g\rho\partial_x \eta$ is independent of z. Hence horizontal acceleration is also independent of z, as is the horizontal velocity, which is now considered uniform. Hence the Euler equation of motion is reduced to the following form,

$$\partial_t u + u\partial_x u = -g\partial_x \eta . \tag{2.8}$$

Now returning to the derived relation (2.7), the integral calculation can be performed in view of the vertical component independency as,

$$\partial_x \left[u \ \eta + h \ \right] = -\partial_t \eta . \tag{2.9}$$

Equations (2.8) and (2.9) constitute the two dimensional, non-linear shallow water equations. Neglecting non-linear terms, thus implicitly considering small surface displacements and velocities, the system is reduced to the following form,

$$\partial_t u = -g\partial_x \eta \tag{2.10}$$

$$\partial_x \left(uh \right) = -\partial_t \eta \tag{2.11}$$

By eliminating η from the above system the resulting equation is given as,

$$\partial_{tt} u = g\partial_{xx} \left(uh \right) \tag{2.12}$$

Equation (2.12) can finally be rewritten in terms of the velocity potential as,

$$\partial_{tt} \varphi = g\partial_x \left(h\partial_x \varphi \right) \tag{2.13}$$

Systems (2.8)-(2.9) and (2.10)-(2.11) can be alternatively derived from the swallow water asymptotic forms of the hyperbolic functions that appear in the velocity potential and surface displacement equations for the propagating wave in 2-D. For a more in depth analysis refer to the work of Stoker [2].

2.2 Long Waves

Water waves propagating in swallow water are often referred to as long waves, typically with a wavelength several times larger than water depth, $(h < 20^{-1} L)$. The study of the transformations undergone by these waves while approaching the shore, are essential to coastal engineering design.

The following analysis presents some key results in the study of progressive waves approaching shallow waters.

As their amplitude decreases progressive waves can be considered sinusoid. After solving the velocity potential problem described by (2.2), modifying boundary conditions (2.3),

(2.4) and (2.5) for a constant bathymetry h, and assuming a periodic lateral boundary condition the vertical displacement of the free water surface is given by :

$$\eta(x,t) = \frac{H}{2}\cos(kx - \omega t) \ . \tag{2.14}$$

Where ω is the angular velocity of the progressive wave, defined as $\omega = 2\pi / T$, k is the wave number, defined as $2\pi / L$, H is the vertical distance from crest to trough and L is the wavelength. The velocity potential is given as:

$$\Phi = -\frac{\mathrm{H}}{2\omega} g \frac{\cosh k(h+z)}{\cosh kh}\sin(kx - \omega t). \tag{2.15}$$

The horizontal and vertical particle velocities derived from eq. (2.14) are given by :

$$u = \frac{H}{2\omega} gk \frac{\cosh k(h+z)}{\cosh kh}\cos(kx - \omega t), \tag{2.16}$$

$$w = \frac{H}{2\omega} gk \frac{\sinh k(h+z)}{\cosh kh}\sin(kx - \omega t). \tag{2.17}$$

Finally the dispersion relation is given as :

$$\omega^2 = gk \tan kh \tag{2.18}$$

As previously stated, in shallow water theory, it holds that $kh < 10^{-1}\pi$, hence equations (2.15)-(2.17) can be adapted for small kh in the following sense:

$$u_s = \frac{H}{2\omega} gk \cos(kx - \omega t), \tag{2.19}$$

$$w_s = \sin(kx - \omega t)\left(\frac{H}{2\omega} gk^2 h + \frac{gHkz}{2\omega}\right), \tag{2.20}$$

$$\omega_s^2 = gk^2 h. \tag{2.21}$$

The wave celerity defined as the ratio $C = \omega / k$ is given from (2.21) as

$$C = \sqrt{gh}. \tag{2.22}$$

Equation (2.21) shows that celerity, the velocity of the propagating wave does not depend on the surface elevation. For more information on the engineering properties of long waves the reader is referred to [1].

2.3 Flexural wave propagation in elastic media

In this section, a brief review will be given on the propagation of transverse waves in elastic systems. The reader will be given a strength-of-materials viewpoint regarding the engineering models examined and the dispersion characteristics of the corresponding waves . A more in depth analysis can be found in [3] and [4].

2.3.1 Euler-Bernoulli beam theory

Before detailing the specifics of the theory, assumptions must be explicitly stated for clarity. The reader unfamiliar with the classical beam theory must note that the material is assumed linear, elastic and under the small deformations assertion. A prismatic bar is considered with a vertical symmetry in its cross section. Transverse loads are assumed to act on the xz plane only, while the normal remain straight and perpendicular to the centroidal axis after deformation (*see* figure *5*).

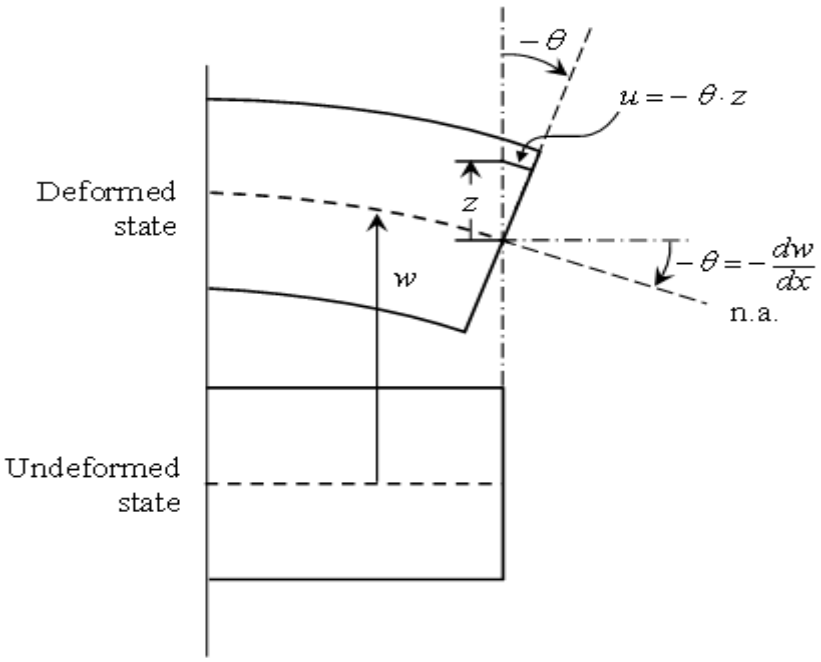

Figure 5 Schematic diagram of beam in bending

The kinematic conditions of the theory ensure that the cross sections are infinitely rigid in their plane and remain plane after bending. The angle of rotation of a cross section is given by $\theta = dw / dx$, while the horizontal displacement $u = -z\theta$,due to the small deformation consideration mentioned earlier, $w = w(x)$.

Hence it can be easily derived that ,

$$\varepsilon_{xx} = -\partial_x \left(z \partial_x w \right) = -z \partial_{xx} w \ , \tag{2.23}$$

$$\sigma_{xx} = -Ez \partial_{xx} w \ , \tag{2.24}$$

$$M = -\int_A \sigma_{xx} z dA = EI \partial_{xx} w, \tag{2.25}$$

Where M is the bending moment and $I_x = \int_A z^2 dA$ is the moment of inertia for a given plane. From the equation of motion in the vertical direction,

$$\partial_x V = q(x,t) - \rho A \partial_{tt} w \, , \tag{2.26}$$

where ρ is the density. Since it holds that $\partial_{xx} M = \partial_x V$, from moment equilibrium, the dynamic Euler-Bernoulli beam equation is derived,

$$\partial_{xx} \left(EI \partial_{xx} w \right) + \rho A \partial_{tt} w = q(x,t) \, . \tag{2.27}$$

At this point it must be noted that material and geometrical homogeneity are not mathematical restrictions in the Euler-Bernoulli theory. Hence, beam cross section and material properties may be allowed to vary longitudinally. On the contrary, the small deflections assumption is imperative for the derivation of (2.27). The linear normal and shear stress distributions for a thin, elastic beam is shown in figure 6.

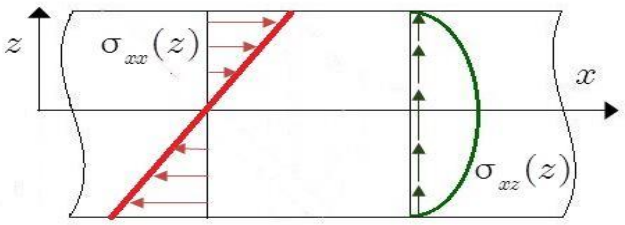

Figure 6 Normal and Shear Stress distributions within a thin elastic beam

For a freely vibrating, homogeneous, elastic beam of uniform cross section, equation (2.27) becomes,

$$\partial_{xxxx} w + \frac{1}{a^2} \partial_{tt} w = 0 \tag{2.28}$$

where $a^2 = \dfrac{EI}{\rho A}$

In order to investigate the dispersive characteristics of the elastic wave within the beam, a harmonic wave of the form $w(x,t) = Ae^{i(kx-\omega t)}$ is assumed to be the solution of equation (2.28), where A is the wave amplitude. After substitutions,

$$k^4 - \frac{\omega^2}{a^2} = 0 \quad \text{or} \quad \omega(k) = \pm\frac{4a\pi^2}{\lambda^2} \tag{2.29}$$

The dispersion relation (2.30) is used for the determination of the phase velocity $c = \frac{\omega(k)}{k} = \pm\frac{2\pi a}{\lambda}$ and the group velocity $c_g = \frac{\partial\omega}{\partial k} = \pm 2ak$. The group velocity is twice the phase velocity.

References

[1] Dean R. G. and Dalrymple R. A. (1991) *Water wave mechanics for engineers and scientists*, Singapore: World scientific Publishing Co.

[2] Stoker J. J. (1957) *Water Waves: The mathematical Theory with Applications*, New York: Wiley-Interscience.

[3] Fung Y. C and Pin Tong (2001) *Classical and Computational Solid Mechanics*, World Scientific Publishing Co.

[4] Graff K. F. (1975) *Wave motion in Elastic Solids*, Oxford: Clarendon Press.

CHAPTER 3

Hydroelasticity: Governing Equations

The governing equations for the general 2-D hydroelastic problem of a thin floating plate are presented. Due to the small amplitude, long wave, forcing assumption, the linear shallow water hydroelastic equations are employed. In addition, the Euler-Bernoulli beam theory is used for the determination of the thin floating structure deflection field and the corresponding bending moment and shear force. Several configurations corresponding to different hydroelastic problems are analysed. Among them, of most importance are the freely floating plate, simulating the response of VLFS and ice floes and the floating cantilever, more appropriate for the analysis of long wave – ice shelf interactions.

3.1 Mathematical formulation of the general hydroelastic problem

This introductory section is aimed to present the 2D problem of hydroelastic interaction between linear water waves of arbitrary wavelength and thin floating flexural strips. The configuration to be considered includes a floating cantilever and a freely floating plate as well. The corresponding initial boundary value problem in the xz plane is shown in the schematic below, (figure 7). Assuming a two dimensional coordinate system, the x-axis spans horizontally while the z-axis spans vertically upwards. The fixed end is placed at $x = 0$ and the free, undisturbed water surface lays over $0 < x < \infty$, $z = 0$. The plates span horizontally along $0 < x < \infty$, where L_1 and L_2 are their lengths. The plates may be of

variable thickness described by the functions $\tau_1(x)$ and $\tau_2(x)$. Additionally the plates are assumed to extend infinitely in the y- direction (perpendicular to the page). The undisturbed, fluid of density ρ_w, is enclosed within the domain $\Omega: 0 < x < \infty$, $-H(x) < z < 0$, where $H(x)$ depicts the variable bathymetry of the problem .The fluid is assumed to be inviscid, incompressible and restrained by an impermeable seabed.

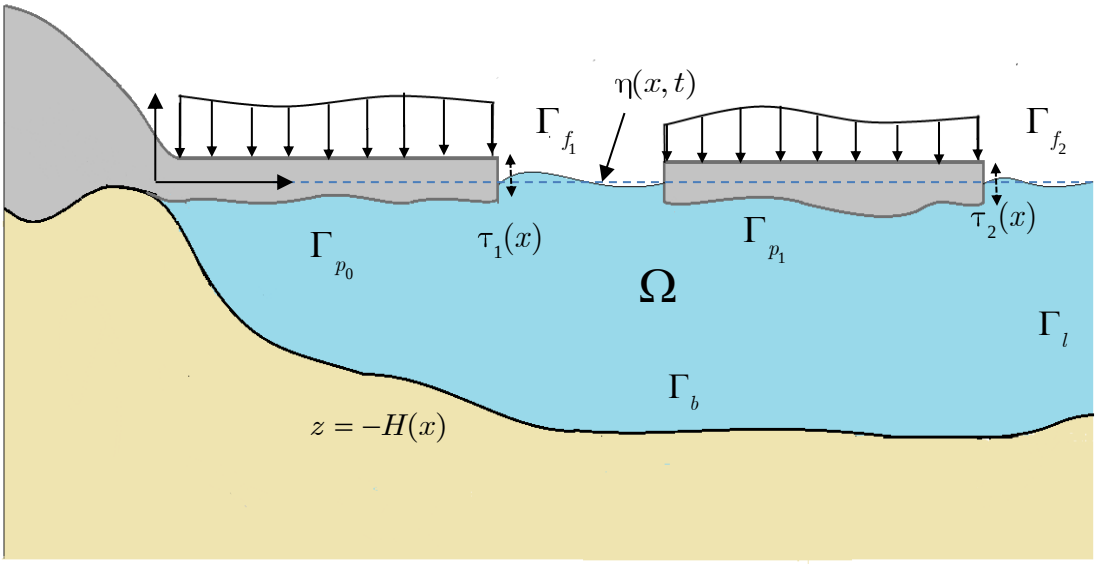

Figure 7 Schematic of the general 2-D hydroelastic problem

The velocity potential defined for the fluid region $\varphi(x,z,t)$, satisfies the Laplace equation,

$$\nabla^2\varphi = 0 \text{ in } \Omega. \tag{3.1}$$

At the seabed, the impermeable bottom assumption results to the following condition,

$$\nabla\varphi \cdot \mathbf{n} = 0 \text{ on } \Gamma_b, \tag{3.2}$$

where $\mathbf{n}$ is the outer vertical vector on the boundary.

The following dynamic condition is valid for the free water surface after setting in equation (2.5), $P = P_{atm}$ and differentiating with respect to time,

$$\partial_{tt}\varphi + g\partial_z\varphi = 0 \text{ on } \Gamma_{f_1} \text{ and } \Gamma_{f_2} \tag{3.3}$$

As the plate is considered thin compared to its length scale, the Euler-Bernoulli beam theory is adopted. Hence, at the plate boundary, the pressure exerted by the floating body prescribes the following condition,

$$m(x)\partial_{tt}\eta + \partial_{xx}(D(x)\partial_{xx}\eta) = q_i(x,t) + p_i - P_{atm} \quad \text{on } \Gamma_{p_i}, \text{ for } i = 0,1 \tag{3.4}$$

,where $m(x) = \rho_p \tau_i(x)$ is the mass per unit length , with ρ_p being the plate density,

while $D(x) = \dfrac{E\tau_i^3(x)}{12(1-\nu^2)}$ is the flexural rigidity of the plates , $q_i(x,t)$ is the vertical variable load on the plates, $\eta(x,t)$ is the free water surface elevation which coincides with the beam deflection and p is the pressure on the fluid (*see* [3]). At the lateral boundary, the velocity potential is assumed to vanish, hence

$$\partial_x \varphi = 0 \ \left(x \to \infty\right) \text{on } \Gamma_l . \tag{3.5}$$

The initial excitation is given by a free water surface disturbance caused by an incoming waveform, described as

$$\eta(x,0) = \eta_0(x), \tag{3.6}$$

It is obvious that the above formulation of the potential BVP can be trivially extended in order to accommodate the presence of multiple freely floating plates.

3.2 The Shallow Water Approximation

In this section, the general one dimensional hydroelastic problem of a floating plate over shallow water will be formulated. Three reductions of the general configuration given will also be formulated.

3.2.1 Multi-body configuration

Since long wave forcing is the subject of the present analysis, the shallow water approximation can be employed in order to achieve a reduction of the above problem, subject to realistic physical constraints. The linear shallow water equations are coupled with the dynamic equation of the plate, constructing a one-dimensional system in the domain $\mathbb{R}_0^+$. The general problem will be initially formulated for N number of freely floating plates (in series). The problems that will be considered next are immediate reduction of the general problem.

The hydroelastic coupling takes place at the regions Ω_{2n}, while the linearised shallow water equations reduce to the wave equation in Ω_{2n+1}, for $n = 0,1,\ldots N$. The lengths of the one-dimensional domains are denoted as L_n, where $n = 1,\ldots N$. Hence it holds that,

$$\Omega_0 \equiv \left(0, L_1\right),\ \Omega_1 \equiv \left(L_1, L_1 + L_2\right),$$

$$\Omega_{2n} \equiv \left(\sum_{k=0}^{n-1} L_{2k+1} + \sum_{k=1}^{n} L_{2k}, \sum_{k=0}^{n} L_{2k+1} + \sum_{k=1}^{n} L_{2k},\right),$$

$$\Omega_{2n+1} \equiv \left(\sum_{k=0}^{n} L_{2k+1} + \sum_{k=1}^{n} L_{2k}, \sum_{k=0}^{n} L_{2k+1} + \sum_{k=1}^{n+1} L_{2k},\right), \text{ for } n = 1,2\ldots N.$$

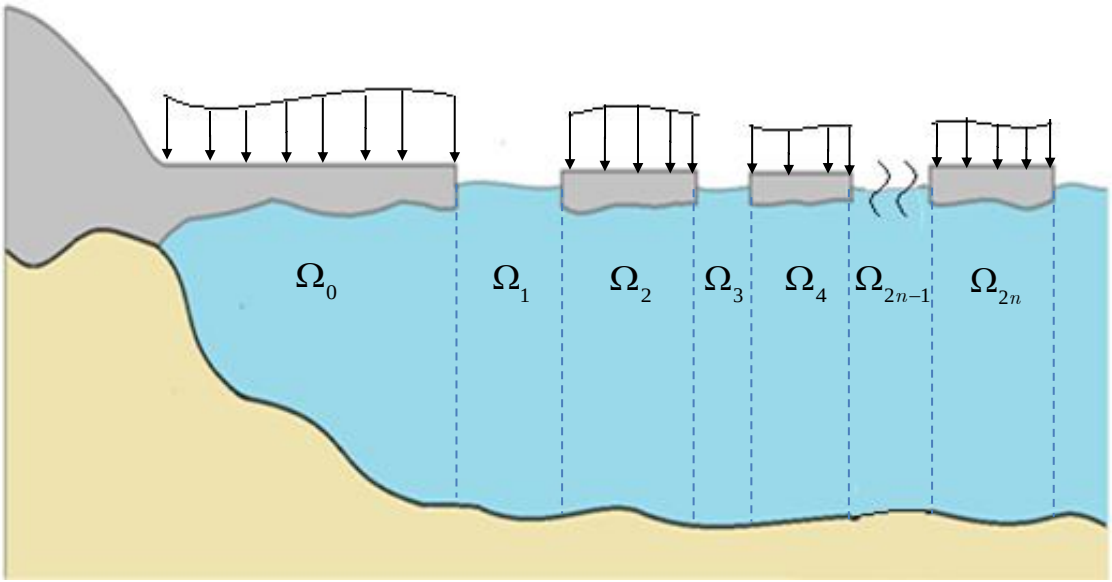

Figure 8 Schematic diagram of the reduced shallow water, hydroelastic problem

Accounting for the plate draft in the regions of the hydroelastic coupling, the following bathymetry function is defined,

$$b(x) = \begin{cases} H(x) - d_{2n}(x), & in \quad \Omega_{2n} \\ H(x), & in \quad \Omega_{2n+1} \end{cases}, \text{ for } n = 0,1,2,\ldots N \tag{3.7}$$

Where, according to the Archimedes principle, the variable plate draft is

$$d_{2n}(x) = \frac{\rho_p}{\rho_w} \tau_{2n}(x) \quad \text{(see also [1] and [2])} \tag{3.8}$$

Hence again for $n = 0,1,\ldots N$ it holds that,

$$m(x)\partial_{tt}\eta_{2n} + \partial_{xx}(D(x)\partial_{xx}\eta_{2n}) + \rho_w g\eta_{2n} + \rho_w \partial_t \varphi_{2n} = q_{2n}(x,t) \text{ in } \Omega_{2n} \times \left(0, \mathrm{T}\right], \tag{3.9}$$

$$\partial_t \eta_{2n} + \partial_x(b(x)\partial_x \varphi_{2n}) = 0 \text{ in } \Omega_{2n} \times \left(0, T\right], \tag{3.10}$$

$$\partial_{tt}\varphi_{2n+1} - g\partial_x(b(x)\partial_x \varphi_{2n+1}) = 0 \text{ in } \Omega_{2n+1} \times \left(0, T\right]. \tag{3.11}$$

The velocity potentials φ_{2n} correspond to the fluid under the plates, at the regions of the hydroelastic coupling, while φ_{2n+1} with the rest of the fluid domain. Similarly, η_{2n} is the water surface elevation that coincides with plate deflection at the corresponding regions while η_{2n+1} is the free surface water elevation.

It must be noted that for the free fluid regions the upper surface elevation and the velocity potential are linked through the following relation, due to the validity of equation (2.12) under shallow water assumptions,

$$\eta_{2n+1} = -g^{-1}\partial_t \varphi_{2n+1} \tag{3.12}$$

At the fixed boundary $(x = 0)$ the condition for the velocity potential corresponds to an impermeable boundary and is

$$\partial_x \varphi_0(0,t) = 0, \tag{3.13}$$

Additionally, as the one plate is considered fixed on one edge, the condition for the free surface elevation that coincides with plate deflection becomes,

$$\eta_0(0,t) = \partial_x \eta_0(0,t) = 0. \tag{3.14}$$

At the free edges of the plates $(x_j = \sum_{k=1}^{j} L_k), j = 1, 2, \ldots N+1$, the conditions of zero bending moment, denoted by m_{b2n} and zero shear force denoted by f_{s2n}, are given by,

$$m_{b2n}(x_j,t) = f_{s2n}(x_j,t) = 0. \tag{3.15}$$

Moreover, the conditions of pressure and mass continuity for the fluid at the same free edges, prescribe that (*see also* [1], [2])

$$\varphi_{2n}(x_j^-,t) = \varphi_{2n+1}(x_j^+,t),\ b(x_j^-)\partial_x \varphi_{2n} = b(x_j^+)\partial_x \varphi_{2n+1}. \tag{3.16}$$

At initial time $t = 0$, the plates are considered to be at rest while and incoming long wave is generated as a free surface elevation $s(x)$ in domain Ω_{2N+1}. The appropriate initial conditions read,

$$\eta_{2n}(x,0) = \partial_t \eta_{2n}(x,0) = \varphi_{2n}(x,0) = 0 \ \text{ in } \Omega_{2n}, \tag{3.17}$$

$$\varphi_{2n+1}(x,0) = 0, \ \ \partial_t \varphi_{2n+1}(x,0) = 0 \ \text{ in } \Omega_{2n+1} \text{ for } n = 0,1,..N-1, \tag{3.18}$$

$$\varphi_{2N+1}(x,0) = 0, \ \ \partial_t \varphi_{2N+1}(x,0) = -gs(x), \text{ in } \Omega_{2n+1} \text{ for } n = N. \tag{3.19}$$

The reduced one-dimensional system (3.9)-(3.11) with the boundary, interface and initial conditions (3.13)-(3.19), is a valid equivalent of the two-dimensional, potential IBVP described by (3.1)-(3.6) for incoming waves of considerable larger length compared to depth.

Using a characteristic length L_c, we introduce the non-dimensional variables:

$$\tilde{x} = L_c^{-1} x, \ \tilde{t} = g^{1/2} L_c^{-1/2} t,$$

$$\tilde{\eta}_{2n} = L_c^{-1} \eta_{2n}, \ \tilde{\varphi}_{2n+1} = g^{-1/2} L_c^{-3/2} \varphi_{2n+1} \text{ and } Q_{2n} = (\rho_w g L_c)^{-1} q_{2n}(x,t).$$

After dropping tildes, eq. (3.9)-(3.11) are re-written in non-dimensional form as

$$M_{2n}(x)\partial_{tt}\eta_{2n} + \partial_{xx}(K_{2n}(x)\partial_{xx}\eta_{2n}) + \eta_{2n} + \partial_t \varphi_{2n} = Q_{2n}(x,t) \ , \ \text{ in } \Omega_{2n} \times (0,T] \tag{3.20}$$

$$\partial_t \eta_{2n} + \partial_x (B(x)\partial_x \varphi_{2n}) = 0 \text{ , in } \Omega_{2n} \times (0,T] \tag{3.21}$$

$$\partial_{tt}\varphi_{2n+1} - \partial_x (B(x)\partial_x \varphi_{2n+1}) = 0 \text{ , in } \mathbb{R}^+ \times (0,T] \tag{3.22}$$

where $M_{2n}(x) = m_{2n}(x) \ (\rho_w L_c)^{-1}, K_{2n}(x) = D_{2n}(x) \ (\rho_w g L_c^4)^{-1}, \ B(x) = b(x) L_c^{-1}$.

The non-dimensional bending moment and shear force are given in the non-unifrom thickness case as,

$$M_b(x,t) = K\partial_{xx}\eta \ \text{ and} \tag{3.23}$$

$$V(x,t) = \partial_x (K\partial_{xx}\eta) \tag{3.24}$$

Hence the boundary conditions (3.13)-(3.14) are expressed in nondimensional form as,

$$\partial_x \varphi_0(0,t) = 0, \tag{3.25}$$

$$\eta_0(0,t) = \partial_x \eta_0(0,t) = 0, \tag{3.26}$$

$$M_{b2n}(L_c^{-1}x_j, t) = V_{2n}(L_c^{-1}x_j, t) = 0. \tag{3.27}$$

,while the interface conditions are,

$$B(L_c^{-1}x_j^{-})\partial_x \varphi_{2n}(L_c^{-1}x_j^{-}, t) = B(L_c^{-1}x_j^{+})\partial_x \varphi_{2n+1}(L_c^{-1}x_j^{+}, t), \tag{3.28}$$

$$\partial_t \varphi_{2n}(L_c^{-1}x_j^{-}, t) = \partial_t \varphi_{2n+1}(L_c^{-1}x_j^{+}, t). \tag{3.29}$$

The initial conditions become,

$$\eta_{2n}(x,0) = \varphi_{2n}(x,0) = 0, \text{ in } \Omega_{2n} \tag{3.30}$$

$$\partial_x \varphi_{2n+1}(x,0) = 0, \;\; \partial_t \varphi_{2n+1}(x,0) = 0, \text{ in } \Omega_{2n+1} \text{ for } \; n = 0,1,..N-1 \tag{3.31}$$

$$\partial_x \varphi_{2n+1}(x,0) = 0, \;\; \partial_t \varphi_{2n+1}(x,0) = 0, \text{ in } \Omega_{2N+1}, \tag{3.32}$$

where $S(x) = L_c^{-1} s(x)$.

The non-dimensional IBVP is considered in the following sections describing the method of solution and results.

3.2.2 Problem Π_1 (cantilever)

Considering the aforementioned general case, it is possible to formulate an IBV problem that features a floating cantilever, extending into the ocean. This model may be used for the simulation of the hydroelastic response of ice shelf under long wave An application of this model in geophysics is found, in the study of the hydroelastic response of ice shelves under long wave excitation. Same analysis could be followed in the study of the dynamic response of a partially fixed pontoon type VLFS over shallow water.

The hydroelastic coupling takes place only in region $\Omega_0 \equiv (0, L)$. The free surface fluid occupies the domain $\Omega_2 \equiv (L, +\infty)$. The bathymetry function now has the form

$$b(x) = \begin{cases} H(x) - d(x), & in \;\; \Omega_0 \\ H(x), & in \;\; \Omega_2 \end{cases} \tag{3.33}$$

where the draft of the plate is given by,

$$d = \rho_p \rho_w^{-1} \tau(x) \ . \tag{3.34}$$

.

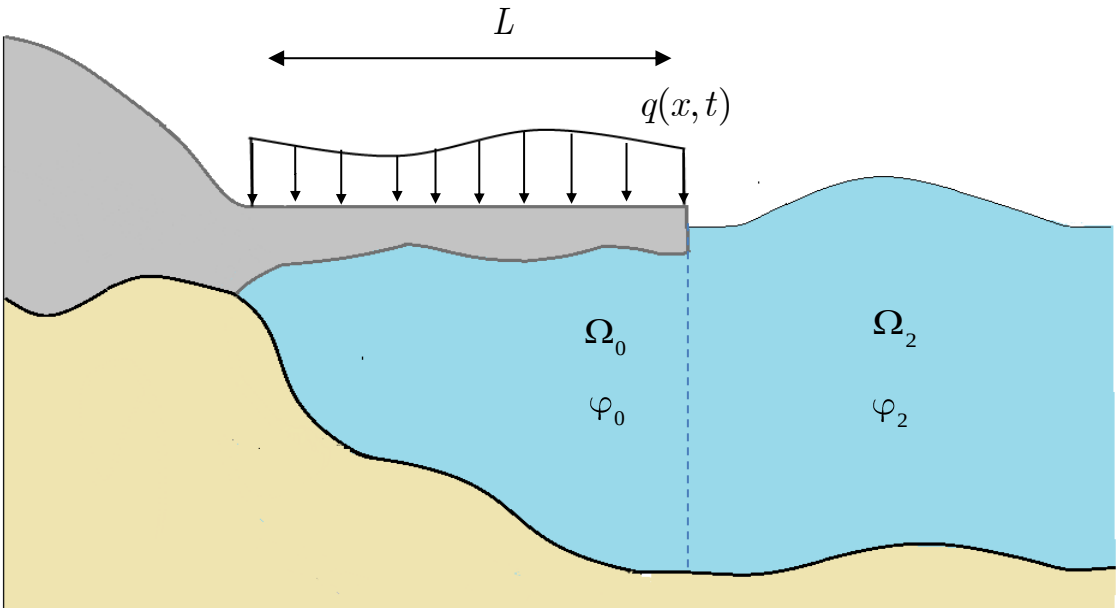

Figure 9 Schematic diagram of problem Π_1

It must be noted that the floating cantilever is assumed to be of great length, so that in regions away from the vicinity of the fixed end, the floating of the beam is characterized by the draft described in equation (3.34).

The resulting non-dimensional system of equations reads,

$$M(x)\partial_{tt}\eta + \partial_{xx}(K(x)\partial_{xx}\eta) + \eta + \partial_t \varphi_0 = Q(x,t) \ \text{ in } \Omega_0 \times (0,T], \tag{3.35}$$

$$\partial_t \eta + \partial_x (B(x)\partial_x \varphi_0) = 0 \ \text{ in } \Omega_0 \times (0,T], \tag{3.36}$$

$$\partial_{tt}\varphi_2 - \partial_x (B(x)\partial_x \varphi_2) = 0 \ \text{ in } \Omega_2 \times (0,T]. \tag{3.37}$$

The boundary conditions at the edges of the plate are expressed as,

$$\eta(0,t) = \partial_x \eta(0,t) = 0, \tag{3.38}$$

$$M_b(L_c^{-1}L,t) = V(L_c^{-1}L,t) = 0. \tag{3.39}$$

The interface conditions now become,

$$B(L_c^{-1}L^-)\partial_x \varphi_0(L_c^{-1}L^-,t) = B(L_c^{-1}L^+)\partial_x \varphi_2(L_c^{-1}L^+,t), \tag{3.40}$$

$$\partial_t \varphi_0(L_c^{-1}L^-,t) = \partial_t \varphi_2(L_c^{-1}L^+,t). \tag{3.41}$$

At initial time, the plate and the fluid of region Ω_0 are considered to be at rest

$$\eta(x,0) = \partial_t \eta(x,0) = \partial_x \varphi_0(x,0) = 0 \quad \text{in} \Omega_0 , \tag{3.42}$$

$$\partial_x \varphi_2(x,0) = 0, \quad \partial_t \varphi_2(x,0) = -S(x) \text{ in } \Omega_2 . \tag{3.43}$$

3.2.3 Problem Π_2 (freely floating)

By following the same line of work, the problem of the freely-floating plate, approximating the case of an unconstrained VLFS or ice floe, can be formulated. Again, the hydroelastic coupling takes place in the domain $\Omega_0 \equiv (0, L)$ alone, (*see* figure (10)) while the wave equation under the assumptions described previously is defined in the regions $\Omega_1 \equiv (-\infty, 0)$ and $\Omega_2 \equiv (L, +\infty)$. The bathymetry is given by,

$$b(x) = \begin{cases} H(x), & in \quad \Omega_1 \\ H(x) - d(x), & in \quad \Omega_0 \\ H(x), & in \quad \Omega_2 \end{cases} \tag{3.44}$$

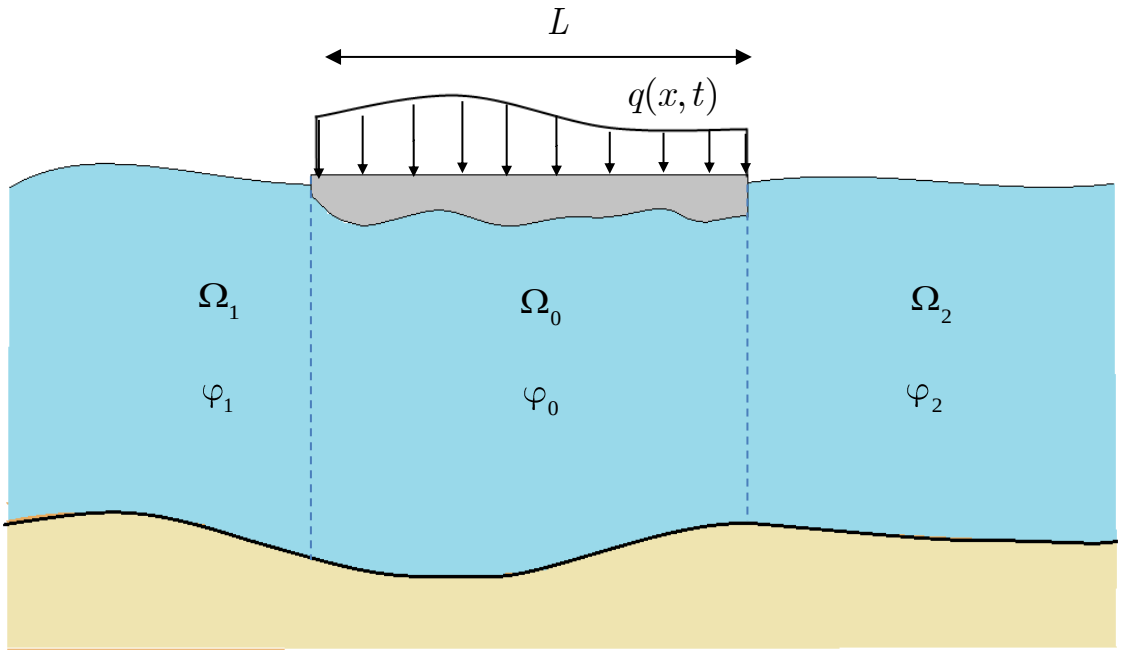

Figure 10 Scematic diagram of Problem Π_2

The plate draft is derived by the expression shown above. The resulting non-dimensional system of equations for the problem of a freely floating heterogeneous, thin, elastic plate over variable shallow water bathymetry reduces to,

$$\partial_{tt}\varphi_1 - \partial_x(B(x)\partial_x\varphi_1) = 0 \ \text{ in } \Omega_1 \times (0,T], \tag{3.45}$$

$$M(x)\partial_{tt}\eta + \partial_{xx}(K(x)\partial_{xx}\eta) + \eta + \partial_t\varphi_0 = Q(x,t) \ \text{ in } \Omega_0 \times (0,T], \tag{3.46}$$

$$\partial_t\eta + \partial_x(B(x)\partial_x\varphi_0) = 0 \text{ in } \ \Omega_0 \times (0,T], \tag{3.47}$$

$$\partial_{tt}\varphi_2 - \partial_x(B(x)\partial_x\varphi_2) = 0 \ \text{ in } \Omega_2 \times (0,T]. \tag{3.48}$$

The boundary conditions at the free edges of the plate are expressed as,

$$M_b(0,t) = V(0,t) = 0, \tag{3.49}$$

$$M_b(L_c^{-1}L,t) = V(L_c^{-1}L,t) = 0, \tag{3.50}$$

The interface conditions now become,

$$B(0^-)\partial_x\varphi_0(0^-,t) = B(0^+)\partial_x\varphi_1(0^+,t), \tag{3.51}$$

$$\partial_t\varphi_0(0^-,t) = \partial_t\varphi_1(0^+,t), \tag{3.52}$$

$$B(L_c^{-1}L^-)\partial_x\varphi_0(L_c^{-1}L^-,t) = B(L_c^{-1}L^+)\partial_x\varphi_2(L_c^{-1}L^+,t), \tag{3.53}$$

$$\partial_t\varphi_0(L_c^{-1}L^-,t) = \partial_t\varphi_2(L_c^{-1}L^+,t). \tag{3.54}$$

At initial time, the plate and the fluid of regions Ω_1 and Ω_0 are considered to be at rest,

$$\partial_x\varphi_1(x,0) = 0, \ \ \partial_t\varphi_1(x,0) = 0 \text{ in } \Omega_1, \tag{3.55}$$

$$\eta(x,0) = \varphi_0(x,0) = 0 \text{ in } \Omega_0, \tag{3.56}$$

$$\partial_x\varphi_2(x,0) = 0, \ \ \partial_t\varphi_2(x,0) = -S(x) \ \text{ in } \Omega_2. \tag{3.57}$$

References

[1]Sturova, I. V. (2009) Time-dependent response of a heterogeneous elastic plate floating on shallow water of variable bathymetry, *Journal of Fluid Mechanics (637)*, p. 305-325.

[2]Stoker J. J. (1957) *Water Waves: The mathematical Theory with Applications*, New York: Wiley-Interscience.

[3]Adrianov, A. (2011) *Hydroelastic analysis of Very Large Floating Structures: Interaction of floating elastic plates and water waves*, Berlin: VDM Verlag Dr. Müller

[4]Wang, C. M., Watanabe, E. & Utsunomiya, T. (eds.) (2008) *Very Large Floating Structures*, New York: Taylor & Francis.

CHAPTER 4

Variational formulations

In the present chapter, the variational formulation of the previously defined problems will be derived. These weak forms are the starting point for the numerical solution of the aforementioned Initial-Boundary Value Problems (IBVPs) via the Finite Element Method. The energy conservation principle is derived for the continuous weak form and ***a priori*** *stability estimates for the weak solutions in the physical energy norm and the maximum norm are proved.*

4.1 Preliminaries and Notation

For every Hilbert space U, we denote by $(\cdot\,,\,\cdot)_U$ the corresponding inner product and $\|\cdot\|_U$, $|\cdot|_U$, the induced norm and seminorm respectively. The standard notation $H^k(\Omega)$ is used for the classical Sobolev (Hilbert) spaces $W^{k,2}(\Omega)$, $k \in \mathbb{N}$. For $T > 0$, we denote the Banach valued function spaces as $L^p(0,T;U)$, $1 \leq p \leq \infty$ and the corresponding norm

$$\|u\|_{L^p(0,T;U)} \doteq \left(\int_0^T \|u\|_U \, dt \right)^{1/p}, \; 1 \leq p < \infty \text{ and } \|u\|_{L^\infty(0,T;U)} \doteq \operatorname*{ess\,sup}_{t \in [0,T]} \|u\|_U .$$

Finally use will be made of the following inequalities,

Young's inequality**:** *Let* $\alpha,\beta \geq 0$, $1 < p < \infty$ *and* q *be the conjugate of* p, *i.e.,* $p^{-1} + q^{-1} = 1$. *Then, for every* $\varepsilon > 0$ *it is*

$$\alpha\beta \leq \frac{\varepsilon\alpha^p}{p} + \frac{\varepsilon^{1-q}\beta^q}{q}$$

Gronwall inequality**:** *Let* $u(t)$, $f(t)$ *be continuous real functions with* $u(t) \geq 0$, *and* $c, T \in \mathbb{R}_+$. *Assume that* $u(t) \leq f(t) + c\int_0^t u(s)ds$, $\forall t \in [0,T]$.

Then, $u(t) \leq e^{ct} f(t)$, $\forall t \in [0,T]$.

4.2 Variational formulation

4.2.1 Problem Π_1 (floating cantilever)

The following assumptions are introduced,

(A1) $S(x) \in L^2(0,T;L^2(\Omega_2))$

(A2) For the bathymetry function it is $B \in L^\infty(\Omega_0 \cup \Omega_2)$. We denote, $C_B = \left\|B(x)\right\|_{L^\infty(\Omega_0 \cup \Omega_2)}$ and assume there exists positive constant c_B such that $\underset{x \in \Omega_0 \cup \Omega_2}{ess\ \inf} B(x) \geq c_B > 0$. That is, the bathymetry attains only positive values so that the seabed never reaches the water free surface in Ω_2 and the lower surface of the floating body in Ω_0.

(A3) It is $M, K \in L^\infty(\Omega_0)$ and there exists positive constants c_M, c_K such that $\underset{x \in \Omega_0}{ess\ \inf} M(x) \geq c_M > 0$ and $\underset{x \in \Omega_0}{ess\ \inf} K(x) \geq c_K > 0$.

The following functional space is defined,

$$U \doteq \ u \in H^2(\Omega_0) : u(0) = \partial_x u\Big|_{x=0} = 0$$

so as to account for the fixed end of the floating cantilever at $x = 0$. In order to derive the variational formulation, equations (3.35), (3.36) and (3.37) are multiplied by $u \in U, -w_0 \in H^1(\Omega_0), w_2 \in H^1(\Omega_2)$ respectively. Assuming enough regularity for the proper definition of all integrals and the application of integration by parts we get ,

$$\int_0^L Mu\partial_{tt}\eta dx + \int_0^L (K\partial_{xx}u\partial_{xx}\eta + u\eta)dx + \int_0^L u\partial_t\varphi_0 dx = \int_0^L uQ(x,t)dx \tag{4.1}$$

$$-\int_0^L w_0\partial_t\eta dx - \left[Bw_0\partial_z\varphi_0\right]_0^L + \int_0^L B\partial_x w_0\partial_x\varphi_0 dx = 0 \tag{4.2}$$

$$\int_L^\infty w_2\partial_{tt}\varphi_2 dx - \left[Bw_2\partial_x\varphi_2\right]_L^\infty + \int_L^\infty B\partial_x w_2\partial_x\varphi_2 dx = 0 \tag{4.3}$$

Adding (4.1), (4.2), (4.3) and using the interface conditions (3.40)-(3.41) and boundary and initial conditions (3.38),(3.39),(3.43),(3.42), we have the following variational form of problem Π_1.

Find $\eta(x,t)$, $\varphi_0(x,t)$ *and* $\varphi_2(x,t)$ *such that for every* $u \in U$, $w_0 \in H^1(\Omega_0)$, $w_2 \in H^1(\Omega_2)$ *it is,*

$$\begin{aligned}\int_0^L uM\partial_{tt}\eta dx + \int_0^L u\partial_t\varphi_0 dx - \int_0^L w_0\partial_t\eta dx + \int_L^{+\infty} w_2\partial_{tt}\varphi_2 dx \\ + a(\eta,u) + b_0(w_0,\varphi_0) + b_2(w_2,\varphi_2) = \int_0^L uQ(x,t)dx\end{aligned}, \tag{4.4}$$

a.e. in $(0,T]$ and with initial contitions,

$$(\eta(x,0),v)_{L^2(\Omega_0)} = (\varphi_0(x,0),w_0)_{L^2(\Omega_0)} = 0, \tag{4.5}$$

$$(\varphi_2(x,0),w_2)_{L^2(\Omega_2)} = 0, \ \ (\partial_t\varphi_2(x,0),w_2)_{L^2(\Omega_2)} = -(S(x),w_2)_{L^2(\Omega_2)} \ . \tag{4.6}$$

The bilinear functionals $a : V \times V \to \mathbb{R}$, $b_0 : H^1(\Omega_0) \times H^1(\Omega_0) \to \mathbb{R}$ and $b_2 : H^1(\Omega_2) \times H^1(\Omega_2) \to \mathbb{R}$ are defined as,

$$a(\eta,u) = \int_0^L (K\partial_{xx}u\partial_{xx}\eta + u\eta)dx, \tag{4.7}$$

$$b_0(w_0,\varphi_0) = \int_0^L B\partial_x w_0\partial_x\varphi_0 dx, \tag{4.8}$$

$$b_2(w_2,\varphi_2) = \int_L^\infty B\partial_x w_2\partial_x\varphi_2 dx. \tag{4.9}$$

4.2.2 Problem Π_2

The assumptions stated in the previous section are modified as,

(A4) $S(x) \in L^2(0,T;L^2(\Omega_2))$

(A5) Set $\mathrm{X} = \bigcup_{n=0}^{2} \Omega_n$.For the bathymetry function it is $B \in L^\infty(X)$. We denote, $C_B = \|B(x)\|_{L^\infty(X)}$ and assume there exists positive constant c_B such that $ess\inf_{x\in X} B(x) \geq c_B > 0$. That is, the bathymetry attains only positive values so that the seabed never reaches the water free surface in Ω_1, Ω_2 and the lower surface of the ice self in Ω_0.

(A6) It is $M, K \in L^\infty(\Omega_0)$ and there exists positive constants c_M, c_K such that $ess\inf_{x\in \Omega_0} M(x) \geq c_M > 0$ and $ess\inf_{x\in \Omega_0} K(x) \geq c_K > 0$.

In order to derive the variational formulation, equations (3.45), (3.46), (3.47) and (3.48) are multiplied by $v \in V, -w_0 \in H^1(\Omega_0), w_1 \in H^1(\Omega_1), w_2 \in H^1(\Omega_2)$ respectively. Assuming enough regularity for the proper definition of all integrals and the application of integration by parts we get

$$\int_{-\infty}^{0} w_1 \partial_{tt}\varphi_1 dx - \left[B w_1 \partial_x \varphi_1\right]_{-\infty}^{0} + \int_{-\infty}^{0} B\partial_x w_1 \partial_x \varphi_1 dx = 0 \qquad (4.10)$$

$$\int_0^L M v \partial_{tt}\eta dx + \int_0^L (K\partial_{xx} v \partial_{xx}\eta + v\eta) dx + \int_0^L v\partial_t \varphi_0 dx = \int_0^L vQ(x,t) dx \qquad (4.11)$$

$$-\int_0^L w_0 \partial_t \eta dx - \left[B w_0 \partial_z \varphi_0\right]_0^L + \int_0^L B\partial_x w_0 \partial_x \varphi_0 dx = 0 \qquad (4.12)$$

$$\int_L^\infty w_2 \partial_{tt}\varphi_2 dx - \left[B w_2 \partial_x \varphi_2\right]_L^\infty + \int_L^\infty B\partial_x w_2 \partial_x \varphi_2 dx = 0 \qquad (4.13)$$

Adding (4.10), (4.11), (4.12),(4.13) and using the interface conditions (3.50)-(3.53) initial and boundary conditions (3.49),(3.50),(3.55)-(3.57) we have the following variational form of problem Π_2.

Find $\eta(x,t), \varphi_0(x,t), \varphi_1(x,t)$ *and* $\varphi_2(x,t)$ *such that for every* $v \in V, w_0 \in H^1(\Omega_0)$, $w_1 \in H^1(\Omega_1)$ *and* $w_2 \in H^1(\Omega_2)$ *it holds that,*

$$\begin{aligned}\int_0^L vM\partial_{tt}\eta dx + \int_0^L v\partial_t\varphi_0 dx - \int_0^L w_0\partial_t\eta dx + \int_L^{+\infty} w_2\partial_{tt}\varphi_2 dx + \int_{-\infty}^0 w_1\partial_{tt}\varphi_1 dx \\ + a(\eta, v) + b_0(w_0, \varphi_0) + b_1(w_1, \varphi_1) + b_2(w_2, \varphi_2) = \int_0^L vQ(x,t)dx\end{aligned}, \quad (4.14)$$

a.e. in $(0,T]$ with initial conditions,

$$(\varphi_1(x,0), w_1)_{L^2(\Omega_1)} = (\partial_t\varphi_1(x,0), w_1)_{L^2(\Omega_1)} = 0, \quad (4.15)$$

$$(\eta(x,0), v)_{L^2(\Omega_0)} = (\partial_t\eta(x,0), v)_{L^2(\Omega_0)} = (\varphi_0(x,0), w_0)_{L^2(\Omega_0)} = 0, \quad (4.16)$$

$$(\varphi_2(x,0), w_2)_{L^2(\Omega_2)} = 0, \ \ (\partial_t\varphi_2(x,0), w_2)_{L^2(\Omega_2)} = -(S(x), w_2)_{L^2(\Omega_2)}. \quad (4.17)$$

The bilinear functionals $a: V \times V \to \mathbb{R}$, $b_0: H^1(\Omega_0) \times H^1(\Omega_0) \to \mathbb{R}$ and $b_1: H^1(\Omega_1) \times H^1(\Omega_1) \to \mathbb{R}$ are defined as

$$a(\eta, v) = \int_0^L (K\partial_{xx}v\partial_{xx}\eta + v\eta)dx, \quad (4.18)$$

$$b_0(w_0, \varphi_0) = \int_0^L B\partial_x w_0\partial_x\varphi_0 dx, \quad (4.19)$$

$$b_1(w_1, \varphi_1) = \int_{-\infty}^0 B\partial_x w_1\partial_x\varphi_1 dx, \quad (4.20)$$

$$\text{and} \quad b_2(w_2, \varphi_2) = \int_L^{\infty} B\partial_x w_2\partial_x\varphi_2 dx. \quad (4.21)$$

4.3 Energy conservation principle

In this section, under the assumption of sufficient regularity for the weak solution of the variational problem presented above, an energy conservation principle will be derived.

4.3.1 Problem Π_1

Theorem 1.1 (Energy conservation principle). Assume that $\partial_t\eta \in L^2(0,T;U)$, $\partial_t\varphi_0 \in L^2(0,T;H^1(\Omega_0))$ and $\partial_t\varphi_2 \in L^2(0,T;H^1(\Omega_2))$. Further, let $Q \equiv 0$. Then, $\forall t \in (0,T]$ it is,

$$\left\|M^{1/2}\partial_t\eta\right\|^2_{L^2(\Omega_0)}+\left\|\partial_t\varphi_2\right\|^2_{L^2(\Omega_2)}+a(\eta,\eta)+b_0(\varphi_0,\varphi_0)+b_2(\varphi_2,\varphi_2)=\left\|S(x)\right\|^2_{L^2(\Omega_2)} \quad (4.22)$$

Proof. By setting $v=\partial_t\eta, w_0=\partial_t\varphi_0, w_2=\partial_t\varphi_2$ in (4.1), (4.2), (4.3) the cancelation

$$-\int_0^L\partial_t\eta\partial_t\varphi_0dx+\int_0^L\partial_t\varphi_0\partial_t\eta dx=0$$

is directly achieved. In the same time all boundary terms appearing in those equations vanish due to the interface conditions (3.40), (3.41). Finally, the term $b_0(\partial_t\varphi_0,\varphi_0)$ attains positive sign.

By invoking the assumed regularity, the following relations hold,

$$\int_0^L M\partial_{tt}\eta\partial_t\eta dx=\frac{1}{2}\frac{d}{dt}\left\|M^{1/2}\partial_t\eta\right\|^2_{L^2(\Omega_0)},\int_L^{+\infty}\partial_{tt}\varphi_2\partial_t\varphi_2dx=\frac{1}{2}\frac{d}{dt}\left\|\partial_t\varphi_2\right\|^2_{L^2(\Omega_2)} \quad (4.23)$$

$$\text{and}\quad a(\eta_t,\eta)=\int_0^L K\partial_{txx}\eta\partial_{xx}\eta dx+\int_0^L\partial_t\eta\eta dx=\frac{1}{2}\frac{d}{dt}a(\eta,\eta). \quad (4.24)$$

Similarly it is,

$$b_0(\partial_t\varphi_0,\varphi_0)=\frac{1}{2}\frac{d}{dt}b_0(\varphi_0,\varphi_0)\ \text{and}\ b_2(\partial_t\varphi_2,\varphi_2)=\frac{1}{2}\frac{d}{dt}b_2(\varphi_2,\varphi_2) \quad (4.25)$$

Using (4.23), (4.24) and (4.25), equation (4.4) becomes,

$$\frac{d}{ds}\left[\left\|M^{1/2}\partial_s\eta\right\|^2_{L^2(\Omega_0)}+\left\|\partial_s\varphi_2\right\|^2_{L^2(\Omega_2)}+a(\eta,\eta)+b_0(\varphi_0,\varphi_0)+b_2(\varphi_2,\varphi_2)\right]=2\int_0^L\partial_s\eta Q(x,s)dx \quad (4.26)$$

Setting $Q=0$, integrating (4.26) with respect to time from $s=0$ to $s=t$ and enforcing initial conditions (4.5) and (4.6), we get (4.22). □

Equation (4.22) in an energy conservation principle, which states that when no forcing is present, the total hydroelastic energy, i.e. the kinetic and strain energy of the beam along with the water free surface kinetic energy and the discharge flux energy of the water column remains constant in time and equals the energy of the initial water free surface elevation in the region outside the hydroelastic interaction. Apart from its theoretical significance and the insights in the physics of these hydroelastic phenomena, the energy conservation principle provides a useful means for the validation of the finite element models to be applied for any numerical solution.

Remark: The bathymetry function B, as defined through relations (3.33) possesses a discontinuity in the form of a finite jump at $x = L$. Thus when defined as a function $B : \Omega_0 \cup \Omega_2 \to \mathbb{R}_+$ the regularity $B \in L^\infty(\Omega_0 \cup \Omega_2)$ is appropriate in order to form a simple realistic model. However, the bathymetry function could be smoother when restricted to the interior of Ω_0 and Ω_2. Similar considerations are valid for problem Π_2.

4.3.2 Problem Π_2 (freely floating plate)

Theorem 1.2 (Energy conservation principle). Assume that $\partial_t \eta \in L^2(0,T;V)$, $\partial_t \varphi_0 \in L^2(0,T;H^1(\Omega_0)), \partial_t \varphi_1 \in L^2(0,T;H^1(\Omega_1))$ and $\partial_t \varphi_2 \in L^2(0,T;H^1(\Omega_2))$

Further, let $Q \equiv 0$. Then, $\forall t \in (0,T]$ it is,

$$\begin{aligned} \left\| M^{1/2} \partial_t \eta \right\|^2_{L^2(\Omega_0)} + \left\| \partial_t \varphi_1 \right\|^2_{L^2(\Omega_1)} + \left\| \partial_t \varphi_2 \right\|^2_{L^2(\Omega_2)} + a(\eta,\eta) + b_0(\varphi_0,\varphi_0) + b_1(\varphi_1,\varphi_1) \\ + b_2(\varphi_2,\varphi_2) = \left\| S(x) \right\|^2_{L^2(\Omega_2)} \end{aligned}, \quad (4.27)$$

Proof. By setting $v = \partial_t \eta, w_0 = \partial_t \varphi_0, w_1 = \partial_t \varphi_1, w_2 = \partial_t \varphi_2$ in (4.10), (4.11), (4.12) and (4.13) the cancelation ,

$$-\int_0^L \partial_t \eta \partial_t \varphi_0 dx + \int_0^L \partial_t \varphi_0 \partial_t \eta dx = 0,$$

is again directly achieved. In the same time all boundary terms appearing in those equations vanish due to the interface conditions (3.50),-(3.53). Finally, the term $b_0(\partial_t \varphi_0, \varphi_0)$ attains positive sign.

By invoking the assumed regularity, the following relations hold

$$\begin{aligned} \int_0^L M \partial_{tt} \eta \partial_t \eta dx = \frac{1}{2} \frac{d}{dt} \left\| M^{1/2} \partial_t \eta \right\|^2_{L^2(\Omega_0)}, \int_{-\infty}^0 \partial_{tt} \varphi_1 \partial_t \varphi_1 dx = \frac{1}{2} \frac{d}{dt} \left\| \partial_t \varphi_1 \right\|^2_{L^2(\Omega_1)}, \\ \int_L^{+\infty} \partial_{tt} \varphi_2 \partial_t \varphi_2 dx = \frac{1}{2} \frac{d}{dt} \left\| \partial_t \varphi_2 \right\|^2_{L^2(\Omega_2)} \end{aligned}, \quad (4.28)$$

$$\text{and } a(\partial_t \eta, \eta) = \int_0^L K \partial_{txx} \eta \partial_{xx} \eta dx + \int_0^L \partial_t \eta \eta dx = \frac{1}{2} \frac{d}{dt} a(\eta,\eta) \quad (4.29)$$

Similarly it is,

$$b_0(\partial_t\varphi_0,\varphi_0)=\frac{1}{2}\frac{d}{dt}b_0(\varphi_0,\varphi_0), b_1(\partial_t\varphi_1,\varphi_1)=\frac{1}{2}\frac{d}{dt}b_1(\varphi_1,\varphi_1)$$
$$b_2(\partial_t\varphi_2,\varphi_1)=\frac{1}{2}\frac{d}{dt}b_2(\varphi_2,\varphi_2) \tag{4.30}$$

Using (4.28), (4.29) and (4.30) equation (4.14) becomes

$$\frac{d}{ds}\left[\left\|M^{1/2}\partial_s\eta\right\|^2_{L^2(\Omega_0)}+\left\|\partial_s\varphi_1\right\|^2_{L^2(\Omega_1)}+\left\|\partial_s\varphi_2\right\|^2_{L^2(\Omega_2)}+a(\eta,\eta)+b_0(\varphi_0,\varphi_0)+b_1(\varphi_1,\varphi_1)+b_2(\varphi_2,\varphi_2)\right]$$
$$=2\int_0^L\partial_s\eta Q(x,s)dx \tag{4.31}$$

Setting $Q=0$, integrating (4.31) with respect to time from $s=0$ to $s=t$ and by using initial conditions (4.15)-(4.17), we get (4.27). □

4.4 Stability estimates for the weak solution

Stability estimates, in the physical energy norm for the hydroelastic problem, will be derived. In addition, a priori estimates for the ice self deformation characteristics in the infinity norm will be proven.

4.4.1 Problem Π_1

Proposition 1.1 Let assumptions **(A1)**, **(A2)**, **(A3)** hold. Assume that $\partial_t\eta\in L^2(0,T;U)$, $\partial_t\varphi_0\in L^2(0,T;H^1(\Omega_0))$ and $\partial_t\varphi_2\in L^2(0,T;H^1(\Omega_2))$. Further let $Q\in L^2(0,T;L^2(\Omega_0))$. Then there exist constants $c_L, C>0$ such that

$$\left\|\partial_t\eta\right\|^2_{L^2(\Omega_0)}+\left\|\eta\right\|^2_{H^2(\Omega_0)}+\left\|\eta\right\|^2_{L^2(\Omega_0)}+\left|\varphi_0\right|^2_{H^1(\Omega_0)}+\left\|\partial_t\varphi_2\right\|^2_{L^2(\Omega_2)}+\left|\varphi_2\right|^2_{H^1(\Omega_2)}$$
$$\le C^{-1}e^{C^{-1}T}\left(\left\|S\right\|^2_{L^2(\Omega_2)}+\left\|Q\right\|^2_{L^2(0,T;L^2(\Omega_2))}\right), \tag{4.32}$$

with $C=\min\ 1,c_M,c_Kc_L,c_B$.

Proof. Integrating (4.26) with respect to time from $s=0$ to $s=t$ and using initial conditions (4.5) and (4.6), we get,

$$\left\|M^{1/2}\partial_t\eta\right\|^2_{L^2(\Omega_0)}+\left\|\partial_t\varphi_2\right\|^2_{L^2(\Omega_2)}+a(\eta,\eta)+b_0(\varphi_0,\varphi_0)+b_2(\varphi_2,\varphi_2)$$
$$=\left\|S\right\|^2_{L^2(\Omega_2)}+2\int_0^t\int_0^L\partial_s\eta Q(x,s)dxds \tag{4.33}$$

From Young's inequality

$$\left|\int_0^L \partial_s \eta Q dx\right| \le \frac{1}{2}\int_0^L (\partial_s \eta)^2 + Q^2 \; dx = \frac{1}{2}\left\|\partial_s \eta\right\|^2_{L^2(\Omega_0)} + \frac{1}{2}\left\|Q\right\|^2_{L^2(\Omega_0)} \tag{4.34}$$

Invoking (A3) it is

$\left\|M^{1/2}\partial_t \eta\right\|^2_{L^2(\Omega_0)} \ge c_M \left\|\partial_t \eta\right\|^2_{L^2(\Omega_0)}$ and

$$a(\eta,\eta) = \int_0^L K \; \partial_{xx}\eta \;^2 dx + \int_0^L \eta^2 dx \ge c_K \left|\eta\right|^2_{H^2(\Omega_0)} + \left\|\eta\right\|^2_{L^2(\Omega_0)}. \tag{4.35}$$

From the equivalence of norm and semi-norm in U, there exist $c_L > 0$ such that

$$a(\eta,\eta) \ge c_L c_K \left\|\eta\right\|^2_{L^2(\Omega_0)} + \left\|\eta\right\|^2_{L^2(\Omega_0)} \tag{4.36}$$

Similarly, we have $b_0(\varphi_0,\varphi_0) \ge c_B \left|\varphi_0\right|^2_{H^1(\Omega_0)}$ and $b_2(\varphi_2,\varphi_2) \ge c_B \left|\varphi_2\right|^2_{H^1(\Omega_2)}$. From relations (4.33)-(4.36) it is,

$$\begin{aligned} C\left(\left\|\partial_t \eta\right\|^2_{L^2(\Omega_0)} + \left\|\eta\right\|^2_{L^2(\Omega_0)} + \left\|\eta\right\|^2_{L^2(\Omega_0)} + \left|\varphi_0\right|^2_{H^1(\Omega_0)} + \left\|\partial_t \varphi_2\right\|^2_{L^2(\Omega_2)} + \left|\varphi_2\right|^2_{H^1(\Omega_2)}\right) \\ \le \left\|S\right\|^2_{L^2(\Omega_2)} + \int_0^t \left\|\partial_s \eta\right\|^2_{L^2(\Omega_0)} ds + \int_0^t \left\|Q(x,s)\right\|^2_{L^2(\Omega_0)} ds \end{aligned} \tag{4.37}$$

where $C = \min\ 1, c_M, c_K c_L, c_B$

Application of Gronwall's lemma in (4.37) and setting $t = T$, yields the desired result. With the use of Proposition 1.1 one may easily prove the following result for the plate deflection solution.

Theorem 2.1 Let all assumptions stated in Proposition 1.1 hold. Then it is

$$\left\|\partial_t \eta\right\|_{L^2(0,T;L^2(\Omega_0))} + \left\|\eta\right\|_{L^2(0,T;H^2(\Omega_0))} \le \sqrt{2C^{-1}Te^{C^{-1}T}}\left(\left\|S\right\|_{L^2(\Omega_2)} + \left\|Q\right\|_{L^2(0,T;L^2(\Omega_0))}\right), \tag{4.38}$$

with $C = \min\ 1, c_M, c_K c_L, c_B$

Proof. From Proposition 1.1 we get

$$\left\|\partial_t \eta\right\|^2_{L^2(\Omega_0)} + \left\|\eta\right\|^2_{L^2(\Omega_0)} \le C^{-1}e^{C^{-1}T}\left(\left\|S\right\|^2_{L^2(\Omega_2)} + \left\|Q\right\|^2_{L^2(0,T;L^2(\Omega_0))}\right) \tag{4.39}$$

where $C = \min\ 1, c_M, c_K c_L, c_B\ $. Integrating with respect to time $[0,T]$,

$$\left\|\partial_t \eta\right\|^2_{L^2(0,T;L^2(\Omega_0))} + \left\|\eta\right\|^2_{L^2(0,T;H^2(\Omega_0))} \le C^{-1} T e^{C^{-1}T}\left(\left\|S\right\|^2_{L^2(\Omega_2)} + \left\|Q\right\|^2_{L^2(0,T;L^2(\Omega_0))}\right). \tag{4.40}$$

Taking square roots using the norm equivalence in $\mathbb{R}^2$, equation (4.40) yields (4.38). □

For applications, it is of interest to derive a bound on the maximum value of the flexible strip deflection and slope. For this purpose, the following classic embedding result will be used.

Lemma 1 Let $\Omega \subset \mathbb{R}^n$ be a Lipschitz domain. It is $W^{k,p}(\Omega) \hookrightarrow C^\ell(\bar{\Omega})$ if $k - \ell > np^{-1}$.

Using Theorem 2.1 and lemma 1, we get

Theorem 3.1 Let all assumptions stated in Theorem 2.1 hold. Then $\eta \in C^0([0,T];C^1(\bar{\Omega}_0))$ and there exists $C_0 \in \mathbb{R}_+$

$$\left\|\eta\right\|_{C^0([0,T];C^1(\bar{\Omega}_0))} \le \Sigma\ \left\|S\right\|_{L^2(\Omega_2)} + \left\|Q\right\|_{L^2(0,T;L^2(\Omega_0))}\ , \tag{4.41}$$

where $\Sigma = C_0^{-1}\sqrt{C^{-1}e^{C^{-1}T}}$.

Proof . The first part follows directly from lemma 1 assumed regularity for the solution.. From (4.39), and Lemma 1, it is

$$C_0^2 \left\|\eta\right\|^2_{C^1(\bar{\Omega}_0)} \le C^{-1} e^{C^{-1}T}\left(\left\|S\right\|^2_{L^2(\Omega_2)} + \left\|Q\right\|^2_{L^2(0,T;L^2(\Omega_0))}\right), \tag{4.42}$$

Thus it holds

$$\max_{t\in[0,T]} \left\|\eta\right\|^2_{C^1(\bar{\Omega}_0)} \le C_0^{-2} C^{-1} e^{C^{-1}T}\left(\left\|S\right\|^2_{L^2(\Omega_2)} + \left\|Q\right\|^2_{L^2(0,T;L^2(\Omega_0))}\right), \tag{4.43}$$

and (4.41) follows by taking square roots. □

4.4.2 Problem Π_2

Proposition 1.2 Let assumptions **(A4)**, **(A5)**, **(A6)** hold. Assume that $\partial_t \eta \in L^2(0,T;V)$, $\partial_t \varphi_0 \in L^2(0,T;H^1(\Omega_0)), \partial_t \varphi_1 \in L^2(0,T;H^1(\Omega_1))$ and $\partial_t \varphi_2 \in L^2(0,T;H^1(\Omega_2))$.

Further let $Q \in L^2(0,T;L^2(\Omega_0))$. Then there exist constants $C > 0$ such that

$$\begin{aligned}\left\|\partial_t \eta\right\|^2_{L^2(\Omega_0)} + \left\|\eta\right\|^2_{H^2(\Omega_0)} + \left\|\eta\right\|^2_{L^2(\Omega_0)} + \left|\varphi_0\right|^2_{H^1(\Omega_0)} + \left\|\partial_t \varphi_1\right\|^2_{L^2(\Omega_1)} + \left|\varphi_1\right|^2_{H^1(\Omega_1)} \\ + \left\|\partial_t \varphi_2\right\|^2_{L^2(\Omega_2)} + \left|\varphi_2\right|^2_{H^1(\Omega_2)} \le C^{-1} e^{C^{-1}T}\left(\left\|S\right\|^2_{L^2(\Omega_2)} + \left\|Q\right\|^2_{L^2(0,T;L^2(\Omega_1))}\right),\end{aligned} \tag{4.44}$$

with $C = \min\ 1, c_M, c_K, c_B\ .$

Proof. Integrating (4.31) with respect to time from $s = 0$ to $s = t$ and using initial conditions (4.15)-(4.17), we get,

$$\left\|M^{1/2}\partial_t\eta\right\|^2_{L^2(\Omega_0)} + \left\|\partial_t\varphi_1\right\|^2_{L^2(\Omega_1)} + \left\|\partial_t\varphi_2\right\|^2_{L^2(\Omega_2)} + a(\eta,\eta) + b_0(\varphi_0,\varphi_0) + b_1(\varphi_1,\varphi_1) + b_2(\varphi_2,\varphi_2)$$
$$= \left\|S\right\|^2_{L^2(\Omega_2)} + 2\int_0^t\int_0^L \partial_s\eta Q(x,s)dxds \tag{4.45}$$

From Young's inequality,

$$\left|\int_0^L \partial_s\eta Q dx\right| \le \frac{1}{2}\int_0^L\ (\partial_s\eta)^2 + Q^2\ \ dx = \frac{1}{2}\left\|\partial_s\eta\right\|^2_{L^2(\Omega_0)} + \frac{1}{2}\left\|Q\right\|^2_{L^2(\Omega_0)} \tag{4.46}$$

Invoking (A3) it is,

$\left\|M^{1/2}\partial_t\eta\right\|^2_{L^2(\Omega)} \ge c_M\left\|\partial_t\eta\right\|^2_{L^2(\Omega)}$ and

$$a(\eta,\eta) = \int_0^L K\ \ \partial_{xx}\eta\ ^2\, dx + \int_0^L \eta^2 dx \ge c_K\left|\eta\right|^2_{H^2(\Omega)} + \left\|\eta\right\|^2_{L^2(\Omega)}. \tag{4.47}$$

Similarly, we have $b_0(\varphi_0,\varphi_0) \ge c_B\left|\varphi_0\right|^2_{H^1(\Omega_0)}$, $b_1(\varphi_1,\varphi_1) \ge c_B\left|\varphi_1\right|^2_{H^1(\Omega_1)}$ and

$b_2(\varphi_2,\varphi_2) \ge c_B\left|\varphi_2\right|^2_{H^1(\Omega_2)}$.

From relations (4.45)-(4.47) it is,

$$C\left(\left\|\partial_t\eta\right\|^2_{L^2(\Omega_0)} + \left\|\eta\right\|^2_{H^2(\Omega_0)} + \left\|\eta\right\|^2_{L^2(\Omega_0)} + \left|\varphi_0\right|^2_{H^1(\Omega_0)} + \left\|\partial_t\varphi_1\right\|^2_{L^2(\Omega_1)} + \left|\varphi_1\right|^2_{H^1(\Omega_1)}\right)$$
$$+ C\left(\left\|\partial_t\varphi_2\right\|^2_{L^2(\Omega_2)} + \left|\varphi_2\right|^2_{H^1(\Omega_2)}\right)\ \le \left\|S\right\|^2_{L^2(\Omega_2)} + \int_0^t\left\|\partial_s\eta\right\|^2_{L^2(\Omega_0)}ds + \int_0^t\left\|Q(x,s)\right\|^2_{L^2(\Omega_0)}ds \tag{4.48}$$

where $C = \min\ 1, c_M, c_K, c_B$

Application of Gronwall's lemma in (4.48) and setting $t = T$, yields the desired result. □

Similarly to the analysis of problem Π_1, the following stability result for the beam deflection in the energy norm holds,

Theorem 2.2 Let all assumptions stated in Proposition 2.1 hold. Then it is

$$\left\|\partial_t\eta\right\|_{L^2(0,T;L^2(\Omega_0))} + \left\|\eta\right\|^2_{H^2(0,T;H^2(\Omega_0))} \le \sqrt{2C^{-1}Te^{C^{-1}T}}\left(\left\|S\right\|^2_{L^2(\Omega_2)} + \left\|Q\right\|^2_{L^2(0,T;L^2(\Omega_0))}\right) \tag{4.49}$$

with $C = \min\ 1, c_M, c_K, c_B$

Proof. From Proposition 2.1 we get,

$$\left\|\partial_t \eta\right\|^2_{L^2(\Omega_0)} + \left\|\eta\right\|^2_{H^2(\Omega_0)} \leq C^{-1} e^{C^{-1}T} \left(\left\|S\right\|^2_{L^2(\Omega_2)} + \left\|Q\right\|^2_{L^2(0,T;L^2(\Omega_0))} \right) \quad (4.50)$$

where $C = \min\ 1, c_M, c_K, c_B$. Integrating with respect to time $[0, T]$,

$$\left\|\partial_t \eta\right\|_{L^2(0,T;L^2(\Omega_0))} + \left\|\eta\right\|^2_{H^2(0,T;H^2(\Omega_0))} \leq C^{-1} T e^{C^{-1}T} \left(\left\|S\right\|^2_{L^2(\Omega_2)} + \left\|Q\right\|^2_{L^2(0,T;L^2(\Omega_0))} \right). \quad (4.51)$$

The respective stability estimate in the maximum norm is

Theorem 3.2 Let all assumptions stated in Theorem 2.2 hold. Then $\eta \in C^0([0,T]; C^1(\bar{\Omega}_0))$ and there exists $C_0 \in \mathbb{R}_+$ such that

$$\left\|\eta\right\|_{C^0([0,T];C^1(\bar{\Omega}_0))} \leq \Sigma \left\|S\right\|_{L^2(\Omega_2)} + \left\|Q\right\|_{L^2(0,T;L^2(\Omega_0))} , \quad (4.52)$$

where $\Sigma = C_0^{-1} \sqrt{C^{-1} e^{C^{-1}T}}$.

Proof . The first part follows directly from lemma 1 and assumed regularity for the solution. From (4.15), and Lemma 1, it is

$$C_0^2 \left\|\eta\right\|^2_{C^1(\bar{\Omega}_0)} \leq C^{-1} e^{C^{-1}T} \left(\left\|S\right\|^2_{L^2(\Omega_2)} + \left\|Q\right\|^2_{L^2(0,T;L^2(\Omega_0))} \right), \quad (4.53)$$

Thus, taking square roots it holds

$$\max_{t\in[0,T]} \left\|\eta\right\|_{C^1(\bar{\Omega}_0)} \leq C_0^{-1} \sqrt{C^{-1} e^{C^{-1}T}} \left(\left\|S\right\|_{L^2(\Omega_1)} + \left\|Q\right\|_{L^2(0,T;L^2(\Omega_0))} \right), \quad (4.54)$$

which is (4.49). □

References

[1] Kardestuncer H. (1987) *Finite Element handbook,* US: Mc.Graw-Hill, Inc.
[2] Athinson, K & Han, W. (2000) *Theoretical Numerical Analysis a functional analysis framework*, New York: Springer Science and Business Media, Inc.
[3] Grossmann, C., Roos H. & Stynes, M. (2000) *Numerical Treatment of Partial Differential Equations*, Berlin: Springer-Verlag Berlin Heidelberg.
[4] Brezis, H. (1983) *Analyse Fonctionnelle, theorie et applications,* Paris: Masson.

CHAPTER 5

Hydroelastic Finite Elements

Based on the variational formulations presented in the previous chapter, the semi-discretization, by means of the finite element method, for hydroelastic problems Π_1 *(floating cantilever) and* Π_2 *(freely floating plate) will be pursued. As an application of the vertical method of lines, the spatial discretization with finite elements leads to a system of ordinary differential (ODE) equations to be integrated with respect to time with the use of a suitable numerical ODE integration time-stepping procedure. Hydroelastic elements of various polynomial degrees will be constructed and error estimates for the semi-discrete form will be derived.*

5.1 Semi-discrete formulation

The variational problems defined in section 4.2, will be approximated by the use of finite elements. The semi-discrete formulation of the problems Π_1 and Π_2 can be derived from the previous sections in a straight forward manner. Using the super-script h, linked with the discrete length scale, the spatially discrete functions are presented.

In order to carry out the analysis the following subspaces of the respective function spaces defined in Chapter 4 need to be introduced. Let $k_1, k_2 \in \mathbb{N}, u\big|_e$ denote the restriction of the function u inside finite element e and H_i , $i = 1,..,k_1$, L_i , $i = 1,..,k_2$ be Hermite and Lagrange basis function inside e respectively.

$$U^h \doteq \left\{ u^h \in U \ and \ u^h\Big|_e = \sum_{i=1}^{k_1} H_i(x) u_i^h(t) \right\},$$

$$V^h \doteq \left\{ v^h \in H^2(\Omega_0) \ and \ v^h\Big|_e = \sum_{i=1}^{k_1} H_i(x) v_i^h(t) \right\} \text{ and}$$

$$W_j^h \doteq \left\{ w^h \in H_1^h(\Omega_j) \ and \ w^h\Big|_e = \sum_{i=1}^{k_2} L_i(x) w_i^h(t) \right\} \text{ for } j = 0,1,2 .$$

,along with the discrete weight functions $u^h \in U^h, v^h \in V^h, w_0^h \in W_0^h, w_1^h \in W_1^h, w_2^h \in W_2^h$.

So for Π_1, the fixed –edge plate problem , the variational problem is reformulated as,

Π_1 : *Find* $\eta^h(x,t)$, $\varphi_0^h(x,t)$ *and* $\varphi_2^h(x,t)$ *such that for every* $u^h \in U^h \subset U$, $w_0 \in W_0^h$, $w_2 \in W_1^h$ *it is,*

$$\begin{aligned} &\int_{\Omega_0^h} u^h M \partial_{tt} \eta^h dx + \int_{\Omega_0^h} u^h \partial_t \varphi_0^h dx - \int_{\Omega_0^h} w_0^h \partial_t \eta^h dx + \int_{\Omega_1^h} w_2^h \partial_{tt} \varphi_2^h dx \\ &\quad + a^h(\eta^h, u^h) + b_0^h(w_0^h, \varphi_0^h) + b_2^h(w_2^h, \varphi_2^h) = \int_{\Omega_0^h} u^h Q^h(x,t) dx \end{aligned} \tag{5.1}$$

With initial conditions,

$$(\eta^h(x,0), v^h)_{L^2(\Omega_0^h)} = (\varphi_0^h(x,0), w_0^h)_{L^2(\Omega_0^h)} = 0$$

$$(\varphi_2^h(x,0), w_2^h)_{L^2(\Omega_2^h)} = 0, \ \ (\partial_t \varphi_2^h(x,0), w_2^h)_{L^2(\Omega_2^h)} = -(S(x), w_2^h)_{L^2(\Omega_2^h)} \tag{5.2}$$

The semi-discrete formulation of problems Π_2 is given below,

Π_2 :*Find* $\eta^h(x,t)$, $\varphi_0^h(x,t)$, $\varphi_1^h(x,t)$ *and* $\varphi_2^h(x,t)$ *such that for every* $v^h \in H_2^h$, $w_0^h \in W_0^h$, $w_1^h \in W_1^h$ *and* $w_2^h \in W_2^h$ *it holds that,*

$$\begin{aligned} &\int_0^L v^h M \partial_{tt} \eta^h dx + \int_0^L v^h \partial_t \varphi_0{}^h dx - \int_0^L w_0^h \partial_t \eta^h dx + \int_L^{+\infty} w_2^h \partial_{tt} \varphi_2^h dx \\ &+ \int_{-\infty}^0 w_1^h \partial_{tt} \varphi_1^h dx + a^h(\eta^h, v^h) + b_0^h(w_0^h, \varphi_0^h) + b_1^h(w_1^h, \varphi_1^h) + b_2^h(w_2^h, \varphi_2^h) \\ &\qquad = \int_0^L v^h Q^h(x,t) dx \end{aligned} \tag{5.3}$$

with initial conditions,

$$(\varphi_1^h(x,0), w_1^h)_{L^2(\Omega_1)} = (\partial_t \varphi_1^h(x,0), w_1^h)_{L^2(\Omega_1)} = 0$$

$$(\eta^h(x,0), v^h)_{L^2(\Omega_0)} = (\varphi_0^h(x,0), w_0^h)_{L^2(\Omega_0)} = 0 \tag{5.4}$$

$$(\varphi_2^h(x,0), w_2^h)_{L^2(\Omega_2)} = 0, \quad (\partial_t \varphi_2^h(x,0), w_2^h)_{L^2(\Omega_2)} = -(S(x), w_2^h)_{L^2(\Omega_2)}$$

The central idea behind the finite element approximation of the solution to the previously defined variational problems, is the representation of the domain as a collection of disjoint subdomains connected by nodes. The solutions are then approximated within a single element or subdomain as interpolations of nodal values.

Hence, the approximate free surface/plate deflection within each element of the hydroelasticity dominated regions, is expressed as $\eta^h\Big|_e = \sum_{i=1}^{k_1} H_i(x)\eta_i^h(t)$ while the velocity potential for the fluid in both hydroelasticity dominated and free-water surface regions, as $\varphi_j^h\Big|_e = \sum_{i=1}^{k_2} L_i(x)\varphi_i^h(t) \in W_j^h$ for $j = 0,1,2$, where η_i^h, φ_i^h are the nodal unknowns.

The use of C_1 Hermite shape functions is required the interpolation of η^h due to the continuity requirement posed on its first derivative. Additionally, it must be noted that $\eta^h\Big|_e \in U^h$ for Π_1 and $\eta^h\Big|_e \in V^h$ for Π_2. The reader is reminded that Dirichlet boundary condition in problem Π_1 is included in the definition of space U and in extent U^h.

Thus, in terms of the problems in question, the approximation using Hermite shape functions is to be applied in the domain $\Omega_0(\eta)$ of the problems Π_1 and Π_2. The velocity potential is represented by φ_j^h and interpolated using Lagrange shape functions. In the hydroelasticity dominated regions, the coupling between the unknown plate deflection/surface elevation and the unknown velocity potential underneath the plate, mandates the development of a special hydroelastic element featuring a superposition of the resulting DOFs.

5.2 Special Hydroelastic Elements

In the previous section the semi-discrete formulation of the weak problems Π_1, Π_2 and Π_3 were presented. As pointed out the velocity potential and the plate deflection in the hydroelasticity dominated regions of the problems have different continuity requirements for their derivatives. Namely, $\eta^h \in C_1$ while $\varphi^h \in C_0$, meaning that η^h needs to be continuously differentiable in the aforementioned regions while φ^h does not. It is evident that within a single hydroelastic element two different interpolations take place. A series of special hydroelastic elements will be presented ranging from the lowest to the highest degree of interpolation incorporated. This family of elements are denoted as HELFEM (a,b), i.e. Hydroelastic Finite Element Method with polynomial approximation of degree a for the beam deflection and degree b for the velocity potential.

5.2.1 HELFEM (3,1) and HELFEM (3,2)

HELFEM (3,1) is a hydroelastic element featuring two nodes and 6 DOFs. Cubic Hermite Shape functions are used for the interpolation of η^h while linear Lagrange shape functions are used for φ^h, in the sense,

$$\eta^h\Big|_e = \sum_{i=1}^{4} H_i(x)\eta_i^h(t) \text{ and } \varphi_j^h\Big|_e = \sum_{i=1}^{2} L_i(x)\varphi_i^h(t) \in W_j^h \tag{5.5}$$

In HELFEM (3,2) the degree of interpolation of φ^h is increased, while cubic Hermite shae functions are used again for η^h. Hence, the element features 3 nodes with 7 DOFs.

$$\eta^h\Big|_e = \sum_{i=1}^{4} H_i(x)\eta_i^h(t) \text{ and } \varphi_j^h\Big|_e = \sum_{i=1}^{3} L_i(x)\varphi_i^h(t) \in W_j^h \tag{5.6}$$

The shape functions for the two types of element are shown in the figure below,

5.2.2 HELFEM (5,2) and HELFEM(5,4)

HELFEM (5,2) features 3 nodes and 9 DOFs. A quantic Hermite interpolation is used for the approximation of η^h while a quadratic Lagrange interpolation is used for φ^h

$$\eta^h\Big|_e = \sum_{i=1}^{6} H_i(x)\eta_i^h(t) \text{ and } \varphi_j^h\Big|_e = \sum_{i=1}^{3} L_i(x)\varphi_i^h(t) \in W_j^h . \tag{5.7}$$

HELFEM (5,4) has 5 nodes and 11 DOFs. The same quantic Hermite interpolation is used for η^h and a fourth-order Lagrange interpolation for φ^h,

$$\eta^h\Big|_e = \sum_{i=1}^{6} H_i(x)\eta_i^h(t) \text{ and } \varphi_j^h\Big|_e = \sum_{i=1}^{5} L_i(x)\varphi_i^h(t) \in W_j^h. \tag{5.8}$$

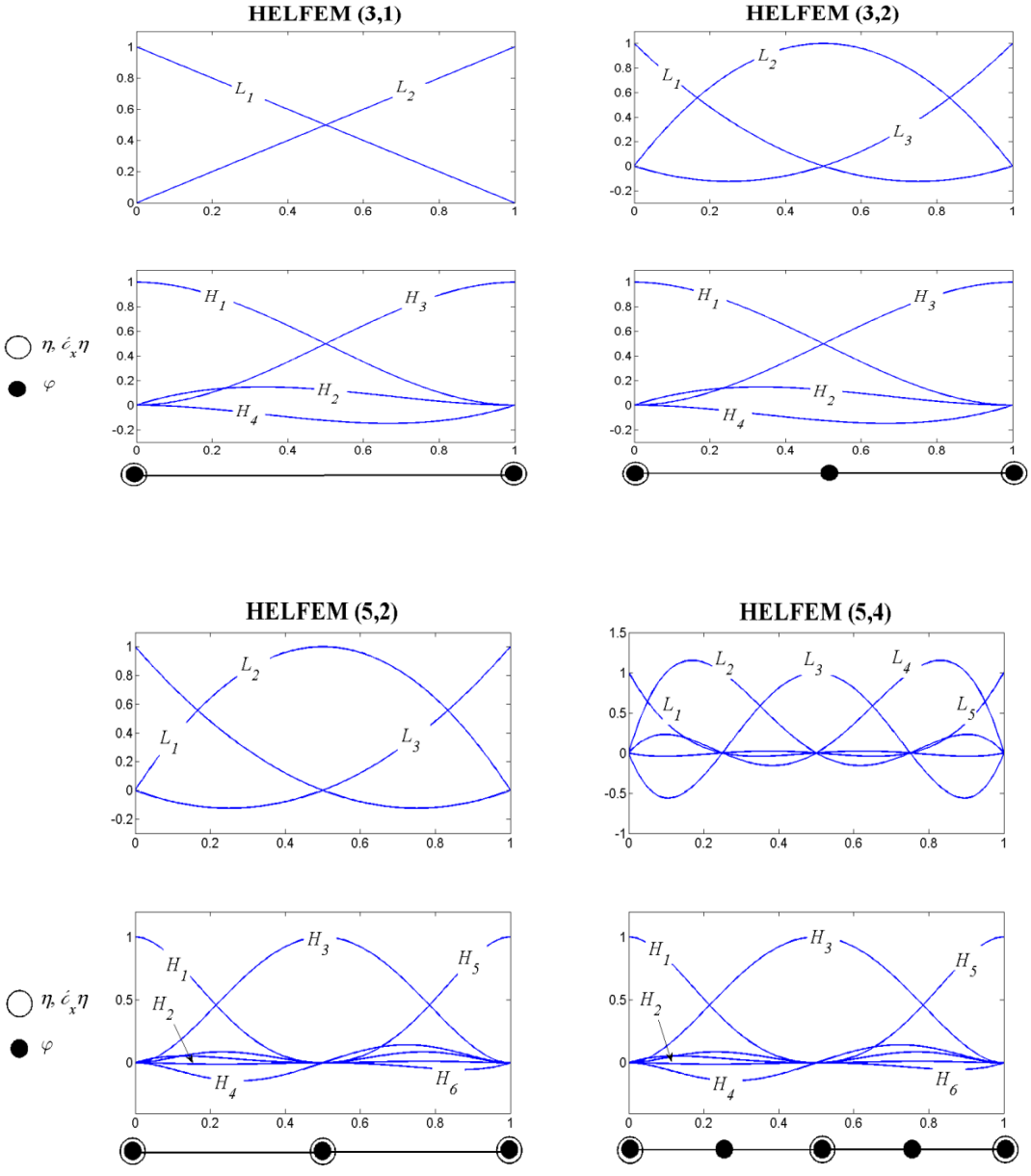

Figure 11 Shape functions for HELFEM (3,1), HELFEM (3,2) and HELFEM (5,2), HELFEM (5,4)

In the following analysis, only elements HELFEM(3,2) and HELFEM(5,4) will be considered, as they appear to exhibit the best balance between simplicity in programming and robustness in the approximation of solutions.

5.2.3 Error Estimates for the Semi-discrete form

In this subsection, error estimates in the energy norm for the semi-discrete form will be derived. To achieve a more compact presentation of the analysis, the error estimate will be proved in for both problems Π_1 and Π_2 in a single result. For this purpose, we introduce the parameter λ such that $\lambda = 0$ for problem Π_1 and $\lambda = 1$ for problem Π_2. The forcing wave is assumed, in both cases, to be generated by a free surface elevation at domain Ω_2. Finally, for simplicity, the notation $(\cdot,\cdot)_{k,\Omega}, \left\| \cdot \right\|_{k,\Omega}, \left| \cdot \right|_{k,\Omega}$ will be used for the inner product, norm and seminorm of $H^k(\Omega)$ respectively.

Assume that V^h is a finite dimensional space of V or $H^2(\Omega_0)$ such that for some integer $r \geq 3$ and $h_0 < 1$ it is,

$$\inf_{u^h \in V^h} \left\| u - u^h \right\|_{0,\Omega_0} + h_0 \left| u - u^h \right|_{1,\Omega_0} + h_0^2 \left| u - u^h \right|_{2,\Omega_0} \leq C h_0^s \left\| u \right\|_{s,\Omega_0}, \text{for } 2 \leq s \leq r$$

when $u \in H^s(\Omega) \cap \mathrm{V}$. Constant r is the order of accuracy of V^h.

Similarly we assume that W_i^h is a finite dimensional subspace of $H^1(\Omega_i), i = 0,1,2$ and $r_0 \geq 2$ such that for $h_i < 1$ it is,

$$\inf_{u^h \in W_i^h} \left\| u - u^h \right\|_0 + h_i \left| u - u^h \right|_1 \leq C h_0^{s_0} \left\| u \right\|_{s_0}, \; 1 \leq s_0 \leq r_0 \text{ when } u \in H^{s_0}(\Omega_i).$$

For the solution of the problem let the following assumption hold,

(A7) Assume that the solution functions of problem Π_1 and Π_2 satisfy the following:

For problem Π_1 it is,

$$\eta \in C^0([0,T];V) \cap C^1([0,T];L^2(\Omega_0)) \cap H^2([0,T];V^*)\ ,$$

$$\varphi_0 \in C^0([0,T];H^1(\Omega_0)),$$

$$\varphi_1 \in C^0([0,T];H^1(\Omega_1)) \cap C^1([0,T];L^2(\Omega_1)) \cap H^2([0,T];H^1(\Omega_1)^*) \text{ and in addition,}$$

$$\partial_{tt}\eta \in L^2(0,T;L^2(\Omega_0)) \text{ and } \eta(t) \in H^s(\Omega_0) \cap V,\ t \in (0,T], s \geq 3,$$

$$\partial_t\varphi_0 \in L^2(0,T;L^2(\Omega_0)) \text{ and } \varphi_0(t) \in H^{s_0}(\Omega_0),\ t \in (0,T], s \geq 2,$$

$$\partial_{tt}\varphi_1 \in L^2(0,T;L^2(\Omega_1)) \text{ and } \varphi_1(t) \in H^{s_0}(\Omega_1),\ t \in (0,T], s_0 \geq 2\,.$$

Finally it is $\eta^h \in H^s(\Omega_0) \cap V^h, \varphi_i^h \in H^{s_0}(\Omega_i), i = 0,1\ ,\ t \in (0,T]$.

For problem Π_2 it is,

$$\eta \in C^0([0,T];H^2(\Omega_0)) \cap C^1([0,T];L^2(\Omega_0)) \cap H^2([0,T];H^2(\Omega_0)^*)\ ,$$

$$\varphi_0 \in C^0([0,T];H^1(\Omega_0)),$$

$$\varphi_1 \in C^0([0,T];H^1(\Omega_1)) \cap C^1([0,T];L^2(\Omega_1)) \cap H^2([0,T];H^1(\Omega_1)^*)$$

$$\varphi_2 \in C^0([0,T];H^1(\Omega_2)) \cap C^1([0,T];L^2(\Omega_2)) \cap H^2([0,T];H^1(\Omega_2)^*) \text{ and in addition,}$$

$$\partial_{tt}\eta \in L^2(0,T;L^2(\Omega_0)) \text{ and } \eta(t) \in H^s(\Omega_0) \cap V,\ t \in (0,T], s \geq 3,$$

$$\partial_t\varphi_0 \in L^2(0,T;L^2(\Omega_0)) \text{ and } \varphi_0(t) \in H^{s_0}(\Omega_0),\ t \in (0,T], s \geq 2,$$

$$\partial_{tt}\varphi_1 \in L^2(0,T;L^2(\Omega_1)) \text{ and } \varphi_1(t) \in H^{s_0}(\Omega_1),\ t \in (0,T], s_0 \geq 2\,,$$

$$\partial_{tt}\varphi_2 \in L^2(0,T;L^2(\Omega_2)) \text{ and } \varphi_2(t) \in H^{s_0}(\Omega_2),\ t \in (0,T], s_0 \geq 2\,.$$

Further assume that $\eta^h \in H^s(\Omega_0) \cap V^h, \varphi_i^h \in H^{s_0}(\Omega_i) \cap W_i^h, i = 0,1\ ,\ t \in (0,T]$.

Let us introduce the quotient space

$$W = H^1(\Omega_0) \setminus \mathbb{R} \doteq\ \ u = v + z \mid v \in H^1(\Omega_0), z \in \mathbb{R}$$

endowed with the quotient norm

$$\left\|u\right\|_W = \inf_{z\in\mathbb{R}} \left\|u+z\right\|_{H^1(\Omega_0)},$$

The following result (see for example [6]) establishes the equivalence of the $H^1(\Omega_0)$ semi-norm and the quotient space norm.

Lemma 2 For every $u\in W$, the quantity $\left|u\right|_{H^1(\Omega_0)}$ is a norm on W, equivalent to the quotient norm $\left\|u\right\|_W$, i.e. there exist a positive constant c_W such that

$$\inf_{r\in\mathbb{R}} \left\|u+r\right\|_{H^1(\Omega_0)} \le c_W \left|u\right|_{H^1(\Omega_0)}, \forall u\in W, \tag{5.9}$$

For the error of the semi-discrete form we have the following estimate,

Theorem 5.1 Let assumption **(A7)** hold and further assume that $\varphi_0(t)\in W, t\in(0,T]$.. Finally, the real parameter λ attains the values $\lambda=0$ and $\lambda=1$ for problems Π_1 and Π_2 respectively. Then, for $h_i<1$, $i=0,1,2$, there exists $c\in\mathbb{R}^+$, $i=0,1,2$, independent of h_i, s, s_0 and $\eta,\varphi_0,\varphi_1,\varphi_2$ such that,

$$\begin{aligned}
&\left\|\partial_t(\eta-\eta^h)\right\|_{0,\Omega_0} + \left\|\eta-\eta^h\right\|_{0,\Omega_9} + h_0^2\left|\eta-\eta^h\right|_{2,\Omega_0} + h_0\left|\varphi_0-\varphi_0^h\right|_{1,\Omega_0}\\
&+\lambda\left\|\partial_t(\varphi_1-\varphi_1^h)\right\|_{0,\Omega_1} + \left\|\partial_t(\varphi_2-\varphi_2^h)\right\|_{0,\Omega_2}\\
&+\lambda h_1\left|\varphi_1-\varphi_1^h\right|_{1,\Omega_1} + h_2\left|\varphi_2-\varphi_2^h\right|_{1,\Omega_2} \le\\
&c\left\|S^h-R^hS\right\|_{0,\Omega_2} + c\left(h_0^s\left\|\eta\right\|_{s,\Omega_0} + \lambda h_1^{s_1}\left\|\varphi_1\right\|_{s_1,\Omega_1} + h_2^{s_2}\left\|\varphi_2\right\|_{s_2,\Omega_2} + h_0^{s_0}\left\|\varphi_0\right\|_{s_0,\Omega_0}\right).\\
&+c\left(h_0^s\left\|\partial_\tau\eta\right\|_{s,\Omega_0} + \lambda h_1^{s_1}\left\|\partial_\tau\varphi_1\right\|_{s_1,\Omega_1} + h_2^{s_2}\left\|\partial_\tau\varphi_2\right\|_{s_2,\Omega_2}\right) + ch_0^s\sqrt{\int_0^t\left\|\partial_{\tau\tau}\eta\right\|_{0,\Omega_0}^2 d\tau}\\
&+\lambda ch_1^{s_1}\sqrt{\int_0^t\left\|\partial_{\tau\tau}\varphi_1\right\|_{0,\Omega_1}^2 d\tau} + ch_2^{s_2}\sqrt{\int_0^t\left\|\partial_{\tau\tau}\varphi_2\right\|_{0,\Omega_2}^2 d\tau} + ch_0^{s_0}\sqrt{\left\|\partial_\tau\varphi_0\right\|_{0,\Omega_0}^2 d\tau}
\end{aligned} \tag{5.10}$$

Proof. Use the Ritz projection R^h to write the error as

$$\eta-\eta^h = y+\psi, \tag{5.11}$$

$$\text{where } y \doteq \eta - R^h \text{ and } \psi \doteq R^h\eta-\eta^h. \tag{5.12}$$

In the same manner it is

$$\varphi_i - \varphi_i^h = y_i + \psi_i \ , \ i = 0,1,2 . \tag{5.13}$$

From the regularity hypotheses and standard elliptic estimates regarding the Ritz projection (see for example [5], [7]) it is

$$\left\|y\right\|_{0,\Omega_0} + h\left|y\right|_{1,\Omega_0} + h_0^2\left|y\right|_{1,\Omega_0} \le Ch_0^s\left\|\eta\right\|_{s,\Omega_0} \ , C \in \mathbb{R}_+ \tag{5.14}$$

$$\left\|y_i\right\|_{0,\Omega_i} + h_i\left|y_i\right|_{1,\Omega_i} \le C_i h_i^{s_0}\left\|\varphi_0\right\|_{s_0,\Omega_i} . \tag{5.15}$$

Similarly we get

$$\left\|\partial_{tt} y\right\|_{0,\Omega_0} \le Ch_0^s\left\|\partial_{tt}\eta\right\|_{s,\Omega_i} , \ \left\|\partial_t y_i\right\|_{0,\Omega_i} \le C_i h_i^{s_0}\left\|\partial_t\varphi_0\right\|_{s_0,\Omega_i} \text{ and } \left\|\partial_{tt} y\right\|_{0,\Omega_i} \le C_i h_i^s\left\|\partial_{tt}\varphi_1\right\|_{s_1,\Omega_i} . \tag{5.16}$$

Setting $v = v^h$, $w_i = w_i^h$ in the variational forms of problems Π_1 and Π_2 and subtracting from the respective continuous variational forms, as presented in *Chapter 4*, we have due to linearity,

$$\begin{aligned} &M\partial_{tt}(\eta - \eta^h), v^h\ _{0,\Omega_0} - \ \partial_t(\eta - \eta^h), w_0^h\ _{0,\Omega_0} + \ \partial_t(\varphi_0 - \varphi_0^h), v^h\ _{0,\Omega_0} \\ &+ \ \partial_{tt}(\varphi_1 - \varphi_1^h), w_1^h\ _{0,\Omega_1} + \ \partial_{tt}(\varphi_2 - \varphi_2^h), w_2^h\ _{0,\Omega_2} \\ &+a(\eta - \eta^h, v^h) + b_0(\varphi_0 - \varphi_0^h, w_0^h) + \lambda b_1(\varphi_1 - \varphi_1^h, w_1^h) + b_2(\varphi_2 - \varphi_2^h, w_2^h) = 0 \end{aligned} \tag{5.17}$$

Using the definition of the Ritz projection

$$a(\eta - \eta^h, v^h) = a(R^h\eta - \eta^h, v^h) = a(\psi, v^h) \ , \tag{5.18}$$

$$b_i(\varphi_i - \varphi_i^h, w_i^h) = b_i(\psi_i, w_i^h), \ \ i = 0,1,2 . \tag{5.19}$$

From (5.17), using (5.18), (5.19) and the error decomposition (5.11) and (5.13)

$$\begin{aligned} &M\partial_{tt}\psi, \partial_t\psi\ _{0,\Omega_0} + \lambda\ \partial_{tt}\psi_1, \partial_t\psi_1\ _{0,\Omega_1} + \ \partial_{tt}\psi_2, \partial_t\psi_2\ _{0,\Omega_2} \\ &+a(\psi, \partial_t\psi) + b_0(\psi_0, \partial_t\psi_0) + b_1(\psi_1, \partial_t\psi_1) + \lambda b_2(\psi_2, \partial_t\psi_2) = \\ &- \ M\partial_{tt} y, \partial_t\psi\ _{0,\Omega_0} + \ \partial_t y, \partial_t\psi_0\ _{0,\Omega_0} - \ \partial_t y_0, \partial_t\psi\ _{0,\Omega_0} \\ &-\lambda\ \partial_{tt} y_1, \partial_t\psi_1\ _{0,\Omega_1} - \ \partial_{tt} y_2, \partial_t\psi_2\ _{0,\Omega_2} \end{aligned} \tag{5.20}$$

Similarly to the proof of the energy conservation principle (see *Chapter 4*) it is,

$$\begin{aligned}
&\frac{1}{2}\frac{d}{d\tau}\left[\left\|M^{1/2}\partial_\tau\psi\right\|^2_{0,\Omega_0}+\lambda\left\|\partial_\tau\psi_1\right\|^2_{0,\Omega_1}+\left\|\partial_\tau\psi_2\right\|^2_{0,\Omega_2}\right]\\
&+\frac{1}{2}\frac{d}{d\tau}\left[a(\psi,\psi)+b_0(\psi_0,\psi_0)+\lambda b_1(\psi_1,\psi_1)+b_2(\psi_2,\psi_2)\right]=\\
&-\ M\partial_{tt}y,\partial_t\psi\ _{0,\Omega_0}+\ \partial_t y,\partial_t\psi_0\ _{0,\Omega_0}-\ \partial_t y_0,\partial_t\psi\ _{0,\Omega_0}\\
&-\ \partial_{tt}y_1,\partial_t\psi_1\ _{0,\Omega_1}-\lambda\ \partial_{tt}y_2,\partial_t\psi_2\ _{0,\Omega_2}
\end{aligned}\tag{5.21}$$

From Young's inequality applied in the L^2 inner products in the right hand side of (5.21)

$$\begin{aligned}
&\frac{1}{2}\frac{d}{d\tau}\left[\left\|M^{1/2}\partial_\tau\psi\right\|^2_{0,\Omega_0}+\lambda\left\|\partial_\tau\psi_1\right\|^2_{0,\Omega_1}+\left\|\partial_\tau\psi_2\right\|^2_{0,\Omega_2}\right]\\
&+\frac{1}{2}\frac{d}{d\tau}\left[a(\psi,\psi)+b_0(\psi_0,\psi_0)+\lambda b_1(\psi_1,\psi_1)+b_2(\psi_2,\psi_2)\right]\le\\
&\left\|M^{1/2}\partial_{\tau\tau}y\right\|^2_{0,\Omega_0}+2\left\|\partial_\tau\psi\right\|^2_{0,\Omega_0}+\left\|\partial_\tau y_0\right\|^2_{0,\Omega_0}+2(\partial_\tau y,\partial_\tau\psi_0)_{0,\Omega_0}\\
&+\lambda\left\|\partial_{\tau\tau}y_1\right\|^2_{0,\Omega_1}+\lambda\left\|\partial_\tau\psi_1\right\|^2_{0,\Omega_1}+\left\|\partial_{\tau\tau}y_2\right\|^2_{0,\Omega_2}+\left\|\partial_\tau\psi_2\right\|^2_{0,\Omega_2}
\end{aligned}\tag{5.22}$$

Integrating (5.22) with respect to τ from $\tau=0$ to $\tau=t$, using initial conditions () and since $M\in L^\infty(\Omega)$.

$$\begin{aligned}
&c_M\left\|\partial_t\psi\right\|^2_{0,\Omega_0}+\lambda\left\|\partial_t\psi_1\right\|^2_{0,\Omega_1}+\left\|\partial_t\psi_2\right\|^2_{0,\Omega_2}\\
&+a(\psi,\psi)+b_0(\psi_0,\psi_0)+\lambda b_1(\psi_1,\psi_1)+b_2(\psi_2,\psi_2)\le\left\|S^h-R^hS\right\|^2_{0,\Omega_1},\\
&+C_M\int_0^t\left\|\partial_{\tau\tau}y\right\|^2_{0,\Omega_0}+\lambda\left\|\partial_{\tau\tau}y_1\right\|^2_{0,\Omega_1}+\left\|\partial_{\tau\tau}y_2\right\|^2_{0,\Omega_2}+\left\|\partial_\tau y_0\right\|^2_{0,\Omega_0}d\tau\\
&+2\int_0^t\left\|\partial_\tau\psi\right\|^2_{0,\Omega_0}+\lambda\left\|\partial_\tau\psi_1\right\|^2_{0,\Omega_1}+\left\|\partial_\tau\psi_2\right\|^2_{0,\Omega_2}dt+2\int_0^t(\partial_\tau y,\partial_\tau y)d\tau
\end{aligned}\tag{5.23}$$

where, as in Chapter 4, $c_M=ess\inf_{x\in[0,\mathrm{L}]}M$.

In order to eliminate $\partial_\tau\psi_0$ form the last term in the rhs of (5.23) so as to employ Gronwall's lemma, we write for $z\in\mathbb{R}$.

$$\begin{aligned}
&\int_0^t(\partial_\tau y,\partial_\tau\psi_0)d\tau=\int_{\Omega_0}\int_0^t\partial_\tau y\partial_\tau(\psi_0+z)d\tau dx\\
&-\int_{\Omega_0}\int_0^t\partial_{\tau\tau}y(\psi_0+z)d\tau dx+\int_{\Omega_0}(\partial_\tau y(\psi_0+z)-\partial_\tau y(0)(\psi_0(0)+z))dx
\end{aligned}\tag{5.24}$$

Select $\partial_t y$ such that $\partial_t y\big|_{t=0}=0$. Finally, interchanging integral signs in (5.24) we have

$$\int_0^t(\partial_\tau y,\partial_\tau\psi_0)d\tau\le\frac{1}{2}\int_0^t\left\|\partial_{\tau\tau}y\right\|^2_{0,\Omega_0}+\left\|\psi_0+z\right\|^2_{0,\Omega_0}dt+\int_{\Omega_0}\partial_\tau y(\psi_0+z)dx\tag{5.25}$$

Using the modified Young's inequality with $p = q = 2$, $\varepsilon > 0$

$$\int_0^t (\partial_\tau y, \partial_\tau \psi_0) d\tau \leq \frac{1}{2}\int_0^t \left\|\partial_{\tau\tau} y\right\|_{0,\Omega_0}^2 + \inf_{z\in\mathbb{R}} \left\|\psi_0 + z\right\|_{0,\Omega_0}^2 dt + \frac{1}{2\varepsilon}\left\|\partial_\tau y\right\|_{0,\Omega_0}^2 + \frac{\varepsilon}{2}\inf_{z\in\mathbb{R}} \left\|\psi_0 + z\right\|_{0,\Omega_0}^2 \quad . \tag{5.26}$$

From inequality (5.26), and the norm definition in the quotient space W inequality (5.23) becomes

$$\begin{aligned}
&c_M \left\|\partial_t \psi\right\|_{0,\Omega_0}^2 + \lambda \left\|\partial_t \psi_1\right\|_{0,\Omega_1}^2 + \left\|\partial_t \psi_2\right\|_{0,\Omega_2}^2 \\
&+c_K \left|\psi\right|_{2,\Omega_0}^2 + \left\|\psi\right\|_{0,\Omega_1}^2 + \lambda c_B \left|\psi_1\right|_{1,\Omega_1}^2 + c_B \left|\psi_2\right|_{1,\Omega_2}^2 \leq \left\|S^h - R^h S\right\|_{0,\Omega_1}^2 \\
&+C_M \int_0^t \left\|\partial_{\tau\tau} y\right\|_{0,\Omega_0}^2 + \lambda \left\|\partial_{\tau\tau} y_1\right\|_{0,\Omega_1}^2 + \left\|\partial_{\tau\tau} y_2\right\|_{0,\Omega_2}^2 + \left\|\partial_\tau y_0\right\|_{0,\Omega_0}^2 d\tau \quad . \\
&+2\int_0^t \left\|\partial_\tau \psi\right\|_{0,\Omega_0}^2 + \lambda \left\|\partial_\tau \psi_1\right\|_{0,\Omega_1}^2 + \left\|\partial_\tau \psi_2\right\|_{0,\Omega_2}^2 dt \\
&+\int_0^t \left\|\partial_{\tau\tau} y\right\|_{0,\Omega_0}^2 + \left\|\psi_0\right\|_W^2 dt + \varepsilon^{-1}\left\|\partial_\tau y\right\|_{0,\Omega_2}^2 + \varepsilon\left\|\psi_0\right\|_W^2
\end{aligned} \tag{5.27}$$

From lemma 2 it is

$$\begin{aligned}
&c_M \left\|\partial_t \psi\right\|_{0,\Omega_0}^2 + \lambda \left\|\partial_t \psi_1\right\|_{0,\Omega_1}^2 + \left\|\partial_t \psi_2\right\|_{0,\Omega_2}^2 \\
&+c_K \left|\psi\right|_{2,\Omega_0}^2 + \left\|\psi\right\|_{0,\Omega_1}^2 + c_W c_B \left\|\psi_0\right\|_W^2 + \lambda c_B \left|\psi_1\right|_{1,\Omega_1}^2 + c_B \left|\psi_2\right|_{1,\Omega_2}^2 \leq \left\|S^h - R^h S\right\|_{0,\Omega_1}^2 \\
&+C_M \int_0^t \left\|\partial_{\tau\tau} y\right\|_{0,\Omega_0}^2 + \lambda \left\|\partial_{\tau\tau} y_1\right\|_{0,\Omega_1}^2 + \left\|\partial_{\tau\tau} y_2\right\|_{0,\Omega_2}^2 + \left\|\partial_\tau y_0\right\|_{0,\Omega_0}^2 d\tau \quad . \\
&+2\int_0^t \left\|\partial_\tau \psi\right\|_{0,\Omega_0}^2 + \lambda \left\|\partial_\tau \psi_1\right\|_{0,\Omega_1}^2 + \left\|\partial_\tau \psi_2\right\|_{0,\Omega_2}^2 dt \\
&+\int_0^t \left\|\partial_{\tau\tau} y\right\|_{0,\Omega_0}^2 + \left\|\psi_0\right\|_W^2 dt + \varepsilon^{-1}\left\|\partial_\tau y\right\|_{0,\Omega_2}^2 + \varepsilon\left\|\psi_0\right\|_W^2
\end{aligned} \tag{5.28}$$

Select now $\varepsilon < c_W c_B$ to get

$$\begin{aligned}
&C_a \left(\left\|\partial_t \psi\right\|_{0,\Omega_0}^2 + \lambda \left\|\partial_t \psi_1\right\|_{0,\Omega_1}^2 + \left\|\partial_t \psi_2\right\|_{0,\Omega_2}^2\right) \\
&+C_a \left(\left|\psi\right|_{2,\Omega_0}^2 + \left\|\psi\right\|_{0,\Omega_1}^2 + \left\|\psi_0\right\|_W^2 + \lambda\left|\psi_1\right|_{1,\Omega_1}^2 + \left|\psi_2\right|_{1,\Omega_2}^2\right) + \leq C_b \left\|S^h - R^h S\right\|_{0,\Omega_1}^2 \\
&+C_b \left(\left\|\partial_\tau y\right\|_{0,\Omega_0}^2 + \int_0^t \left\|\partial_{\tau\tau} y\right\|_{0,\Omega_0}^2 + \lambda \left\|\partial_{\tau\tau} y_1\right\|_{0,\Omega_1}^2 + \left\|\partial_{\tau\tau} y_2\right\|_{0,\Omega_2}^2 + \left\|\partial_\tau y_0\right\|_{0,\Omega_0}^2 d\tau\right) , \\
&+C_b \left(\int_0^t \left\|\partial_\tau \psi\right\|_{0,\Omega_0}^2 + \lambda \left\|\partial_\tau \psi_1\right\|_{0,\Omega_1}^2 + \left\|\partial_\tau \psi_2\right\|_{0,\Omega_2}^2 d\tau + \int_0^t \left\|\psi_0\right\|_W^2 dt\right)
\end{aligned} \tag{5.29}$$

where $C_a = \min(1, c_B, c_W c_B - \varepsilon, c_K)$ and $C_b = \max(2, \varepsilon^{-1}, C_M + 1)$

Application of Gronwall's lemma yields

$$\begin{aligned}&\left\|\partial_t\psi\right\|_{0,\Omega_0}^2+\lambda\left\|\partial_t\psi_1\right\|_{0,\Omega_1}^2+\left\|\partial_t\psi_2\right\|_{0,\Omega_2}^2\\&+\left|\psi\right|_{2,\Omega_0}^2+\left\|\psi\right\|_{0,\Omega_1}^2+\left\|\psi_0\right\|_W^2+\lambda\left|\psi_1\right|_{1,\Omega_1}^2+\left|\psi_2\right|_{1,\Omega_2}^2\le\\&C\left\|S^h-R^hS\right\|_{0,\Omega_1}^2\\&+C\left(\left\|\partial_\tau y\right\|_{0,\Omega_0}^2+\int_0^t\left\|\partial_{\tau\tau}y\right\|_{0,\Omega_0}^2+\lambda\left\|\partial_{\tau\tau}y_1\right\|_{0,\Omega_1}^2+\left\|\partial_{\tau\tau}y_2\right\|_{0,\Omega_2}^2+\left\|\partial_\tau y_0\right\|_{0,\Omega_0}^2d\tau\right)\end{aligned},\quad(5.30)$$

where $C=C_a^{-1}C_be^{C_a^{-1}C_bT}$.

Using again the equivalence of the quotient norm and the H^1 semi-norm in the quotient space W, inequality (5.30) becomes

$$\begin{aligned}&\left\|\partial_t\psi\right\|_{0,\Omega_0}^2+\lambda\left\|\partial_t\psi_1\right\|_{0,\Omega_1}^2+\left\|\partial_t\psi_2\right\|_{0,\Omega_2}^2\\&+\left|\psi\right|_{2,\Omega_0}^2+\left\|\psi\right\|_{0,\Omega_9}^2+C_1\left|\psi_0\right|_{1,\Omega_0}^2+\lambda\left|\psi_1\right|_{1,\Omega_1}^2+\left|\psi_2\right|_{1,\Omega_2}^2\le\\&C\left\|S^h-R^hS\right\|_{0,\Omega_1}^2\\&+C\left(\left\|\partial_\tau y\right\|_{0,\Omega_0}^2+\int_0^t\left\|\partial_{\tau\tau}y\right\|_{0,\Omega_0}^2+\lambda\left\|\partial_{\tau\tau}y_1\right\|_{0,\Omega_1}^2+\left\|\partial_{\tau\tau}y_2\right\|_{0,\Omega_2}^2+\left\|\partial_\tau y_0\right\|_{0,\Omega_0}^2d\tau\right)\end{aligned}.\quad(5.31)$$

From the norm equivalence in $\mathbb{R}^{6+2\lambda}$, it is

$$\begin{aligned}&\left\|\partial_t\psi\right\|_{0,\Omega_0}+\lambda\left\|\partial_t\psi_1\right\|_{0,\Omega_1}+\left\|\partial_t\psi_2\right\|_{0,\Omega_2}\\&+\left|\psi\right|_{2,\Omega_0}+\left\|\psi\right\|_{0,\Omega_9}+\left|\psi_0\right|_{1,\Omega_0}+\lambda\left|\psi_1\right|_{1,\Omega_1}+\left|\psi_2\right|_{1,\Omega_2}\le\\&\tilde{c}\left\|S^h-R^hS\right\|_{0,\Omega_1}\\&+\tilde{c}\left(\left\|\partial_\tau y\right\|_{0,\Omega_0}+\sqrt{\int_0^t\left\|\partial_{\tau\tau}y\right\|_{0,\Omega_0}^2+\lambda\left\|\partial_{\tau\tau}y_1\right\|_{0,\Omega_1}^2+\left\|\partial_{\tau\tau}y_2\right\|_{0,\Omega_2}^2+\left\|\partial_\tau y_0\right\|_{0,\Omega_0}^2d\tau}\right)\end{aligned},\quad(5.32)$$

with $\tilde{c}=\sqrt{(6+2\lambda)\min(1,C_1)C_a^{-1}C_be^{C_a^{-1}C_bT}}$.

Now, add the appropriate terms from the elliptic projection estimates, defined through relations (5.16), into both sides of inequality (5.32). In this way, both the terms, in which the error was decomposed, appear in the left hand side of inequality (5.32). Using the triangle inequality, the fact that $h_i<1,\ i=0,1,2$ and the standard elliptic estimates for the Ritz projection error, we finally derive

$$\begin{aligned}
&\left\|\partial_t(\eta-\eta^h)\right\|_{0,\Omega_0}+\lambda\left\|\partial_t(\varphi_1-\varphi_1^h)\right\|_{0,\Omega_1}+\left\|\partial_t(\varphi_2-\varphi_2^h)\right\|_{0,\Omega_2}+h_0^2\left|\eta-\eta^h\right|_{2,\Omega_0}\\
&+\left\|\eta-\eta^h\right\|_{0,\Omega_9}+h_0\left|\varphi_0-\varphi_0^h\right|_{1,\Omega_0}+\lambda h_1\left|\varphi_1-\varphi_1^h\right|_{1,\Omega_1}+h_2\left|\varphi_2-\varphi_2^h\right|_{1,\Omega_2}\le\\
&c\left\|S^h-R^hS\right\|_{0,\Omega_2}+c\left(Ch_0^s\left\|\eta\right\|_{s,\Omega_0}+\lambda C_1h_1^{s_1}\left\|\varphi_1\right\|_{s_1,\Omega_1}+C_2h_2^{s_2}\left\|\varphi_2\right\|_{s_2,\Omega_2}+C_0h_0^{s_0}\left\|\varphi_0\right\|_{s_0,\Omega_0}\right)\\
&+c\left(Ch_0^s\left\|\partial_\tau\eta\right\|_{s,\Omega_0}+\lambda C_1h_1^{s_1}\left\|\partial_\tau\varphi_1\right\|_{s_1,\Omega_1}+C_2h_2^{s_2}\left\|\partial_\tau\varphi_2\right\|_{s_2,\Omega_2}\right)+ch_0^s\sqrt{\int_0^t\left\|\partial_{\tau\tau}\eta\right\|_{0,\Omega_0}^2d\tau}\\
&+\lambda ch_1^{s_1}\sqrt{\int_0^t\left\|\partial_{\tau\tau}\varphi_1\right\|_{0,\Omega_1}^2d\tau}+ch_2^{s_2}\sqrt{\int_0^t\left\|\partial_{\tau\tau}\varphi_2\right\|_{0,\Omega_2}^2d\tau}+ch_0^{s_0}\sqrt{\left\|\partial_\tau\varphi_0\right\|_{0,\Omega_0}^2d\tau}
\end{aligned}\tag{5.33}$$

and the theorem is proven. □

A more exhaustive analysis on error estimate procedures can be found in [5], [6] and [7].

5.3 Finite element implementation

The semi-descrite formulations of the problems (5.1) and (5.3) will be revisited. The approximations employed for HELFEM (3,1) will be substituted into the above in order to derive the corresponding system of differential equations. Linear Lagrange shape functions will be employed for the approximation of the velocity potential in the free-surface water regions. First degree polynomials are merely chosen to match with HELFEM (3,1) approximation of the velocity potential for the hydroelastic regions, any other degree can be easily incorporated. Hence by direct substitution of (5.5) and (5.6) in (5.1) the following is deduced,

$$\begin{aligned}
&\int_{e(\Omega_o)}\begin{bmatrix}\mathrm{H}_1\\ \mathrm{H}_2\\ \mathrm{H}_3\\ \mathrm{H}_4\end{bmatrix}\mathrm{M}(x)\begin{bmatrix}\mathrm{H}_1 & \mathrm{H}_2 & \mathrm{H}_3 & \mathrm{H}_4\end{bmatrix}\begin{bmatrix}\ddot{\eta}_1\\ \ddot{\theta}_1\\ \ddot{\eta}_2\\ \ddot{\theta}_2\end{bmatrix}dx+\int_{e(\Omega_o)}\begin{bmatrix}\mathrm{H}_1\\ \mathrm{H}_2\\ \mathrm{H}_3\\ \mathrm{H}_4\end{bmatrix}\begin{bmatrix}L_1 & 0 & L_2 & 0\end{bmatrix}\begin{bmatrix}\dot{\varphi}_0^1\\ 0\\ \dot{\varphi}_0^2\\ 0\end{bmatrix}dx\\
&-\int_{e(\Omega_o)}\begin{bmatrix}L_1\\ 0\\ L_2\\ 0\end{bmatrix}\begin{bmatrix}L_1 & 0 & L_2 & 0\end{bmatrix}\begin{bmatrix}\dot{\varphi}_0^1\\ 0\\ \dot{\varphi}_0^2\\ 0\end{bmatrix}dx+\int_{e(\Omega_o)}\begin{bmatrix}L_1\\ 0\\ L_2\\ 0\end{bmatrix}\begin{bmatrix}L_1 & 0 & L_2 & 0\end{bmatrix}\begin{bmatrix}\ddot{\varphi}_2^1\\ 0\\ \ddot{\varphi}_2^2\\ 0\end{bmatrix}dx
\end{aligned}$$

$$+\int_{e(\Omega_o)}\begin{bmatrix}\mathrm{H}_1''\\ \mathrm{H}_2''\\ \mathrm{H}_3''\\ \mathrm{H}_4''\end{bmatrix}K(x)\begin{bmatrix}\mathrm{H}_1'' & \mathrm{H}_2'' & \mathrm{H}_3'' & \mathrm{H}_4''\end{bmatrix}\begin{bmatrix}\eta_1\\ \theta_1\\ \eta_2\\ \theta_2\end{bmatrix}dx+\int_{e(\Omega_o)}\begin{bmatrix}\mathrm{H}_1\\ \mathrm{H}_2\\ \mathrm{H}_3\\ \mathrm{H}_4\end{bmatrix}\begin{bmatrix}\mathrm{H}_1 & \mathrm{H}_2 & \mathrm{H}_3 & \mathrm{H}_4\end{bmatrix}\begin{bmatrix}\eta_1\\ \theta_1\\ \eta_2\\ \theta_2\end{bmatrix}dx$$

$$+\int_{e(\Omega_o)}B(x)\begin{bmatrix}L_1'\\ 0\\ L_2'\\ 0\end{bmatrix}\begin{bmatrix}L_1' & 0 & L_2' & 0\end{bmatrix}\begin{bmatrix}\varphi_0^1\\ 0\\ \varphi_0^2\\ 0\end{bmatrix}dx+\int_{e(\Omega_1)}B(x)\begin{bmatrix}L_1'\\ 0\\ L_2'\\ 0\end{bmatrix}\begin{bmatrix}L_1' & 0 & L_2' & 0\end{bmatrix}\begin{bmatrix}\varphi_2^1\\ 0\\ \varphi_2^2\\ 0\end{bmatrix}dx$$

$$=\int_{e(\Omega_o)}Q(x)\begin{bmatrix}\mathrm{H}_1\\ \mathrm{H}_2\\ \mathrm{H}_3\\ \mathrm{H}_4\end{bmatrix}dx$$

Now, by arranging the vector of element unknowns as,

$x=\begin{bmatrix}\eta_1 & \theta_1 & \eta_2 & \theta_2 & \varphi_0^1 & \varphi_0^2 & \varphi_2^1 & \varphi_2^2\end{bmatrix}^{\mathrm{T}}$, the above is reduced to the form,

$$\mathbf{M}_{loc}\ddot{x}+\mathbf{C}_{loc}\dot{x}+\mathbf{K}_{loc}x=\mathbf{F}, \tag{5.34}$$

where $\mathbf{M}_{loc}$, $\mathbf{C}_{loc}$ and $\mathbf{K}_{loc}$ stand for the element mass, damping and stiffness matrices. It is important to observe that the element mass matrices are singular in every case. By enforcing a global numbering on the nodes the local element matrices are used in order to assembly the global equation,

$$\mathbf{M}_{\mathrm{g}lob}\ddot{x}+\mathbf{C}_{glob}\dot{x}+\mathbf{K}_{glob}x=\mathbf{F}_{glob} \tag{5.35}$$

The technical aspects of the global matrices assembly are left out from the present work. The reader is directed to the relevant literature [1], [2].

5.4 Time integration schemes

The general form (5.12) represents a system of N unknowns, which is the number of the finite elements used for the analysis times the number of dofs per element. The computational problem at hand, rises from the fact that the nodal unknowns at every point in time need to be calculated given their values at some initial time.

As already mentioned the peculiar form of the global mass matrix does not allow the direct inversion of $\mathbf{M}_{glob}$, hence the use of implicit integration schemes is essential. In this study, time marching techniques like implicit Euler, Crank Nicolson and the Newmark method were used. Some introductory comments on the above methods are provided for completeness. The reader is again directed to the relevant bibliography, provided at the end of the chapter.

Implicit Euler, Crank Nicolson and Radau II are all members of the Runge-Kutta family, for the integration of 1st order ODEs. Equation (5.35) is transformed into a first order system by assuming $y = \dot{x}$.

$$\mathbf{A}\dot{U} = \mathbf{B}U + f \tag{5.36}$$

where $\mathbf{A} = \begin{bmatrix} \mathbf{M}_{glob} & \mathbf{0} \\ \mathbf{0} & -\mathbf{I} \end{bmatrix}$, $B = -\begin{bmatrix} \mathbf{C}_{glob} & \mathbf{K}_{glob} \\ \mathbf{I} & \mathbf{0} \end{bmatrix}$ and $U = [x \quad y]$.

The implicit Euler method can be derived through the integration of (5.13) and the use of the left hand rectangle method for derivative approximation,

$$\int_{t_i}^{t_{i+1}} [A]\{\dot{U}\}dt = \int_{t_i}^{t_{i+1}} [B]\{U\}dt + \int_{t_i}^{t_{i+1}} \{f\}dt \Leftrightarrow U_{i+1} = U_i + [A]^{-1}[B]U_{i+1}dt + [A]^{-1}\{f\}dt$$

which yields,

$$U_{i+1} = \left([A] - [B]dt\right)^{-1}\left([A]U_i + \{f\}dt\right) \tag{5.37}$$

The method is 1st degree accurate and L-stable.

The Crank-Nicolson scheme is accordingly derived through the use of the trapezoidal rule

$$\int_{t_i}^{t_{i+1}} [A]\{\dot{U}\}dt = \int_{t_i}^{t_{i+1}} [B]\{U\}dt + \int_{t_i}^{t_{i+1}} \{f\}dt \Leftrightarrow U_{i+1} = U_i + [A]^{-1}[B](U_{i+1} + U_i)\frac{dt}{2} + [A]^{-1}\{f\}dt$$

hence,

$$U_{i+1} = \left([A] - [B]\frac{dt}{2}\right)^{-1}\left(\left([A] + [B]\frac{dt}{2}\right)U_i + \{f\}dt\right) \tag{5.38}$$

Crank-Nicolson is an A-stable, 2nd degree accurate method.

The second order system (5.35) can be directly integrated using an algorithm from the Newmark family of methods. The unknowns at step $n+1$ are given by,

$$\ddot{x}_{n+1} = (x_{n+1} - x_n)/\beta\, dt^2 - \dot{x}_{n+1}/\beta\, dt - (1 - 1/2\beta)\ddot{x}_n, \tag{5.39}$$

$$\dot{x}_{n+1} = (x_{n+1} - x_n)\gamma/\beta\, dt^2 - (\gamma/\beta - 1)\dot{x}_n - (\gamma/2\beta - 1)dt\ddot{x}_n. \tag{5.40}$$

Parameters β and γ define the specific method. For values, $2\beta \geq \gamma \geq 1/2$ the methods are implicit and A-stable.

Substituting (5.39), (5.40) into $\mathbf{M}_{glob}\ddot{x}_{n+1} + \mathbf{C}_{glob}\dot{x}_{n+1} + \mathbf{K}_{glob}x_{n+1} = \mathbf{F}_{glob}$, the unknown displacement x_{n+1} can be calculated at a given timestep.

5.5 Validation of the finite element code

In the present section a procedure exploiting the eigenfunction expansion technique presented by Sturova [3], will attempt to validate the developed finite element code. The author considers that the account of Sturova's method in the first section of the chapter is essential for reader's comprehension. Using the presented technique as a benchmark solution a comparison will follow

5.5.1 Eigenfunction expansion method for a freely floating heterogeneous plate.

Sturova [3] presents a problem tailored technique for the calculation of the time-dependent response of a heterogeneous, thin floating plate under long wave excitation. The floating plate is considered to expand infinitely in the $y-$direction, hence a vertical two-dimensional reduction is possible.

The plate is considered to be neutrally buoyant. The bottom is assumed flat for the free water surface regions while bathymetry is given by $h(x) = H(x) - d(x)$. The schematic of the configuration is shown below,

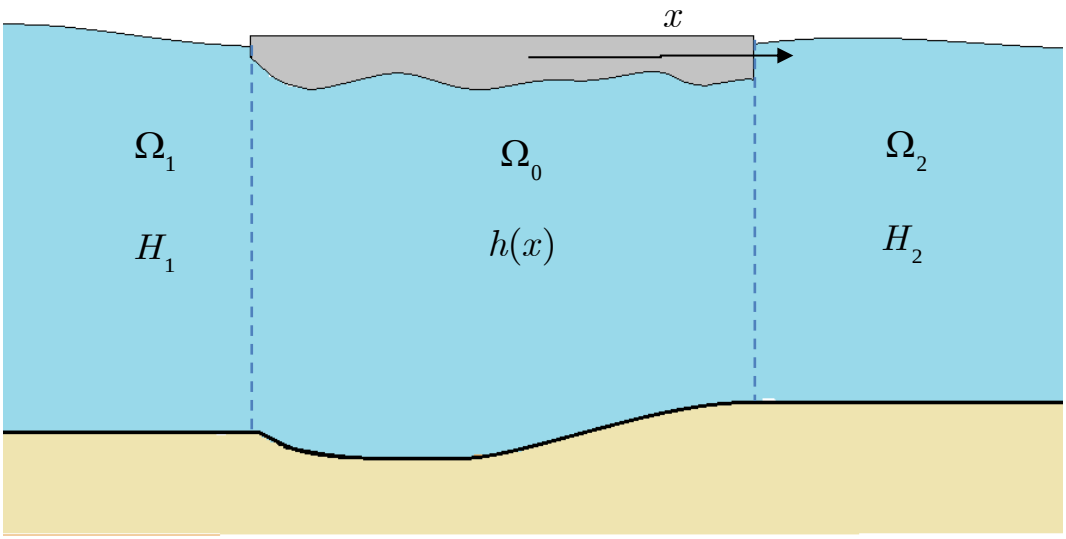

Figure 12 Schematic diagram of the hydroelastic problem solved in [3].

Under the shallow water assumption the system of equations reduce to the presented case of Π_1 (see 3.2.2). For reference the non-dimensional system becomes,

in a subsequent section.

$$\partial_{tt}\varphi_1 - H_1 L^{-1}\partial_{xx}\varphi_1 = 0 \text{ , in } \Omega_1 \times (0,T] \tag{5.41}$$

$$M(x)\partial_{tt}\eta + \partial_{xx}(K(x)\partial_{xx}\eta) + \eta + \partial_t\varphi_0 = Q(x,t) \text{ , in } \Omega_0 \times (0,T] \tag{5.42}$$

$$\partial_t\eta + \partial_x(h(x)\partial_x\varphi_0) = 0 \text{ , in } \Omega_0 \times (0,T] \tag{5.43}$$

$$\partial_{tt}\varphi_2 - H_2 L^{-1}\partial_x\varphi_2 = 0 \text{ , in } \Omega_2 \times (0,T] \tag{5.44}$$

The boundary conditions at the free edges of the plate are expressed as,

$$\partial_{xx}\eta(-1,t) = \partial_{xxx}\eta(-1,t) = 0, \tag{5.45}$$

$$\partial_{xx}\eta(1,t) = \partial_{xxx}\eta(1,t) = 0. \tag{5.46}$$

The interface conditions now become,

$$h(-1)\partial_x\varphi_0(-1,t) = H_1\partial_x\varphi_1(-1,t), \tag{5.47}$$

$$\partial_t\varphi_0(-1,t) = \partial_t\varphi_1(-1,t) \quad \text{and} \tag{5.48}$$

$$h(1)\partial_x\varphi_0(1,t) = H_2\partial_x\varphi_2(1,t), \tag{5.49}$$

$$\partial_t\varphi_0(1,t) = \partial_t\varphi_2(1,t) \tag{5.50}$$

The method of solution seeks the response of the plate as an expansion in the eigenfunctions of the free- free beam in vacuum . Hence ,

$$\eta(x,t)=\sum_{n=0}^{\infty}T_n(t)W_n(x). \tag{5.51}$$

The eigenfunctions W_n are calculated in the domain $[-1,1]$ in a standard mathematical procedure. The reader is directed to [4].

By substituting (5.51) in the beam equation (5.42) and by integrating over length, the following is derived,

$$\begin{aligned}&\sum_{0}^{\infty}\left[T_n\left(\int_{-1}^{1}K(x)\partial_{xx}W_m\partial_{xx}W_n dx+\delta_{nm}\right)+\ddot{T}_n\left(\int_{-1}^{1}M(x)W_mW_n dx\right)\right].\\&+\int_{-1}^{1}\partial_t\varphi_0 W_m=-\int_{-1}^{1}Q(x,t)W_m\end{aligned} \tag{5.52}$$

The velocity potential in the coupling region must satisfy equation (5.43), hence an acceptable form for φ_0 is,

$$\varphi_0(x,t)=\sum_{0}^{\infty}\partial_t T_n\psi_n+Q(x)u(t)+v(t). \tag{5.53}$$

where $\psi_n=\int_0^x\frac{V_n(\xi)}{h(\xi)}d\xi$ or equivalently $\psi_n'=-\frac{V_n(\xi)}{h(\xi)}$, $Q(x)=\int_0^x\frac{1}{h(\xi)}d\xi$ and $V_n=\partial_t W_n$.

The excitation if provided by an initial disturbance of the free water surface in region Ω_2. The disturbance is divided into two propagating waves in opposite directions, featuring zero dispersion. Ultimately, the wave propagating along the x direction towards the plate will have a velocity potential of the form $\psi_0(x+\sqrt{H_2}t)$ while the free surface displacement will be $\zeta_0(x+\sqrt{H_2}t)$. It also holds that $\zeta_0=\sqrt{H_2}\partial_x\psi_0$

Given the above, the solution for $\varphi_2(x,t)$ is given by,

$$\varphi_2(x,t)=\psi_0(x+\sqrt{H_2}t)+\psi(x,t) \tag{5.54}$$

,where $\psi_0(x+\sqrt{H_2}t)$ is the velocity potential of the propagating wave and $\psi(x,t)$ is the velocity potential of the reflected wave

$$\psi(x,t)=\begin{cases}A\left(t-\dfrac{x-1}{\sqrt{H_2}}\right) & ,1<x<1+\sqrt{H_2}t\\ 0 & ,x>1+\sqrt{H_2}t\end{cases}. \tag{5.55}$$

In region Ω_1 the velocity potential of the transmitted wave is given as ,

$$\phi_1(x,t) = \begin{cases} B\left(\dfrac{x+1}{\sqrt{H_1}} + t\right) & ,-(1+\sqrt{H_1}t) < x < -1 \\ 0 & ,x < -(1+\sqrt{H_1}t) \end{cases} \tag{5.56}$$

Equations (5.54), (5.55), (5.56) and (5.53) are used in order to reconstruct the interface conditions (5.47) - (5.50). It holds that,

$$-\sum_0^\infty \partial_t T_n V_n(-1) + u(t) = \sqrt{H_1}\partial_x B \tag{5.57}$$

$$\sum_0^\infty \partial_{tt} T_n \psi_n(-1) + Q(-1)\partial_t u(t) + \partial_t v(t) = \partial_t B \tag{5.58}$$

$$-\sum_0^\infty \partial_t T_n V_n(1) + u(t) = \sqrt{H_2}\ \zeta_0 - \partial_x A \tag{5.59}$$

$$\sum_0^\infty \partial_{tt} T_n \psi_n(1) + Q(1)\partial_t u(t) + \partial_t v(t) = \zeta_0 + \partial_t \mathrm{A} \tag{5.60}$$

In compliance with the above the third term of the left hand side of (5.) can be rewritten as,

$$\int_{-1}^{1} \frac{\partial \phi_0}{\partial t} W_m = \int_{-1}^{1} \left(\sum_0^\infty \partial_{tt} T_n \psi_n + Q(x)\partial_t u(t) + \partial_t v(t) \right) W_m \tag{5.61}$$

Equations (5.57)-(5.60) can be solved for $\partial_t v$, resulting in

$$\partial_t v = \left(\sum_0^\infty \partial_t T_n V_n(1) + u \right) H_2^{-1/2} - \sum_0^\infty \partial_{tt} T_n \psi_n(1) - Q(1)u + 2\zeta_0 \,. \tag{5.62}$$

Equation (5.62) can be substituted in (5.61) and in turn in (5.52). One will immediately realise that finding the response of the plate in now subject to the calculation of $u(t)$ and T_n .

When a vector of unknowns is defined as $x = \begin{bmatrix} T_0 & \ldots & T_{n-1} & u \end{bmatrix}^T$, the problem is reduced to a form identical to (5.35) and any of the time marching techniques mentioned can be utilised in the calculation of the plate response.

5.5.2 Comparison of the finite element solution and the eigenfunction expansion method [3] .

The technique developed by Sturova can be used to validate the finite element solution. A freely floating plate with 500 m length, which correspondes to the length of domain Ω_0 in

problem Π_2, is examined. The plate has variable thickness given by the function $F(x) = 1 + 0.5(1 + x)$ and floats over a flat shallow bottom.. An initial disturbance in the plate, of the form $\eta_0 = 0.5 + 0.5\cos(x - 5)$, is assumed. As time progresses, the initial disturbance dissipates through the elastic plate and into to the adjacent fluid layer regions. A total of 40 modes is used for the modal expansion technique in order to ensure convergence A total of 20 HELFEM (5,4) elements were used for the FE solution. Figure 13 shows the excellent agreement between the two methods.

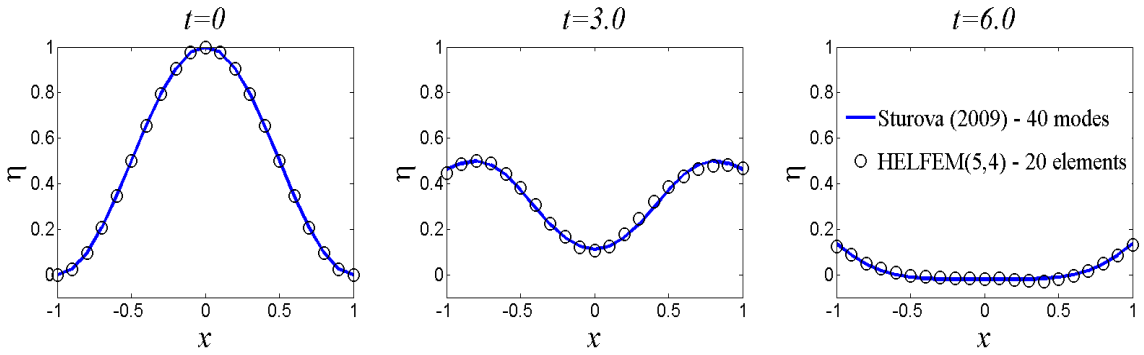

Figure 13 Comparison between the FE solution and the eigenfunction expansion method presented in [3]

References

[1] Hughes, J. R. (2000) *The Finite Element Method: Linear Static and Dynamic Finite Element Analysis*, Dover Publications.

[2] Bathe, K. J. (1996) *Finite Element Procedures*, Michigan: Prentice-Hall

[3] Sturova, I. V. (2009) Time-dependent response of a heterogeneous elastic plate floating on shallow water of variable bathymetry, *Journal of Fluid Mechanics (637)*, p. 305-325.

[4] Timoshenko, S. (1928) *Vibration Problems in Engineering*, New York: D. Van Nostrand Company Inc.

[5] Kardestuncer H. (1987) *Finite Element handbook*, US: Mc.Graw-Hill, Inc.

[6] Athinson, K & Han, W. (2000) *Theoretical Numerical Analysis a functional analysis framework*, New York: Springer Science and Business Media, Inc.

[7] Grossmann, C., Roos H. & Stynes, M. (2000) *Numerical Treatment of Partial Differential Equations*, Berlin: Springer-Verlag Berlin Heidelberg.

CHAPTER 6

Results and Discussion

In this section the results of the finite element model will be presented. Two examples will be used in the study of t problems Π_1 *and* Π_2**.** *In addition the results presented at the European Geosciences Union Assembly will be discussed and finally, a case study of the Sulzberger Ice Shelf will be investigated in order to illustrate the geophysical application of the model.*

6.1 Initial conditions

The initial conditions in the following examples are provided in the form of an initial Heaviside pulse. A Heaviside pulse provides a reasonable mathematical expression of the physical phenomena like sea bottom dislocation [1] or a storm surge [3]. In the first case, a section of the sea bottom is uplifted due to a seismic event; the sudden uplift, produces the same form of disturbance on the surface, (*see* figure 14) In the case of storm surges, low pressure weather systems cause the ocean surface to rise. Both phenomena are identified as causes of long wave generation. The ocean surface disturbance generates waves propagating in all directions, which are considered long. The solution to the one dimensional wave equation, valid for the fluid layer under shallow water theory assumptions (refer to *section 2.1*), will form two linear waves propagating in opposite

directions. Since their superposition must provide the initial pulse, the amplitude of each of the generated waves is half of the one initially provided.

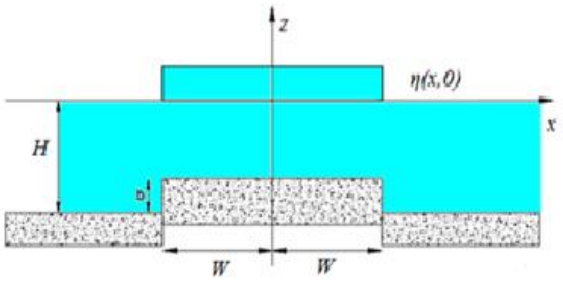

Figure 14 Sea bottom dislocation generating an ocean surface disturbance

However, a mollified Heaviside function is used in the following examples in order to ease the computational demands of the problem and provide more realistic initial conditions for the hydroelastic problem. The initial upper surface elevation (see figure 15) is given as,

$$\eta_0 = \mathrm{A} e^{-x^{-\mu(x_0+w^2)}} e^{-x^{-\mu(x-x_0+w)(x-x_0-w)}} \quad , \tag{6.1}$$

where x_0 is the location and w is the half wavelength of the heaviside pulse. The positive constant μ is a parameter controlling the smoothness of the function. With a decreasing μ the pulse assumes a bell-like shape, while as the parameter increases the step function is generated.

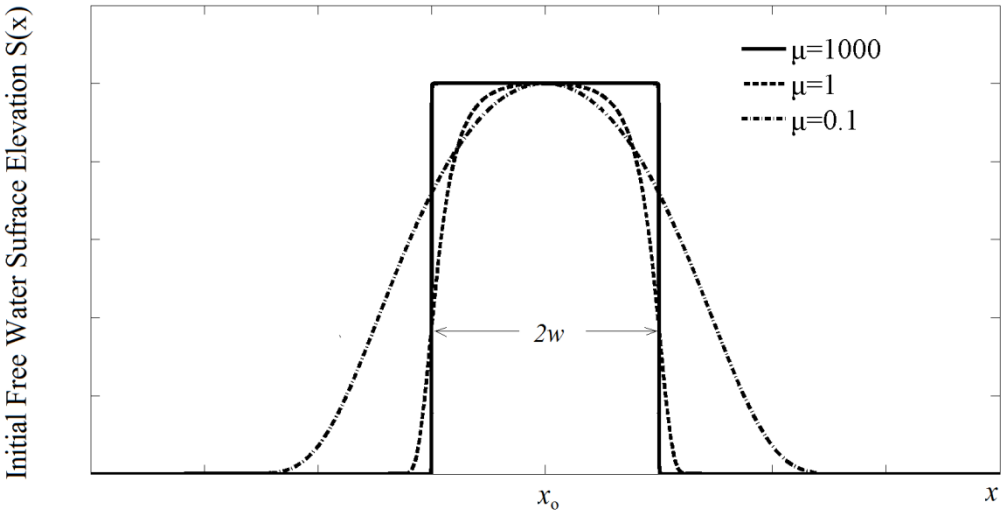

Figure 15 Initial upper surface elevation.

6.2 Example Π_1

The finite element solution of the problem Π_1, for a given configuration is examined below. A length of 1 km is chosen for the cantilever. The bathymetry is assumed to vary linearly underneath the plate, beginning from as shallow as 10 m and reaching 20 m. The bathymetry in the free water region, Ω_2 is considered flat. The thickness of the cantilever decreases from 4 m at the fixed end to 2 m at the free end. The configuration is shown in the figure 16.

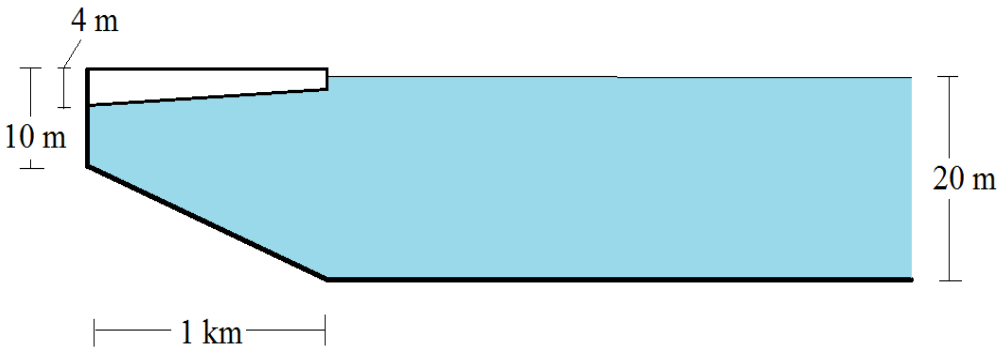

Figure 16 Configuration for example Π_1

The initial excitation was given by (6.1), with $\mu = 50$, $w = 100$ and $A = 0,2\,\text{m}$.

For the calculation of the plate transient response, 100 HELFEM (5,4) were employed. Time integration was performed by means of the Crank-Nicolson scheme. A total of 8000 time increments was used.

Figure 17 provides a visual representation of the upper surface elevation against time. The snapshots in figure 18 picturing a time-series of upper surface elevation, shows important details of the solution. The initial pulse, generated in region Ω_2, is separated into two propagating waves in opposite directions. Each wave, propagating in constant speed, features half the amplitude of the initial disturbance. The form of the linear wave propagating to the left, remains intact as no dispersive effects apply, as depicted by the linear trail left by the compilation of snapshots in figure 17. Hence, any noticeable deviation in wave amplitude is attributed to computational error. The formation of the

travelling waves is also visible in the first three snapshots $(t = 1, 2 \text{ and } 3)$ of figure 18.The wave that impacts the freely-floating plate is partially reflected. Reflected waves are visible as smaller trails travelling to the right in figure 17 while they are less noticeable in figure 18 due to their small amplitude compared to the main wave. After the impact, wave passes under the plate and the hydroelastic wave begins to propagate.

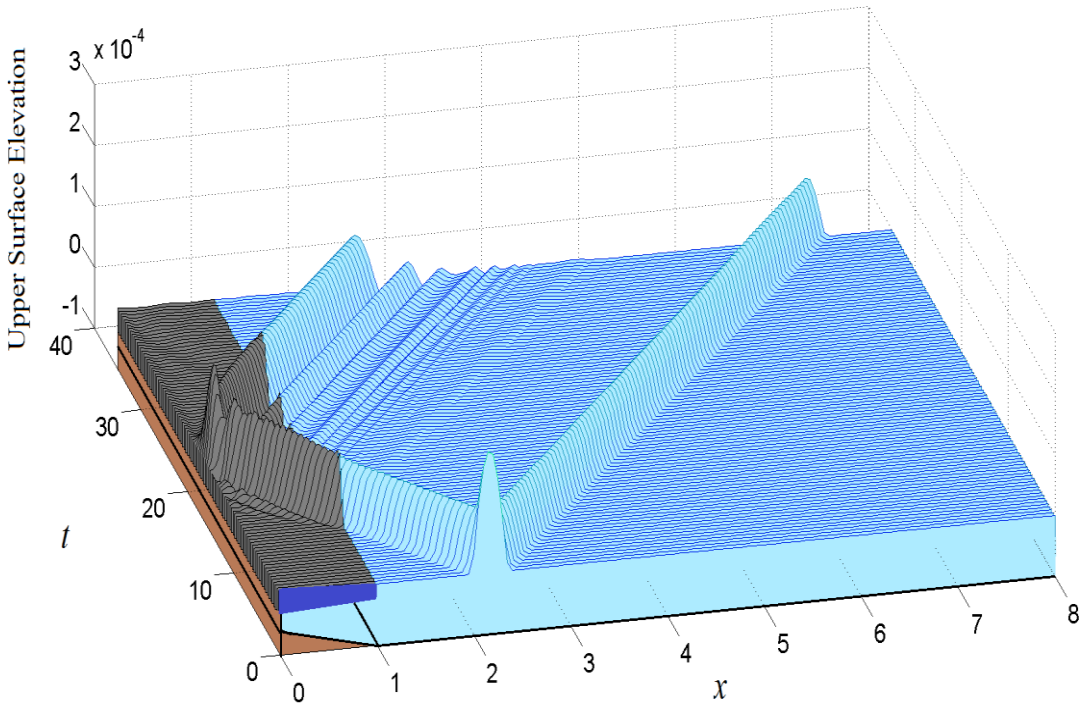

Figure 17 Space-time plot of the wave propagation, for example Π_1 (floating cantilever)

Signs of dispersion are immediately visible, as smaller amplitude waves precede the main pulse within the solid. Dispersive effects are particularly visible in $t = 4 \sim 17$ of figure 18.

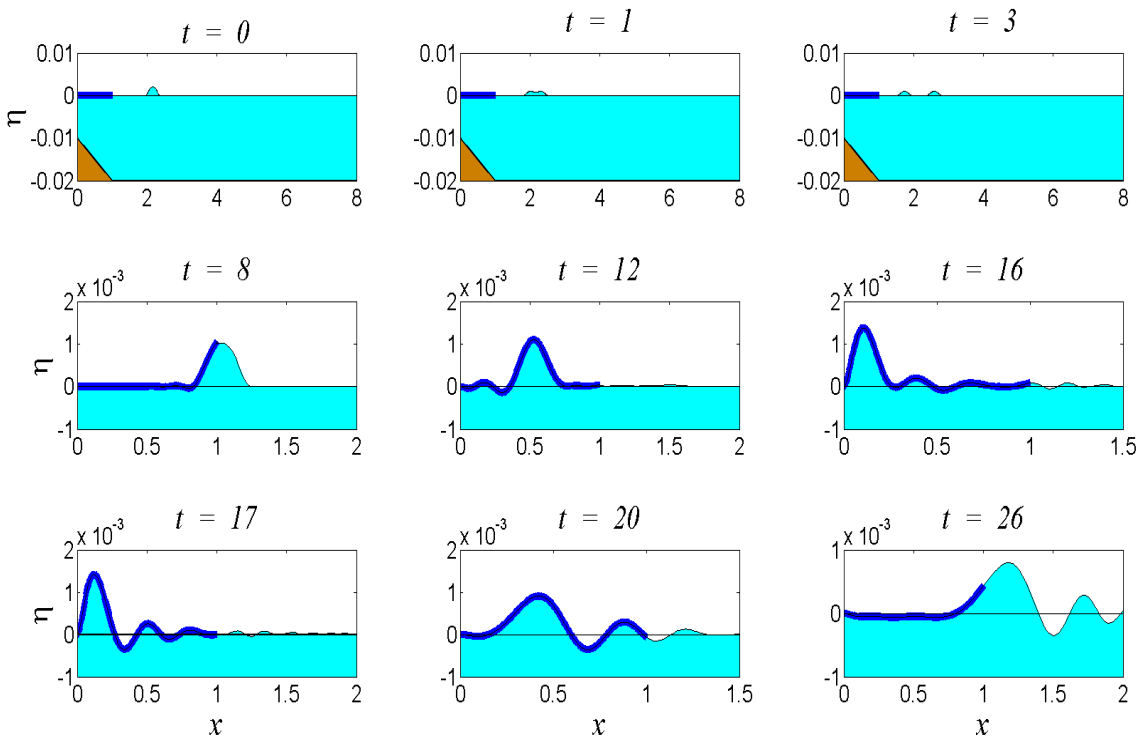

Figure 18 Solution for the upper surface elevation/displacement at distinct moments in time

In figure 17 shorter waves seem to generate and propagate at a different speed as soon as the wave impacts the plate, i.e. enters domain Ω_0.

When the, hydroelastic wave reaches the fixed boundary, it is fully reflected and propagates away from plate. Due to the dispersion of the wave, smaller amplitude waves have reached the boundary and reflected before the main pulse. The impact of the main pulse with the fixed boundary is visible in $t = 16{,}17$ of fig. 18. The train of smaller waves propagating away from the plate into the fluid region are clearly visible in both figures.

Three of the snapshots in figure 18, namely $t = 8{,}12$ and 17 are accompanied by the distributions of bending moment and shear force along the length of the plate at the given moments in time, shown in figure 19. The excitation is seen to propagate in the plate, towards the fixed boundary from (a) to (c). At (a) the pulse impacts the plate, causing the propagation of flexural waves. Flexural waves carry a shift in curvature resulting in variations in bending moment and shear force distributions. In (b) the main pulse has traversed approximately half the length of the plate, while the dispersed waves preceding it have almost reached the fixed-edge. In (c) the main pulse is seen to impact the boundary.

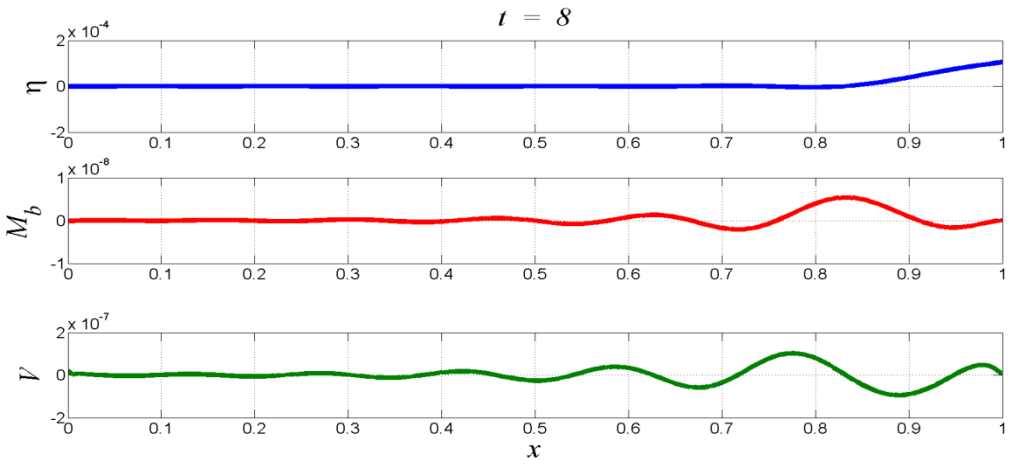

(a)

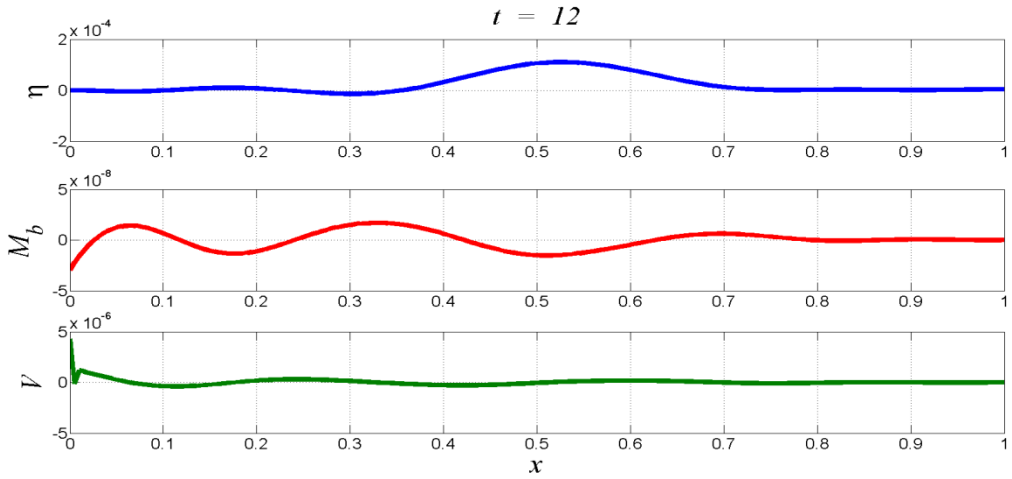

(b)

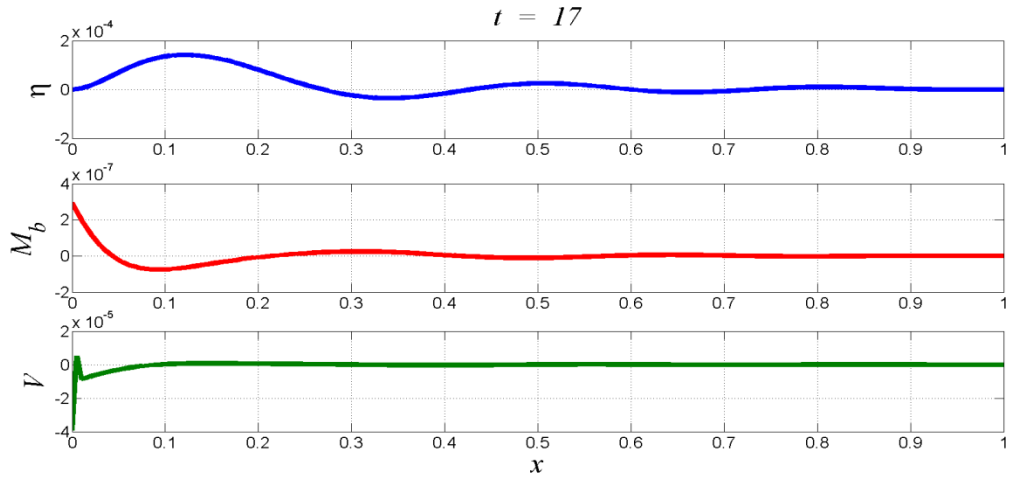

(c)

Figure 19 Deflection, bending moment and shear force profiles at $t = 8,12$ and 17

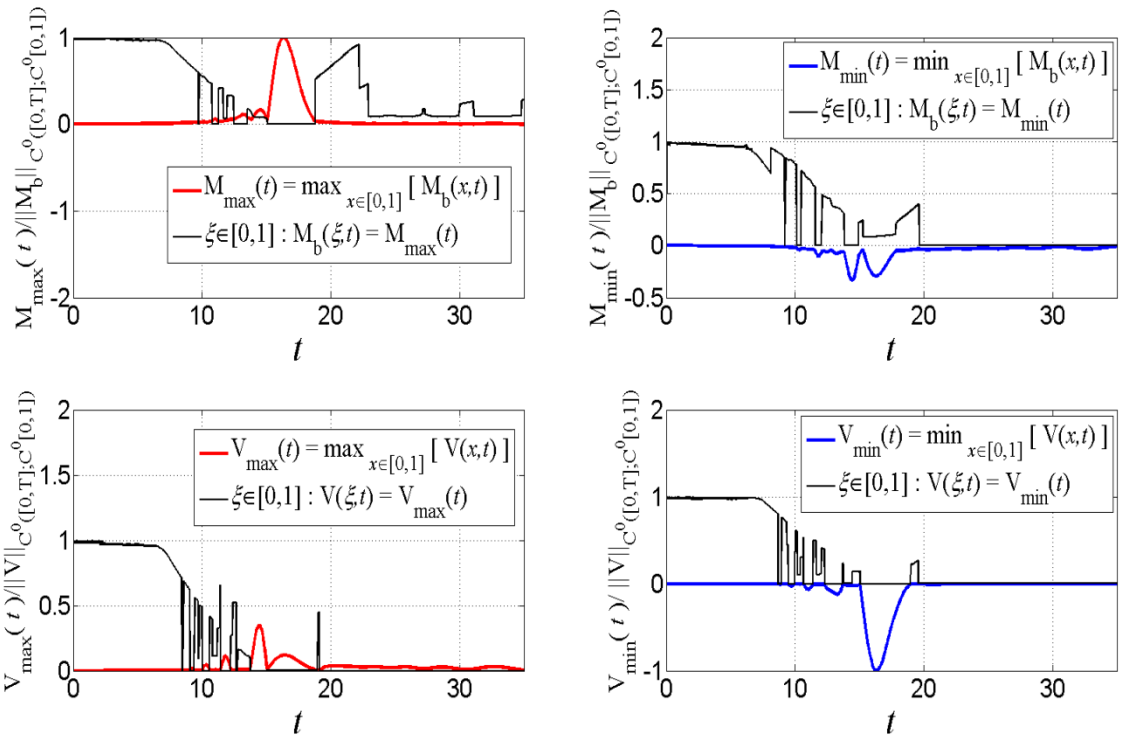

Figure 20 Maximum bending moment and hear force values and their location, against time

Both the maximum bending moment and shear force values seem to increase as the flexural wave propagates.

Figure 20 provides additional information by showing the spatial distributions of the non-dimensional bending moment and shear force extreme values against time. The non-dimensionalisation was carried out to the maximum bending moment and shear force value accordingly. The extrema location is given as a function of the non-dimensional variable ξ denoted by the black line. The figure clearly shows that the maximum values in both shear force and bending moment occur at the fixed end, where $\xi = 0$. Positive or hogging moment effects are seen to be dominant, while the maximum shear force is negative.

The energy conservation principle, presented in *Chapter 4*, is illustrated in figure 21. Prior to the impact with the free edge of the cantileaver plate, the non-dimentional energy is solely comprised by the energy of the waves propagating in domain Ω_2 and is given by the quantity *(blue, dash-dotted line)*,

$$\left\|\partial_t \varphi_2\right\|^2_{L^2(\Omega_2)} + b_2(\varphi_2, \varphi_2) \tag{6.2}$$

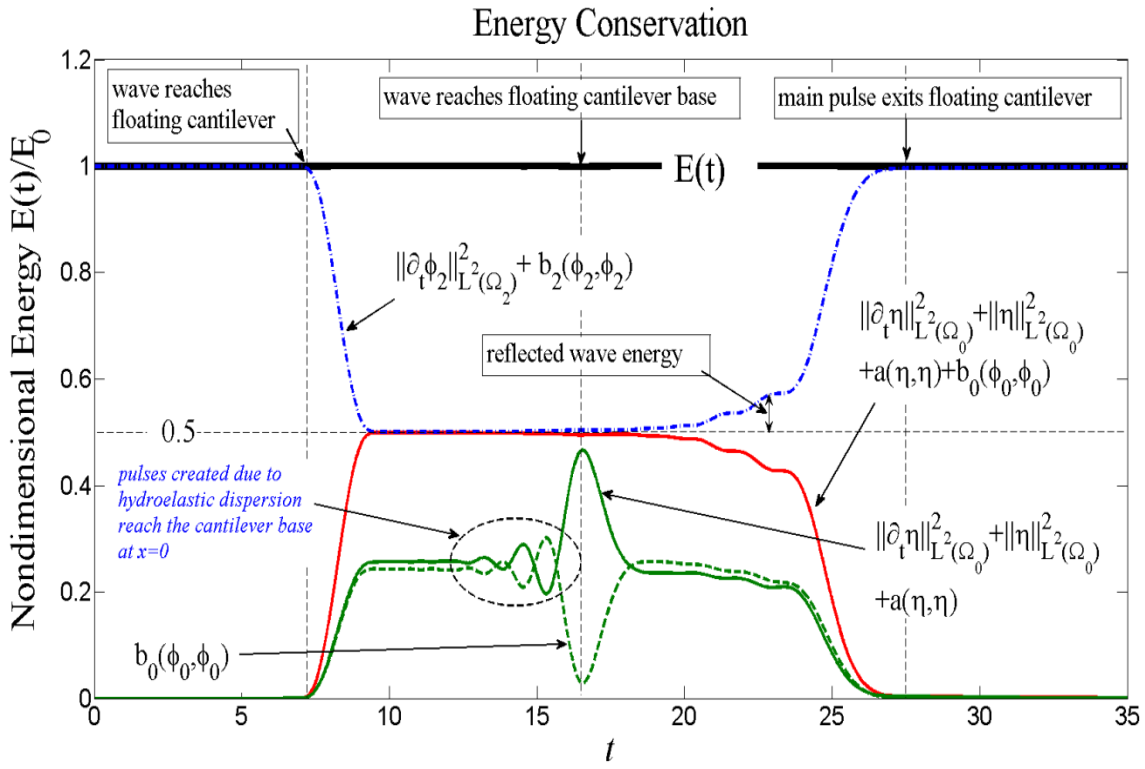

Figure 21 The energy conservation principle for problem Π_1 (floating cantilever)

After the impact, the non-dimensional energy is equally divided between domains Ω_0 and Ω_2. In the fluid region, the linear wave propagating to the positive of the x axis gives rise to the quantity in (6.1). As the second wave enters Ω_0, the energy inflow is divided between the energy of the hydroelastic wave *(green, continuous line)* given by the quantity,

$$\left\|\partial_t \eta\right\|^2_{L^2(\Omega_0)} + \left\|\eta\right\|^2_{L^2(\Omega_0)} + a(\eta,\eta) \tag{6.3}$$

and the energy of the wave propagating in the fluid underneath the plate in Ω_0 *(green dashed line)* which is identified as,

$$b_0(\varphi_0,\varphi_0) \tag{6.4}$$

The superposition of the two curves gives the total non-dimensional energy in Ω_0 *(red continuous line)*. The symmetrical oscillations of the quantities (6.3) and (6.4), seen in figure (3) are due to the impact of the preceding dispersed waves and the main pulse. Close to the fixed edge, the maximum bending moment increases which in turn increases the

hydroelastic energy. Simultaneously an increase in elastic energy is translated into a reduction on wave energy. The phenomenon is observed with every impact at the fixed boundary.

As seen in figure 21, the total energy is divided equally between Ω_0 and Ω_1, a fact that is easily explained through the formation of identical linear waves, after the initial pulse. Moments after the impact with the free-edge of the plate and the inflow of energy in the hydroelasticity dominated region, discrepancies are visible and the total energy in not equally divided. An increase of the total energy in Ω_1 is shown due to the reflected wave re-entering the domain. In fact, as it is observed in figure 21, the total energy in Ω_0 is slowly decreasing up to the impact of the main hydroelastic pulse with the fixed boundary. This decrease is attributed to the initial reflected wave at the free end and the reflection of the smaller, dispersed waves. After the impact, as the larger dispersed waves preceding closely the main pulse are propagating away, into Ω_1 the drop in energy is sharper.

6.3 Example Π_2

In this section an example of a freely floating plate over variable bathymetry will be examined. Domains Ω_1 and Ω_2 are taken as 3000 m and 6000 m long, respectively. The length of the floating plate is assumed to be 1000 m. The water depth in Ω_1 is considered constant at 10 m, while in Ω_0 the depth increases linearly from 10 to 20 m which is taken as the constant depth in Ω_2. The thickness of the plate is taken as constant at 4 m. The configuration is shown in the figure below,

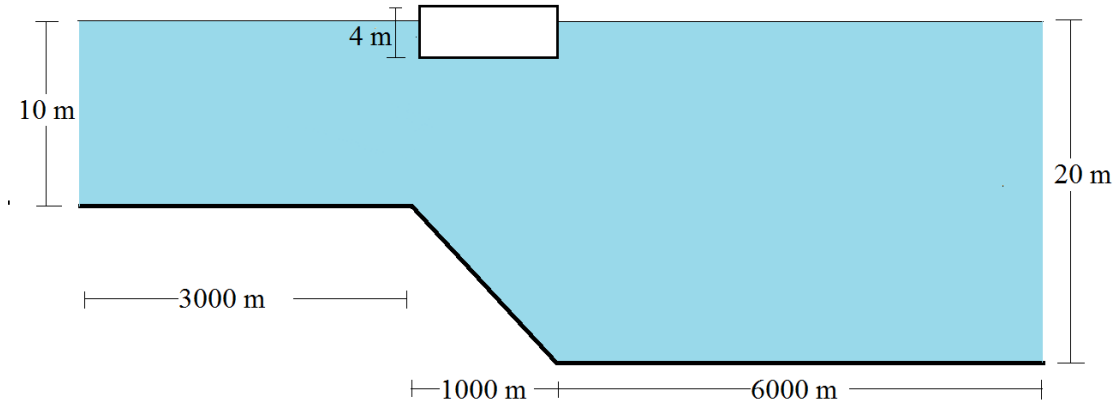

Figure 22 Configuration for example Π_2

The initial excitation was given by (6.1), with $\mu = 50$, $w = 100$ and $A = 0,2\,\mathrm{m}$.

The response was approximated by the use of 300, 100 and 600 finite elements in the regions Ω_1, Ω_0 and Ω_2. HELFEM (5,4) was employed for the hydroelasticity-dominated region Ω_2 while 4th order Lagrange elements were used in the free water surface regions. As seen in the previous example, the initial surface excitation forms two travelling waves. The wave propagating to the right, impacts the freely floating plate and then exits into a second free surface water region. The same visual representation of the upper surface elevation against time given for Π_1, is provided in figure 23.Snapshots of the surface elevation in various moments in time are shown in figure 24. In figure 23, the same linear trail is observed for the wave propagation in the positive x axis away from.

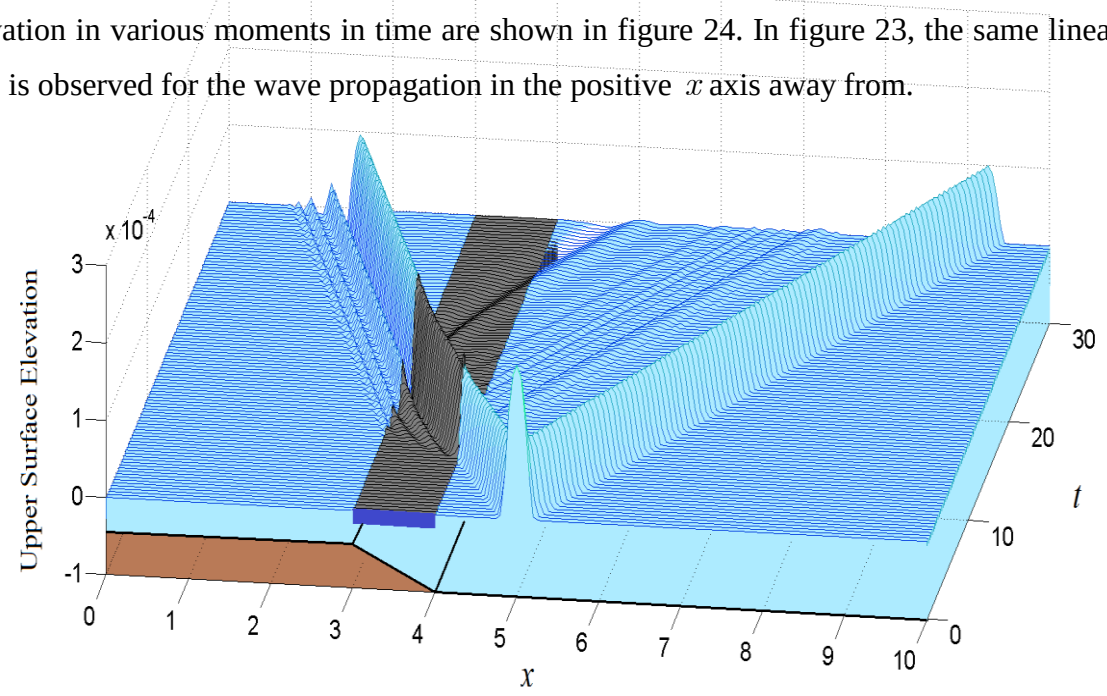

Figure 23 Space-time plot of the wave propagation, for example Π_2 (floating plate)

Upon impact with the free edge of the plate, the incoming wave is partially reflected. As it was before, the reflected waves are visible in figure 23 propagating away from the plate and into Ω_2. As the hydroelastic wave propagates in the plate it becomes dispersed. Signs of dispersion are visible in both figures. In figure 23, there are clear signs of waves propagating in a different speed, preceding the main excitation inside the plate. These smaller waves exit Ω_0 as the larger wave follows. The dispersion of the hydroelastic wave is clearly visible in $t = 4 \sim 16$ of figure 24.

It is observed that the wave train in Ω_1 propagates at a smaller speed, exhibited by the sharply inclined trajectory, compared with the one propagating in Ω_2.

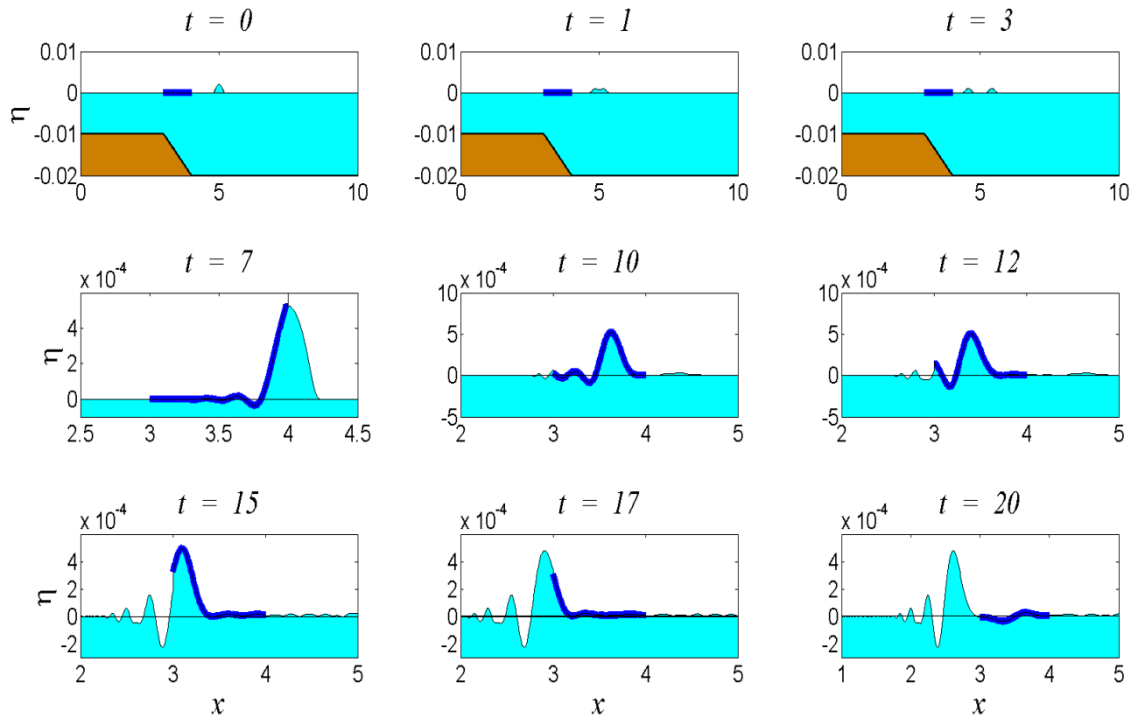

Figure 24 Solution for the upper surface elevation/displacement at distinct moments in time

Distributions of the bending moment and shear force for $t = 7, 12 \text{ and } 17$ are shown in figure 25. Once again the wave is seen to impact the plate at (a). In (b) the wave has traversed half of the plate length and is finally seen to exit the plate at (c).The change in curvature due to the flexural wave propagation gives the corresponding bending moment and shear force profiles. Maximum values for both quantities seem to occur at the vicinity of $t = 12$. A more complete picture regarding the bending moment and shear force extrema are given in figure 26.

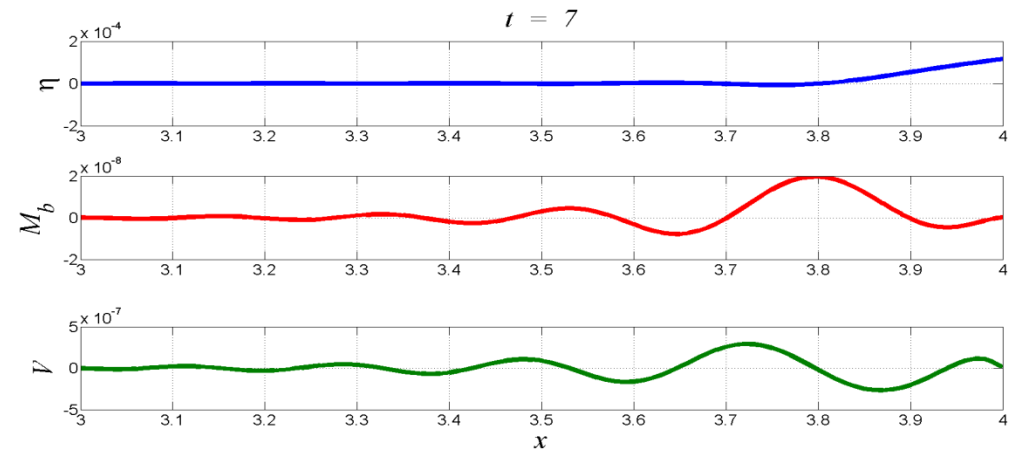

(a)

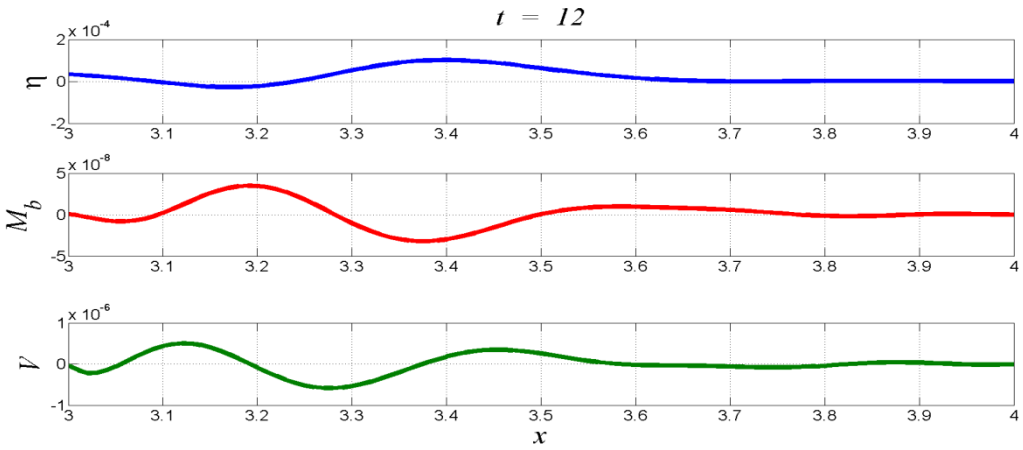

(b)

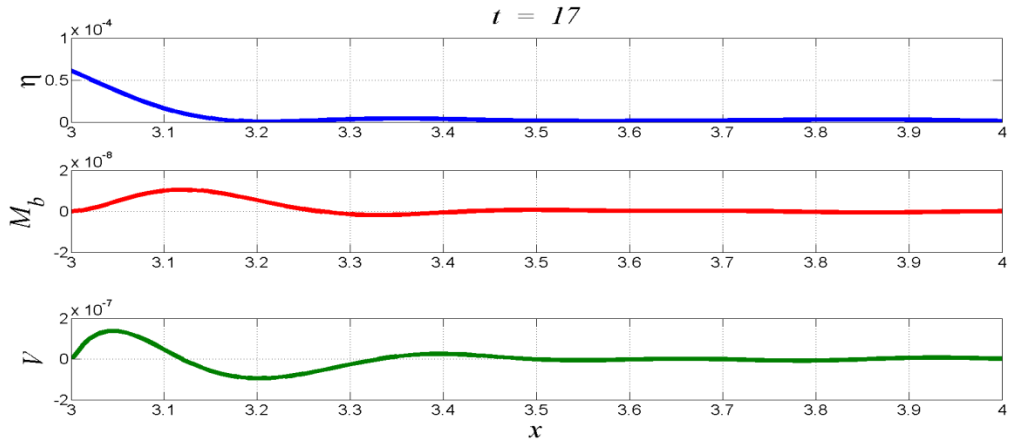

(c)

Figure 25 Elevation, bending moment and shear force profiles at $t = 7,12$ and17

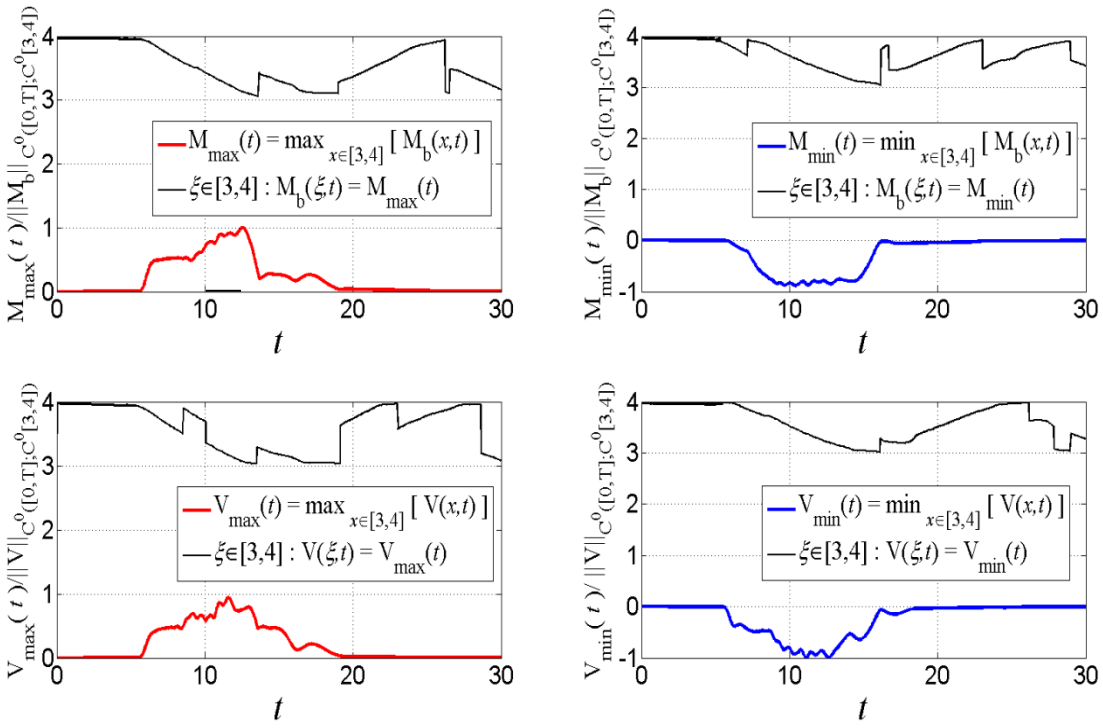

Figure 26 Maximum bending moment and hear force values and their location, against time

Once again the extrema location is given as a function of the non-dimensional variable ξ denoted by the black line. Both bending moment and shear force maximum values seem to occur at $t = 12 - 13$.

It can be observed that positive and negative bending moment values are of the same magnitude, as is the case for the shear force.

The energy conservation principle presented in a previous section is illustrated, for the given example, in figure 27. The non-dimensional energy shown in the y axis initially amounts to the energy of the propagating waves in region Ω_2 (blue dot-dashed line) represented by the quantity

$$\left\| \partial_t \phi \right\|^2_{L^2(\Omega_2)} + b_2(\phi_2, \phi_2) \ . \tag{6.5}$$

After the impact on the floating strip at $t \simeq 3{,}5$, the total non-dimensional energy is given by the equal sum of the wave energy still propagating in Ω_2 the energy of the hydroelastic wave in the elastic plate and the fluid in Ω_2 (continuous red line) given by the quantity

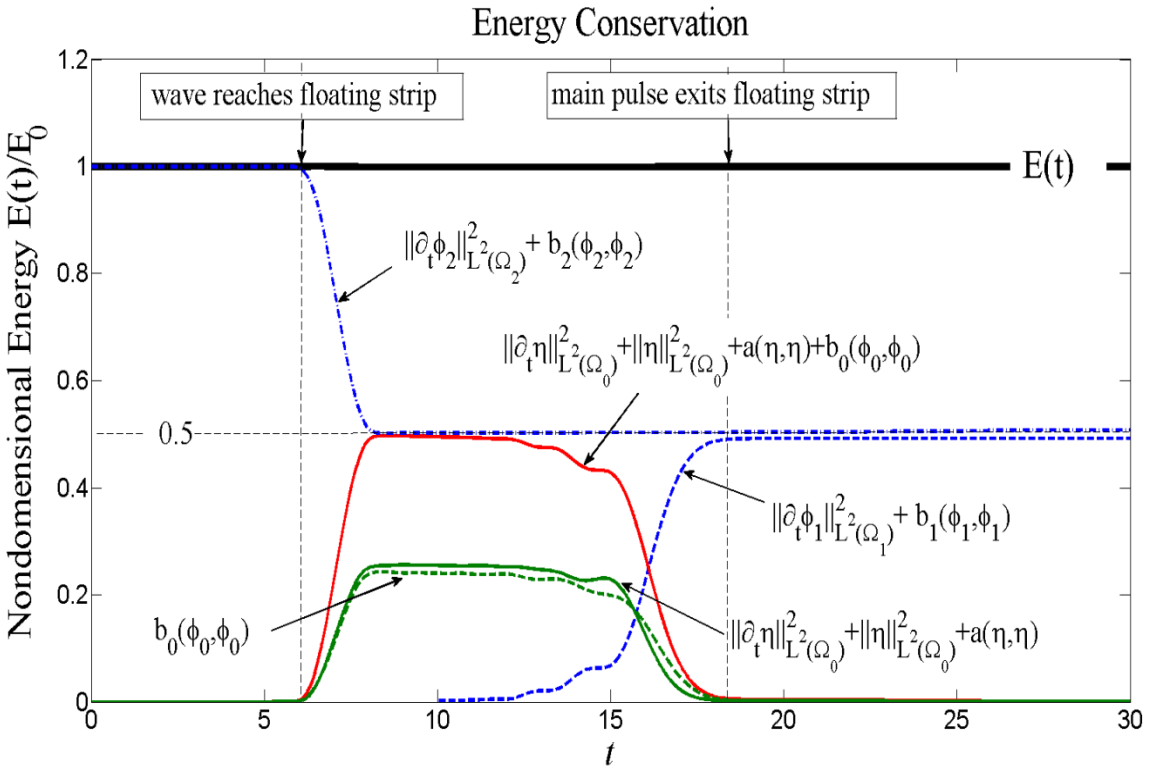

Figure 27 The energy conservation principle for problem Π_2 (floating plate)

$$\left\|\partial_t\eta\right\|^2_{L^2(\Omega_0)} + \left\|\eta\right\|^2_{L^2(\Omega_0)} + a(\eta,\eta) + b_0(\phi_0,\phi_0)\ . \tag{6.6}$$

A few seconds after the impact, the wave passes into Ω_1. The first of the dispersed waves travelling at a greater speed enter Ω_1 at approximately $t \simeq 7.5$. The inflow of energy in the domain is given by the blue dashed line, showing an increase of the quantity

$$\left\|\partial_t\phi\right\|^2_{L^2(\Omega_1)} + b_1(\phi_1,\phi_1) \tag{6.7}$$

,against time. Thus, the non-dimensional energy is now given by the sum of the energies of the propagating waves within the fluid layers Ω_1, Ω_2 and the energy of the hydroelastic wave and the fluid in domain Ω_0. When the elastic strip is finally at rest ($t \simeq 16$), the total energy is given by the sum of (6.5) and (6.7). In figure 8 the energy contributions of the fluid and the elastic strip in Ω_0, are also shown against time. The superposition of the curves representing the quantities $\left\|\partial_t\eta\right\|^2_{L^2(\Omega_0)} + \left\|\eta\right\|^2_{L^2(\Omega_0)} + a(\eta,\eta)$ and $b_0(\phi_0,\phi_0)$ generates the energy quantity (6.6).

6.4 Analysis of two floating cantilever configurations

The following results were presented at the European Geoscience Union Assembly in May 2014, as collaboration between Dr Papathanasiou, Professors Theotokoglou and Belibassakis and the author [2]. The scope of the given work was the hydroelastic analysis of ice shelves under long wave excitation. The effects of variable plate thickness and variable bathymetry were examined. The two separate configurations used for the analysis are shown in figure 28. Configuration A features a plate with constant thickness over linearly varying bathymetry, while configuration B shows a plate with stepped thickness over the same topography.

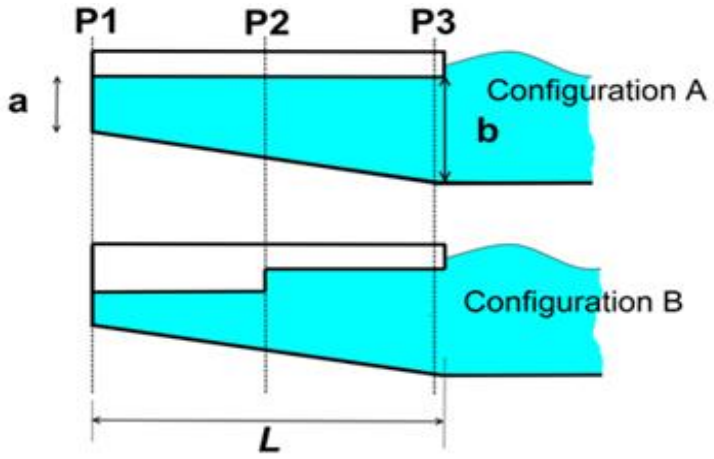

Figure 28 Configurations A and B

- **Configuration A**

The length of the plate is taken as 100 km. The smallest depth, denoted by a, located underneath the fixed edge as shown in figure 29 is 200 m. The largest depth b, underneath the free edge, is 400 m. The initial upper surface disturbance is a step pulse with a wavelength of 20 km and amplitude of 2 m.

Figure 30 shows a series of snapshots of the upper surface elevation at different moments in time, illustrating the evolution of the phenomenon. Figure 31 shows the bending moment and shear force distributions at selected moments in time ($t = 8, 34$ and 30). As seen in the previous examples, the initial upper surface displacement forms two identical travelling waves, propagating in opposite directions, with constant speed. The wave that impacts the free end of the plate is partially reflected while it continues to propagate,

passing under the plate and providing the initial flexural excitation. The hydroelastic wave shows dispersive characteristics, visible in figure 30 as smaller waves preceding the main excitation. When reaching the fixed edge (*x=0*), the wave is fully reflected and subsequently propagates away from the plate origin. At approximately $t = 8$, the hydroelastic wave begins to propagate in the plate, at $t = 30$ it impacts the fixed boundary and at $t = 34$, upon reflection, it is seen propagating towards the free end.

A parametric study of the effects of bottom topography was carried out. The maximum and minimum non-dimensional bending moment and shear force as well as the maximum absolute deflection of the plate were plotted for various ratios a / b (see figure 28). Figure 29 shows a direct link between the depth underneath the plate and the observed quantities. Maximum absolute values seem to increase as the depth decreases.

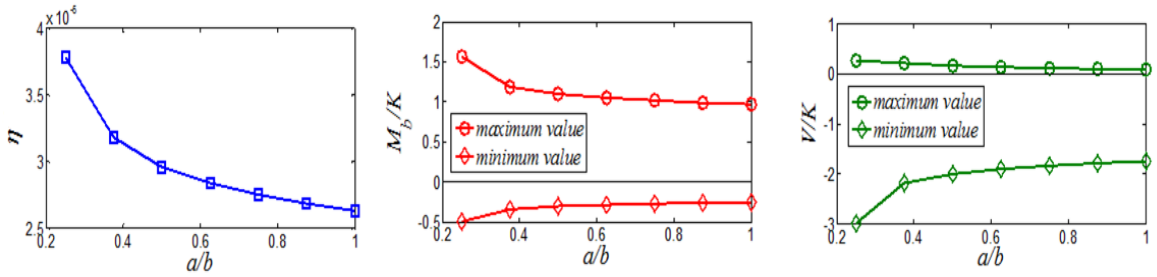

Figure 29 Parametric study of the bottom topography variation

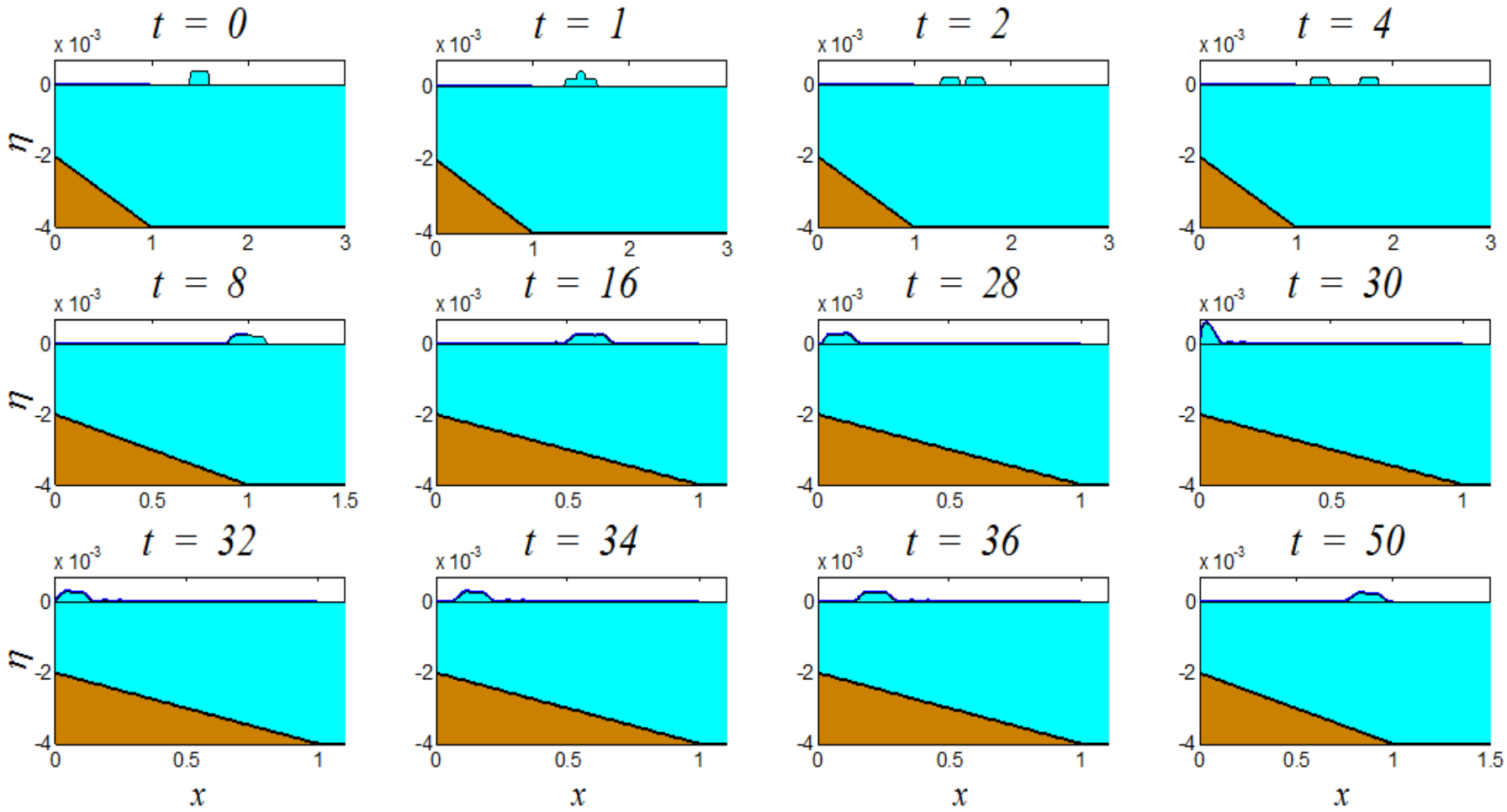

Figure 30 Solution for the upper surface elevation/displacement at distinct moments in time

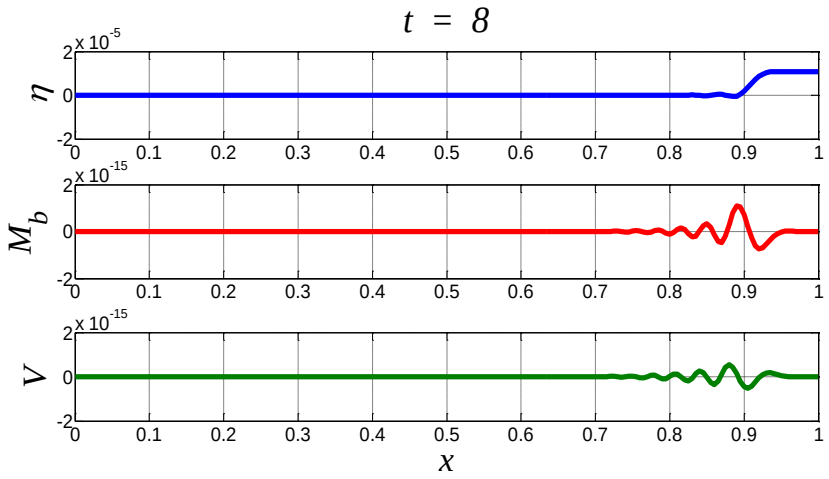

(a)

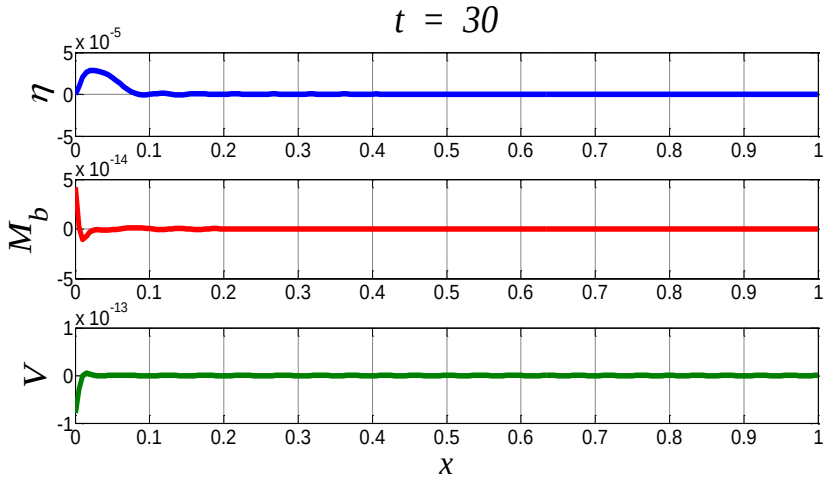

(b)

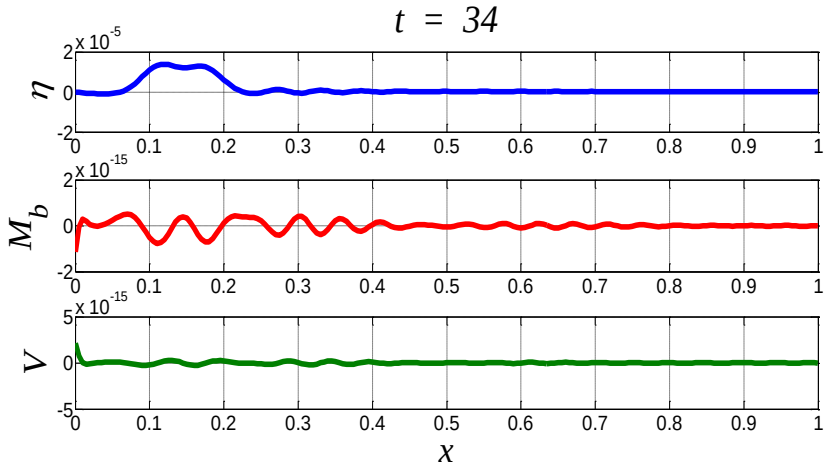

(c)

Figure 31 Deflection, bending moment and shear force profiles at $t = 8, 30$ and 34

- **Configuration B**

Configuration B is examined in order to establish the effects of cross sectional variation. While the same bathymetry and initial excitation profiles as in configuration A are selected, a stepped thickness is used for the plate. A constant thickness of 150 m is assumed from the fixed end to the plate midpoint and a thickness of 100 m from that point to the free edge.

Figure 32 shows the upper surface elevation at different moments in time, while figure 33 shows bending moment and shear force distributions in selected moments.

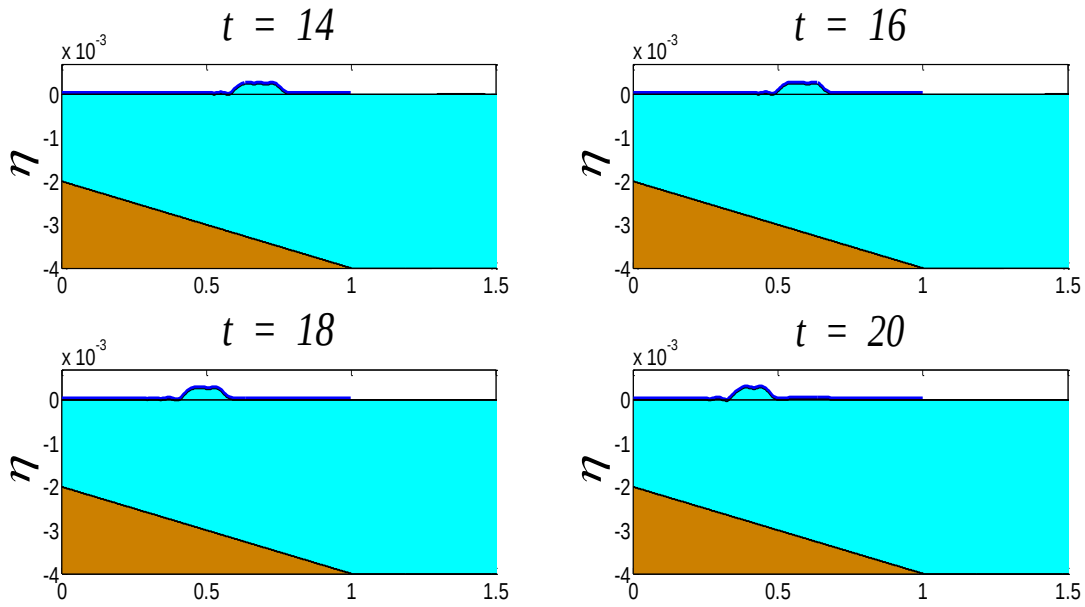

Figure 32 Solution for the upper surface elevation/displacement at distinct moments in time

Kinks can be observed in all bending moment and shear force distributions at point P2, due to the variation in thickness.

Figure 34 shows a comparison between the bending moment and shear force values against time for configurations A and B.

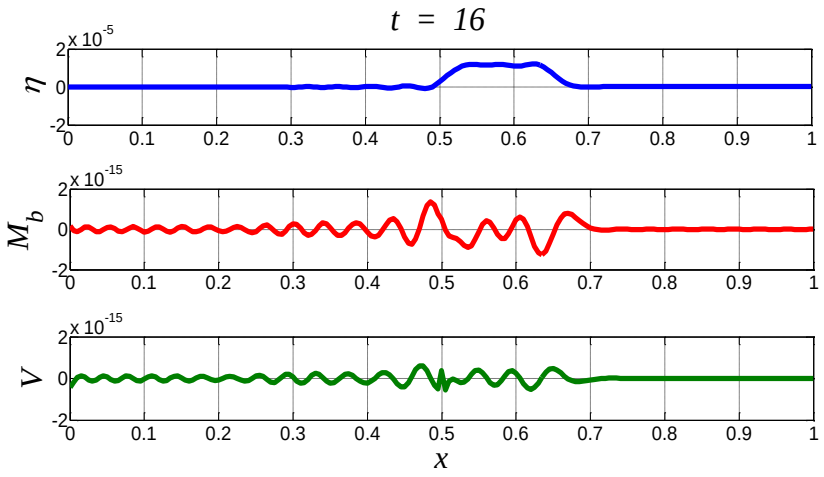

(a)

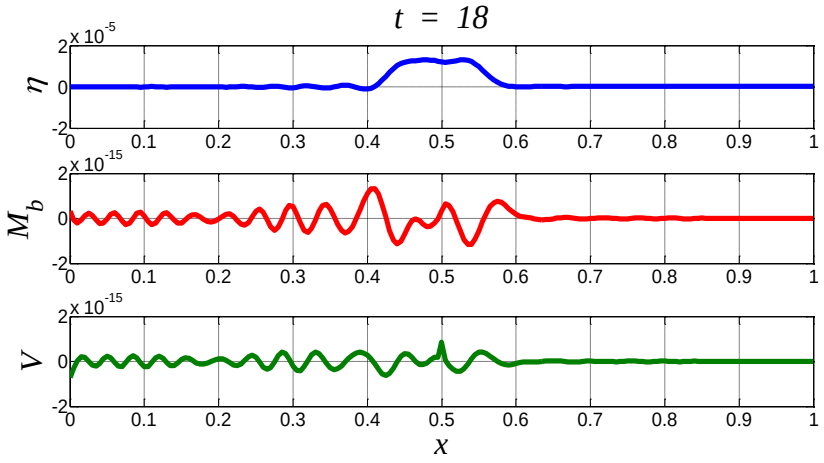

(b)

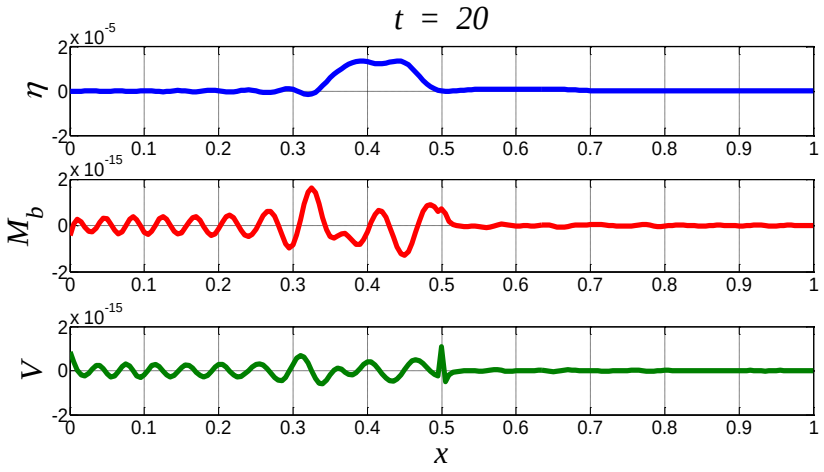

(c)

Figure 33 Deflection, bending moment and shear force profiles at $t = 16, 18$ and 20

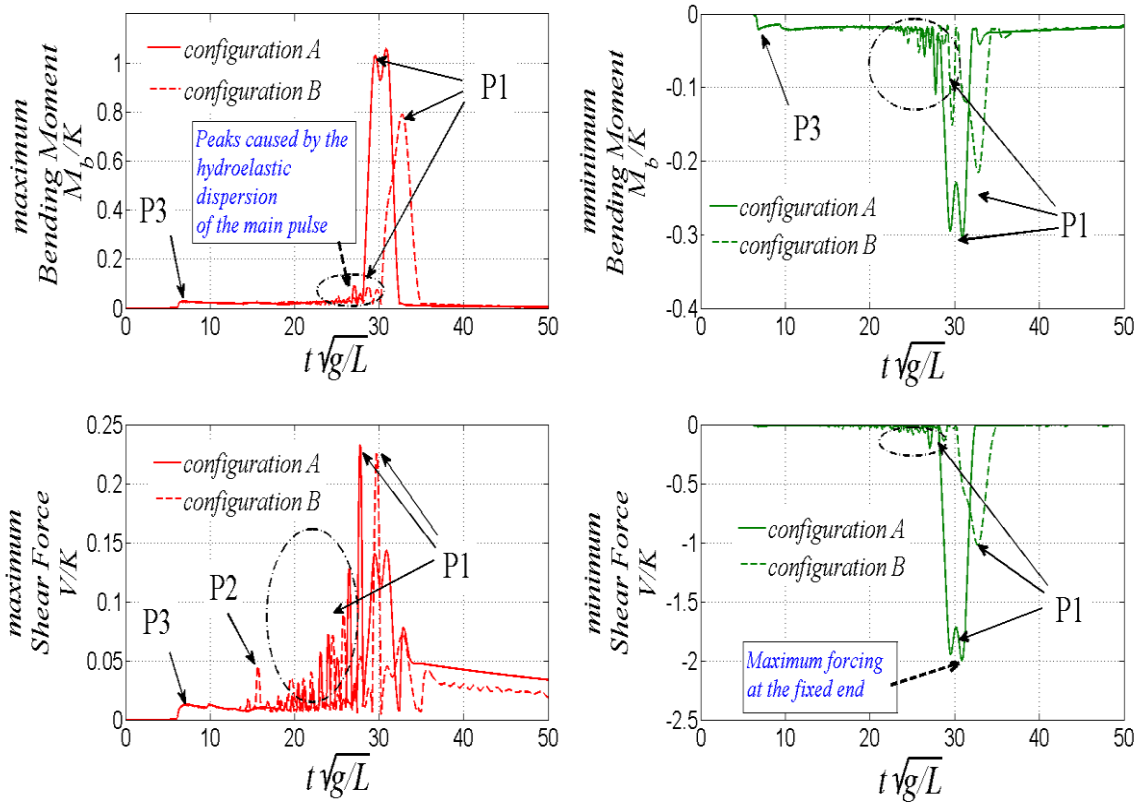

Figure 34 Comparison of the maximum/minimum bending moment and shear force values between configurations A and B.

At point P1 (fixed edge), the positive bending moment is greater for configuration B. In all cases, it is evident that the hydroelastic dispersion of the main pulse is intensified for configuration B, after point P2. The dispersion of the hydroelastic wave manifest itself through the formation of escalating peaks, regarding the bending moment and shear force values at P1, preceding the arrival of the main pulse at the same point. Due to the cross-sectional variation, configuration B features a sudden increase of maximum shear force at point P2 for $t\cong 15.5$.

6.5 Case study- Honshu Tsunami

In this section the Sulzberger Ice shelf calving event of 2011 will be studied. The developed numerical tool will be utilized in order to calculate and interpret the response of the ice shelf under tsunami excitation.

Brunt *et al.* [4] documents the calving event and offers observational data reinforcing the theory of calving due to tsunami impact. The tsunami generated by the Honshu earthquake on the 11th of March, reached the Sulzberger Ice Shelf tip, located East of the Ross Ice shelf. The dimensions of the ice shelf are documented as 160 km wide and 100 km long from the continent to the ocean front. The front on the Eastern front of the ice shelf, between Vollmer island and Guest Peninsula (*see* figure 35) is thin, under 80 m. Decades before the event, rifts on that front had created a rectangular region 10 and 6 km in dimensions.

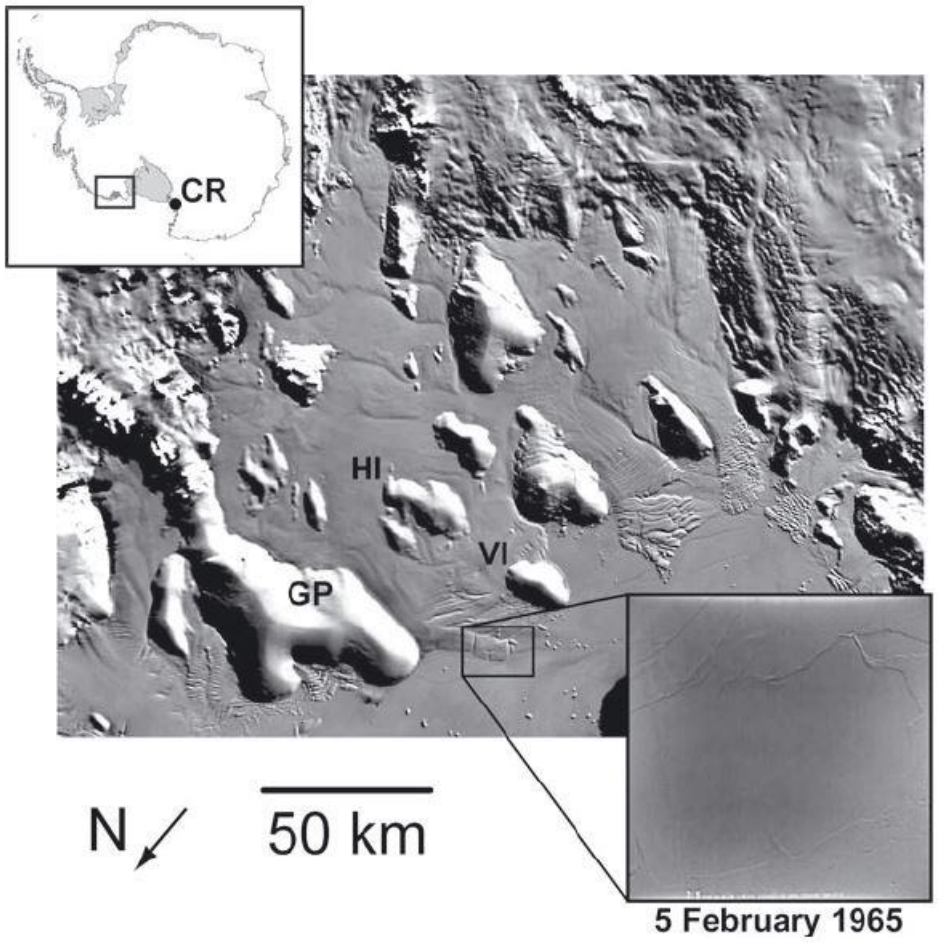

Figure 35 The Sulzberger Ice Shelf (source: Brunt *et al.* [3])

European Space Agency Envisat images reveal that the Sulzberger Ice shelf eastern front was intact on the 11th of March. The projected arrival time, factoring ocean depth and reflections was calculated as 18.3 hours after origin time on 6.45 UTC on 11th of March.

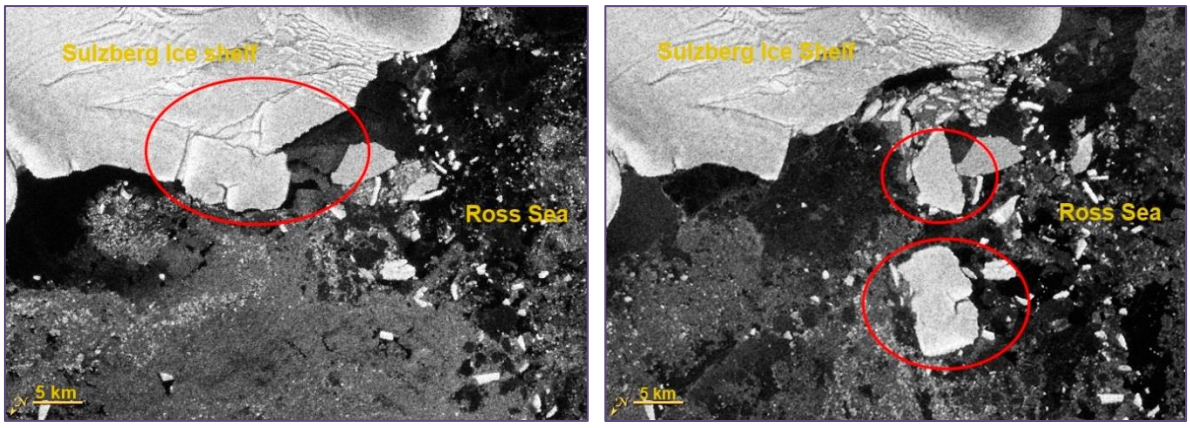

(a) **(b)**

Figure 36 Envisat ASAR images of the Sulzberg ice Shelf (a) *11 March 2011* (b) *16 March 2011*

Satellite images verified the projections and a few days later the separation of two large icebergs is clearly seen.

The Sulzberger Ice shelf is simulated by a fixed edge plate spanning over 100 km. The depth in front of the ice shelf tip is taken as 150 m, varying linearly until 800 m over a distance of 100 km (*see* figure 37)

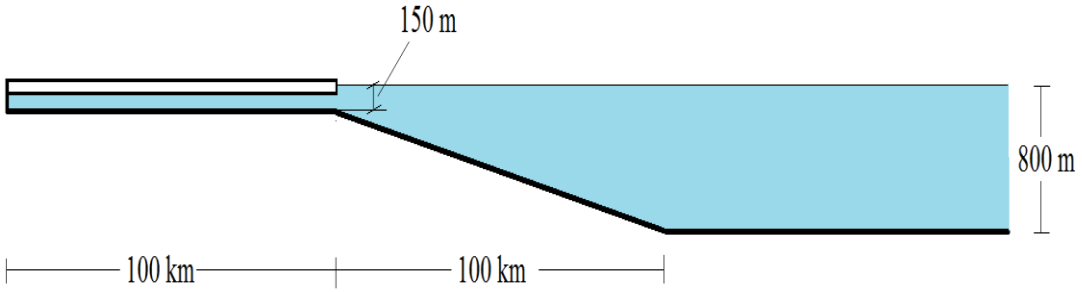

Figure 37 Configuration for the simulation of the Sulzberger Ice Shelf and Honshu Tsunami.

The initial excitation is given by (6.1), with $\mu = 100$, $w = 2000$ and $A = 0,4\,\mathrm{m}$.

The present example is a geophysical application of the developed hydroelastic model. As seen in the first example for problem Π_1 (see *section 6.2*) the maximum bending moment and shear force values appear at the fixed boundary of the plate. Calving

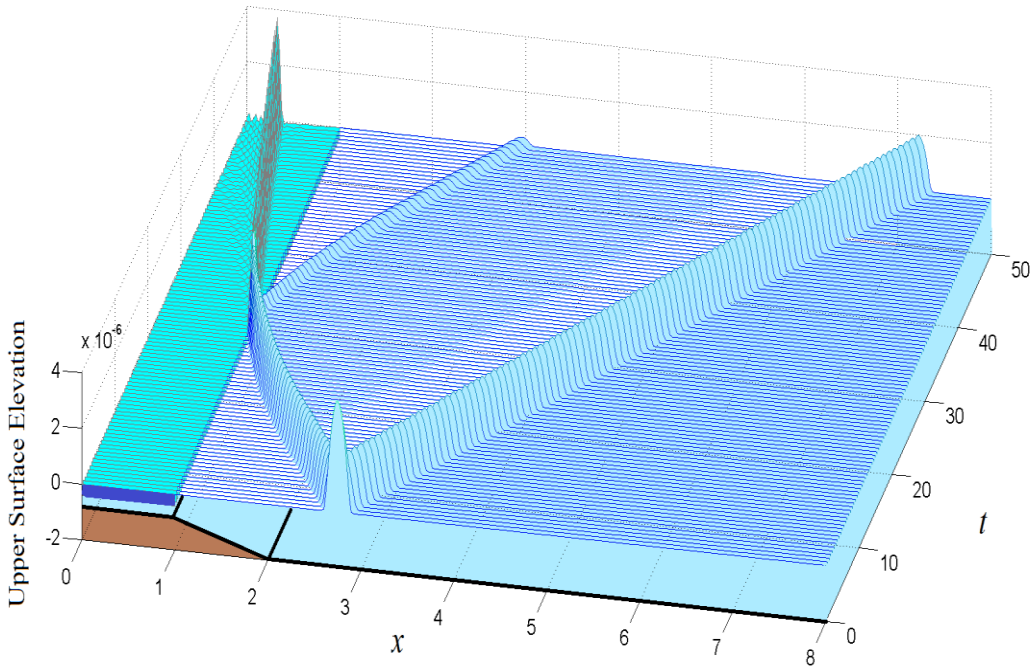

Figure 38 Space-time plot of the wave propagation, for the Sulzberger Ice shelf case study.

events, however are bound to happen at a values significantly lower than the maximum. Hence, it is of interest to examine in detail the hydroelastic wave propagation before its reflection at the fixed edge.

As shown in figure 38 the form of the linear wave propagating to the left, remains intact as no dispersive effects apply, as depicted by the linear trail left by the compilation of snapshots in figure 39.The formation of the travelling waves from the initial pulse is in the first three snapshots $(t = 0, 0.5, 1, 1.5 \text{ and } 5)$ of figure 39. The wave that propagates towards the plate, enters the region of linearly varying bathymetry, resulting in a decreasing velocity. The phenomenon is visible through the trail curve of the propagating wave. The reflected wave upon impact with the free edge is shown in both figures. As the reflected wave traverses the variable bathymetry region, it follows the same curved trail. After the impact, wave passes under the plate and the hydroelastic wave begins to propagate. Signs of dispersion are discernible in figure 39. $(t = 27, 30 \text{ and } 40)$.

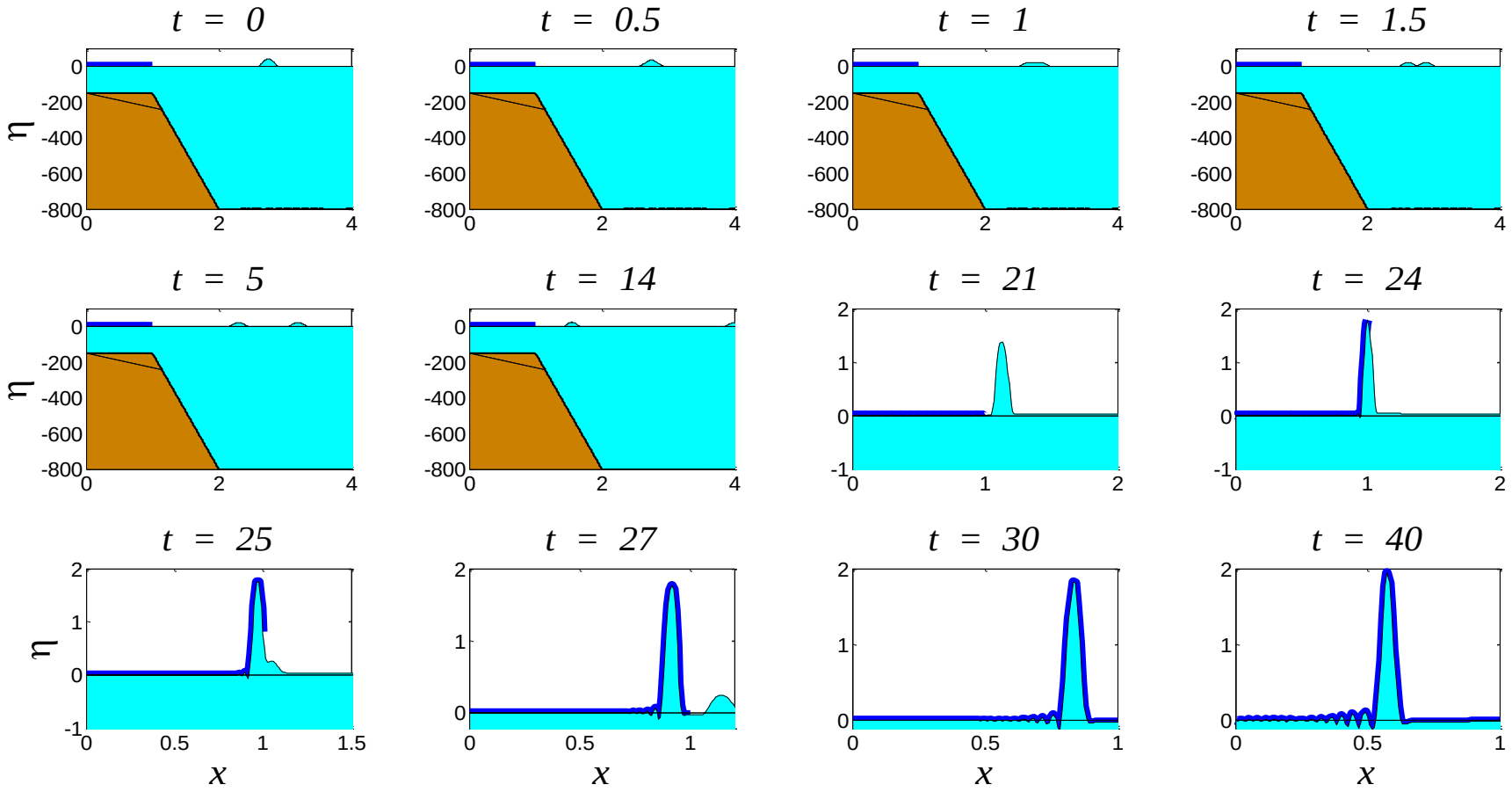

Figure 39 Solution for the upper surface/displacement at distinct moments in time

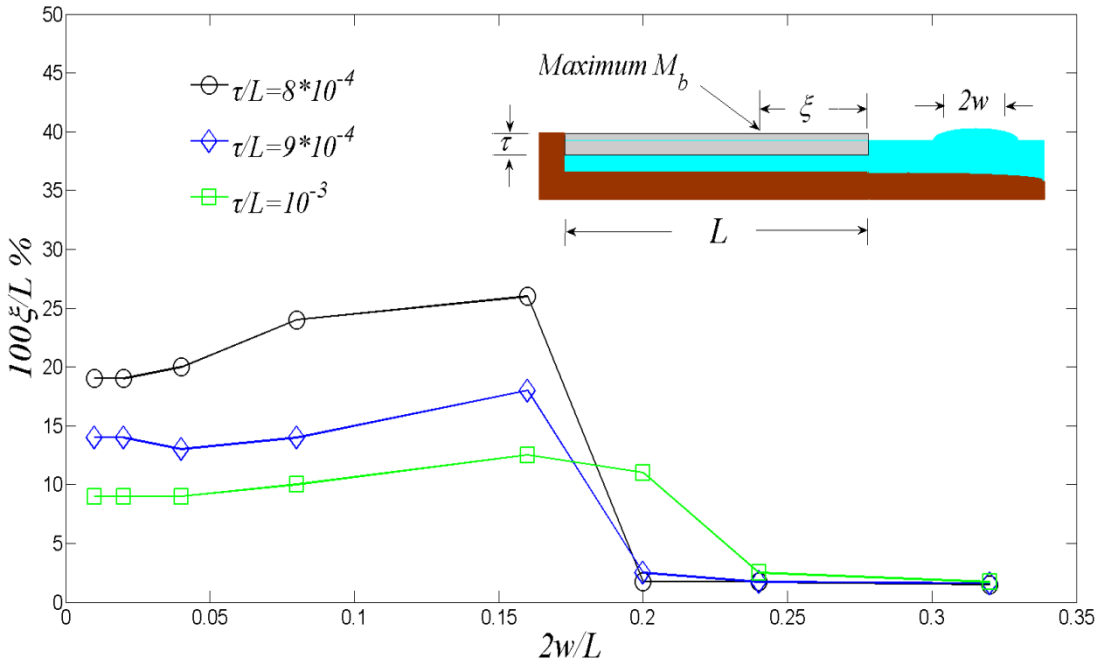

Figure 40 Distance (ξ) from the ice shelf free edge, where maximum absolute value of the bending moment appears as a function of the tsunami wavelength.

The effects of the plate thickness and the wavelength of the incoming tsunami, on the location of the bending moment maximum absolute value are examined. The distance of the location of the extreme value from the free edge, is plotted against the various wavelengths in figure 40. It is seen that for either short or long wavelengths, the distance is relatively irrelevant of the wavelength, while there is a dependency on plate thickness. The location of the extreme bending moment value is closer to the free edge for thicker plates.

The above assertion seems to agree with the observations of Squire [5] who noticed, while performing parametric studies on a semi-infinite ice sheet that the location of maximum strain is insensitive to wave period but dependent on the ice sheet thickness.

However, in figure 40 a sudden drop in distance ξ is visible and consistent for all thicknesses, linking shorter with greater wavelengths. When examining the maximum bending moment and shear force values against time for thickness $\tau = 80\,\mathrm{m}$ and $\tau = 90\,\mathrm{m}$ for short non-dimensional wavelength like 0.04 as shown in figure 41 the maximum bending moment is negative. As the wavelength increases, as shown in figure 42 the maximum bending moment value is now positive.

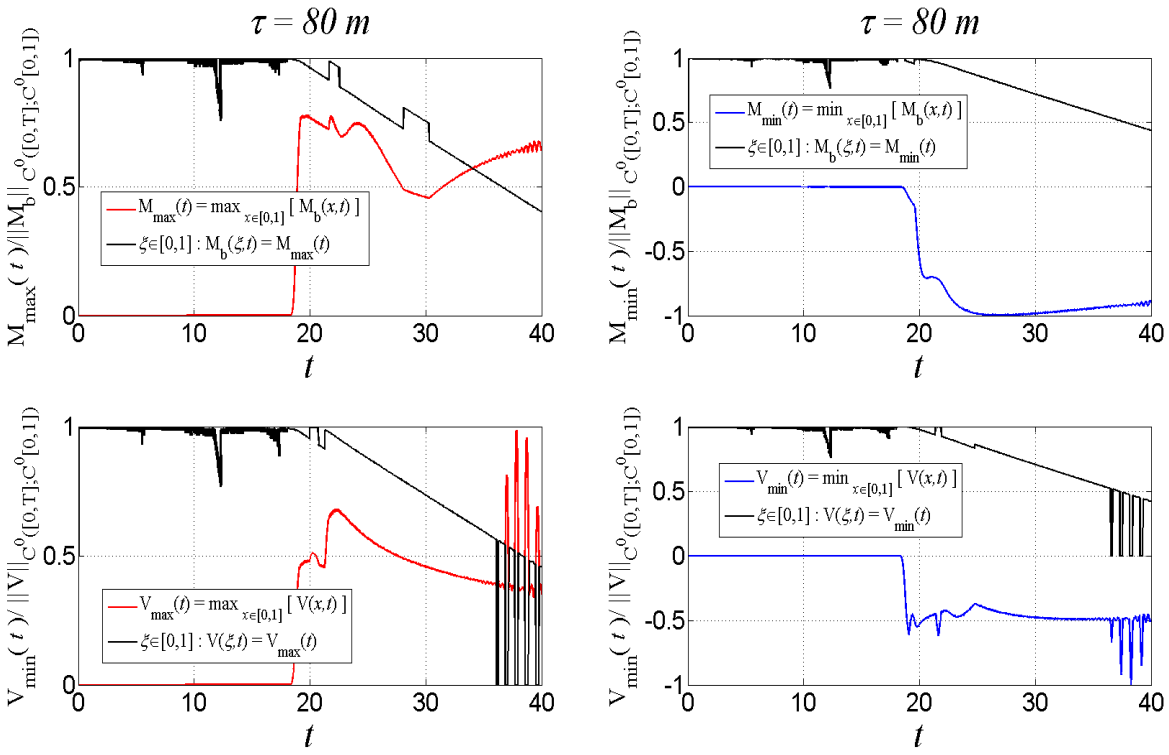

(a)

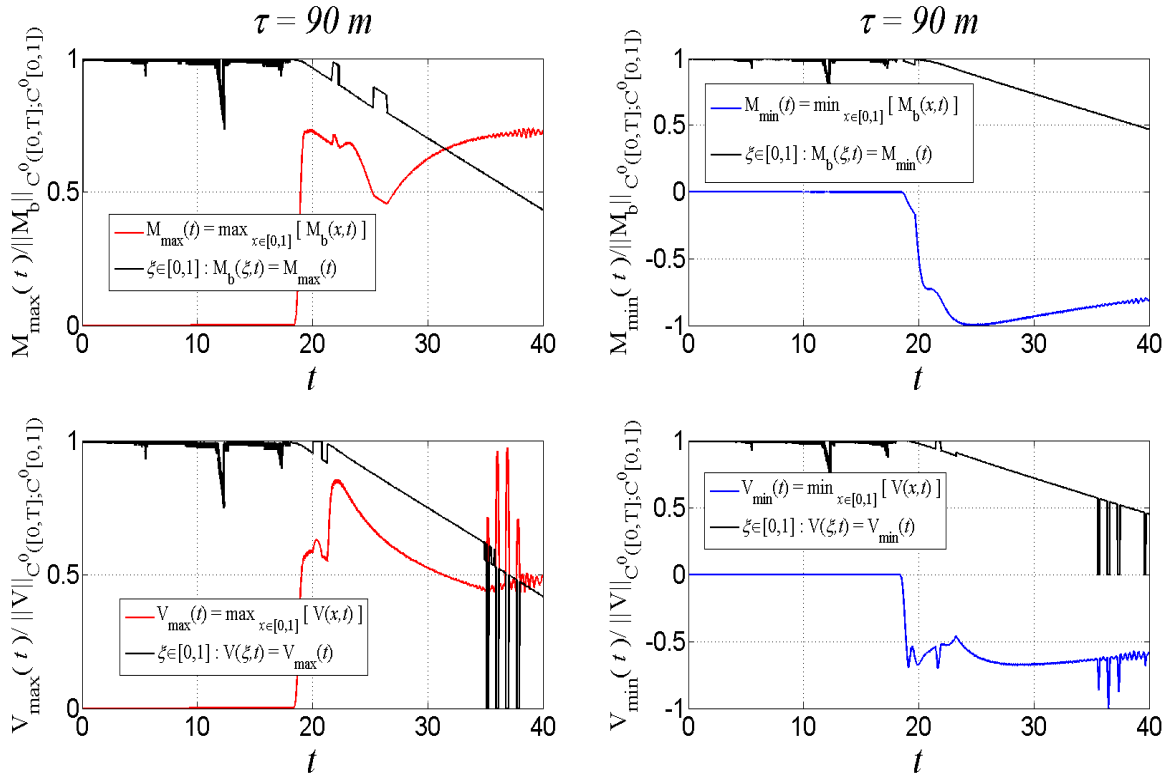

(b)

Figure 41 Maximum bending moment and hear force values and their location, against time. **(a)** $\tau = 80\,\mathrm{m}$ and $w = 2000$, **(b)** $\tau = 90\,\mathrm{m}$ and $w = 2000$

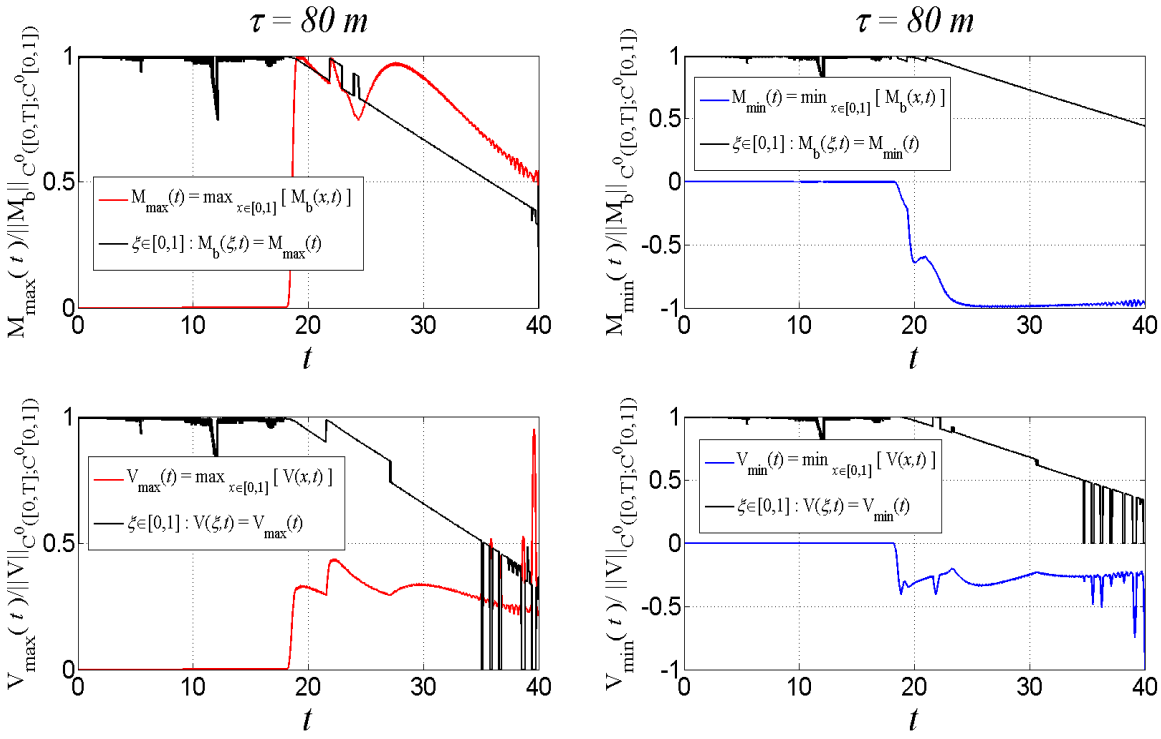

(a)

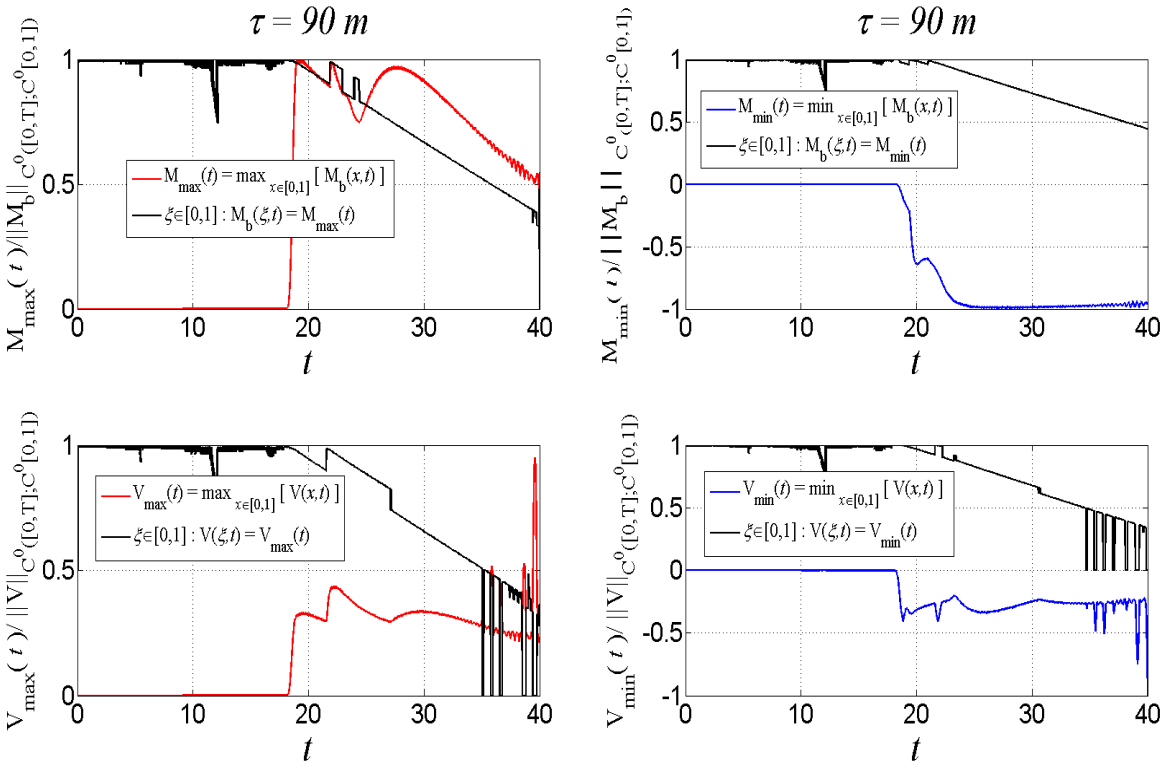

(b)

Figure 42 Maximum bending moment and hear force values and their location, against time. **(a)** $\tau = 80\,\mathrm{m}$ and $w = 4000$,**(b)** $\tau = 90\,\mathrm{m}$ and $w = 4000$

6.6 Conclusions

Two examples were studied for problems Π_1 and Π_2. The dispersive characteristics of the hydroealastic wave were verified in both occasions along with the principle of energy conservation. The Finite Element solution was given the necessary physical interpretation

Additionally, the results presented at the European Geosciences Union Assembly revealed a direct link between plate thickness variation and bending moment and shear force distributions for the floating cantilever problem. Shear force increases at the point of variation.

Finally, the Honshu Tsunami case study revealed that the maximum bending moment remains insensitive to the wavelength of the incoming tsunami while it displays a correlation with plate thickness.

The aim of the present thesis was to employ the finite element method in the study of the hydroelastic response of elastic floating bodies under long wave excitation. Due the course of this work,

- The 1-D general hydroelastic problem of a floating body, under shallow water assumptions was formulated. The problems of a cantilever plate Π_1 and a freely floating plate Π_2 were studied.
- The variational form of problems Π_1 and Π_2 was derived. The solution stability estimates and the energy conservation principle were studied for both problems.
- The variational form was used in the development of special hydroelastic elements, featuring various degrees of interpolation. Error estimates of the semi-discrete form are also presented.
- The finite element solution is compared against the eigenfunction expansion method presented by Sturova. The solutions were found in excellent agreement. Additional validation of the finite element solution is provided by the energy conservation principle.
- Two examples in realistic scales were examined along with a geophysical case study.

6.7 Future research

With the objectives of the present thesis achieved, future directions of the present work may include,

- Introduction of non-linearities in the 1-D model either for the fluid and/or the solid components. The non-linear shallow water equations can be used as the fluid model and/or the non-linear Euler-Bernoulli for the floating body.
- Expansion of the thin plate/ shallow water model in 2-D.
- Study of additional configurations. Development of a 1-D multi-body model, suitable for the simulation of the Marginal Ice Zone or connected VLFSs.

References

[1] Okal, E. A. and Synolakis, C. (2003) A Theoretical Comparison of Tsunamis from Dislocations and Landslides, *Pure and Applied Geophysics (160),* p. 2177-2188,

[2] T. K. Papathanasiou, A. Karperaki, E. E. Theotokoglou and K. A. Belibassakis, Hydroelastic analysis of ice shelves under long wave excitation, European Geosciences Union general assembly 2014, 27 April-2 May, Vienna, Austria

[3] Kardestuncer H. (1987) *Finite Element handbook,* US: Mc.Graw-Hill, Inc.

[4] Brunt K. M. *et al.* (2011) Antarctic ice shelf calving triggered by the Honsu (Japan) Earthquake and tsunami, March 2011, *Journal of Glaciology 57(205),* p. 785-788.

[5] Squire, V. A. (1993) The breakup of shore fast sea ice, *Cold Regions Science and Technology (21),* p. 211-218.

Page intentionally left blank